Technische Universität München
TUM School of Medicine and Health

Spatial metabolomics for therapy response prediction in gastric and lung cancer patients

Jun Wang

Vollständiger Abdruck der von der TUM School of Medicine and Health der Technischen Universität München zur Erlangung des akademischen Grades einer

Doktorin der Naturwissenschaften (Dr. rer. nat.)

genehmigten Dissertation.

Vorsitz: Prof. Dr. Dieter Saur

Prüfer der Dissertation:
1. Prof. Dr. Gil G. Westmeyer
2. Prof. Dr. Bernd Reif

Die Dissertation wurde am 14.11.2023 bei der Technischen Universität München eingereicht und durch die TUM School of Medicine and Health am 13.03.2024 angenommen.

Jun Wang

Spatial metabolomics for therapy response prediction in gastric and lung cancer patients

Technische Universität München
TUM School of Medicine and Health

Abstract

Gastric cancer (GC) and lung squamous cell carcinoma (SCC) are significant contributors to global cancer morbidity and mortality. Patient therapy response differs markedly among current therapeutic regimens within GC and SCC. To address this issue, the state-of-art studies focus on developing molecular classification systems based on multiple molecular levels, such as genomics, transcriptomics and proteomics, which could be a valuable tool for aid in selecting specific treatment approaches. However, molecular classifications based on metabolomics is still lacking and its application for therapy response prediction remains to be comprehensively investigated. This cumulative thesis has the goal to investigate the tissue metabolome by spatial metabolomics for therapy response prediction. Matrix-assisted laser desorption ionization imaging mass spectrometry (MALDI-IMS) will be applied and it will demonstrate how metabolites were measured directly from tissue sections with cellular spatial resolution and how metabolites impacted therapy response.

As a result, this thesis reveal tumor- and stroma-specific subtypes which have distinct tissue metabolite patterns, prognostic value and association with clinical features in GC and SCC. An independent GC cohort confirms that the patient subtypes are associated with trastuzumab therapy response. An independent SCC cohort confirms that the patient subtypes are associated with chemotherapy response.

Overall, this thesis underlines the potential of MALDI mass spectrometry imaging in precision medicine by including two publications. Clinical relevant patient subtypes derived by tissue-based spatial metabolomics are a valuable addition to existing molecular classification systems in

GC and SCC. Metabolic differences of the subtypes and their associations with clinical molecular features might support the development of personalized therapy decision.

Zusammenfassung

Magenkrebs (GC) und Plattenepithelkarzinom der Lunge (SCC) tragen erheblich zur weltweiten Krebsmorbidität und -mortalität bei. Das Therapieansprechen der Patienten bei der Behandlung von GC und SCC variiert. Um dieses Problem zu adressieren, konzentrieren sich aktuelle Studien auf die Entwicklung molekularer Klassifikationssysteme auf der Grundlage mehrerer molekularer Ebenen, wie zum Beispiel Genomik, Transkriptomik und Proteomik, die ein wertvolles Hilfsmittel zur Unterstützung bei der Auswahl spezifischer Behandlungsansätze sein können. Molekulare Klassifikationen auf der Grundlage von Metabolomics und ihr Zusammenhang mit dem Therapieansprechen müssen hingegen noch umfassend untersucht werden. Diese kumulative Dissertation hat das Ziel, den Zusammenhang zwischen dem Therapieansprechen und gewebebasierter Metabolomik. Matrixunterstützte laser desorptions iolisations imaging massenspektrometrie (MALDI-IMS) findet Anwendung und zeigt, wie Metaboliten direkt aus Gewebeschnitten mit zellulärer räumlicher Auflösung gemessen werden und wie diese Metaboliten das Ansprechen auf die Therapie beeinflussen.

Demzufolge weisen die etablierten tumor- und stromaspezifischen Subtypen unterschiedliche Gewebemetabolitenmuster, einen prognostischen Wert und eine Assoziation mit klinischen molekularen Merkmalen bei GC und SCC auf. Eine unabhängige GC Kohorte bestätigen, dass die Patientensubtypen mit dem Ansprechen auf die Trastuzumab-Therapie assoziiert sind. Eine unabhängige SCC Kohorte bestätigen, dass die Patientensubtypen mit dem Ansprechen auf die Chemotherapie assoziiert sind.

Zusammenfassend zeigt diese Dissertation, das Potenzial der MALDI-Massenspektrometrie-Bildgebung in der gewebenbasierten Präzisionsmedizin anhand von zwei Veröffentlichungen auf. Klinisch relevante Patientensubtypen, die durch gewebebasierte räumliche Metabolomik abgeleitet werden, sind eine wertvolle Ergänzung zu bestehenden molekularen Klassifikationssystemen in GC und SCC. Metabolische Unterschiede der Subtypen und ihre Assoziation mit klinischen molekularen Merkmalen könnten die Entwicklung einer personalisierten Therapieentscheidung erweitern und unterstützen.

Acknowledegments

First of all, I am obliged to thank my PhD supervisors Prof. Axel Walch and Prof. Gil Westmeyer giving me the unique opportunity to work on these interesting and challenging topics on spatial metabolomics with clinical relevance during my PhD. I also want to give my appreciation to Dr. Na Sun for my routine guidance. I have always greatly enjoyed the scientific discourse with them that led to new exciting concepts and ideas. From them, I learned that it will always pay off to try all things in the best possible way. I was given exceptional freedom to develop my own ideas, which made me encounter several challenges to overcome but ultimately made me into an independent researcher and thinker.

Second of all, I would like to the members of my thesis committee (Prof. Axel Walch, Prof. Gil Westmeyer and Prof. Bernd Reif) supporting me with valuable suggestions during our joint thesis committee meetings. Furthermore, I'd like to thank Uli and Christina for support with immunofluoresence analysis. Another special thanks goes to Claudia for her support with tissue microarrays preparation. They are the best technician that I have encountered throughout my scientific career. A very special thanks goes to Uli, she has taught me many important insights about life.

In general, I would like to thank my amazing colleagues and office mates, that I shared my everyday life with over the years. You made my PhD some much more rich and enjoyable and many of you have become good friends. In particular, I want to thank Thomas, who I first encountered in the lab when I arrived at the lab in winter 2019. He

taught me a lot with patience, even if I was a beginner at that time in our MALDI–IMS technology research field. He sparked my interest in many topics beyond science, was often my lifesaver and has become a good friend. Verena and Achim were always extremely helpful with any problem whenever I approached them. They always answered with good heart and their professional scientific vision. Thank them very much for being a excellent support and a good friend.

I would also like to thank my Chinese colleagues: Jian Shen and Qian Wang. They offered always exceptional support when I was feeling down and we have shared so many unforgettable moments together. I'd like to thank them in particular for being a great support and distraction from the daily routine over the years. We spent an unforgettable life and always had a good laugh together.

Moreover, I would like to thank my boyfriend, my mother and father for their help during my PhD life. My boyfriend always gave me support and the confidence to become a good scientist at any time. My parents always gave me the encouragements to explore all my interests. Without their unconditional support, I could not be the person that I am today and I want to thank them for that wholeheartedly.

At the end, I would like to thank all the persons that I forgot to mention or can not mention by their names. They were good companions over all this time without whom I would not be able to accomplish my PhD. Thank them all.

Contents

Part I

Preface

This dissertation is a cumulative publication-based doctoral thesis, which was carried out between November 2019 and November 2023 under the supervision of Prof. Axel Walch in the Reserach Unit Analytical Pathology at the Helmholtz Center Munich (HMGU) and Prof. Gil Westmeyer in the faculty of Chemistry at the Technical University of Munich (TUM). It is based on two studies that has been separately published in the international peer-reviewed scientific journals called Clinical Cancer Research [1] and npj Precision Oncology [2]. The first part of this dissertation primarily serves as an introduction to the motivation and developments of related state-of-art research, followed by summaries of each published article in Part IV, discussion in Part V and conclusion in Part VI.

Part II

Acronyms

MALDI	Matrix Assisted Laser Desorption ionization
IMS	Imaging Mass Spectrometry
GC	Gastric Cancer
SCC	Lung Squamous Cell Carcinoma
NSCLC	Non-Small Cell Lung Cancer
LUAD	Lung Adenocarcinoma
HER2	Human Epidermal Growth Factor Recepter 2
MIB1	E3 ubiquitin- protein ligase
DEFA–1	human alpha defensin 1
MSI	Microsatellite Instability
PD–L1	Programmed Death–Ligand 1
PD–1	programmed cell death protein 1
EBV	Epstein-Barr Virus
TP53	Tumor Protein p53
EMT	Epithelial–Mesenchymal Transition
MSS	Microsatellite Stability
MMR	Mismatch Repair Protein
ACRG	Asian Cancer Research Group
TCGA	the Cancer Genome Altas
TMA	Tissue Microarray
FF	Fresh Frozen
FFPE	Formalin-Fixed Paraffin-Embedded
IHC	Immunohistochemistry
FISH	Fluorescence In Situ Hybridization
t–SNE	t–Distributed Stochastic Neighbor Embedding
sPLSDA	Sparse Partial Least Squares Discriminant Analysis
HMDB	Human Metabolome Database
KEGG	Kyoto Encyclopedia of Genes and Genomes
SPACiAL	Spatial Correlation Image Analysis

TILs	Tumor Infiltrating Lymphocytes
CD3	Cluster of Differentiation 3
CD8	Cluster of Differentiation 8
FOXP3	Forkhead Box P3
CPS	Combined Positive Score
OS	Overall Survival
DFS	Disease Free Survival
DNA	Deoxyribonucleic Acid
EGFR	Epidermal Growth Factor Receptor
CDKN2A	Cyclin Dependent Kinase Inhibitor 2A
NFE2L2	Nuclear Factor Erythroid-derived 2-like 2
KEAP1	Kelch-like ECH-associated Protein 1
PIK3CA	Phosphatidylinositol-4,5-bisphosphate 3-kinase Catalytic Subunit Alpha
ALK	Anaplastic Lymphoma Kinase
ROS1	ROS proto-oncogene 1
PTEN	Phosphatase and Tensin Homolog
MLL2	Mixed Lineage Leukemia 2
PI3K	Phosphoinositide 3-kinases
CDK4/6	Cyclin-dependent Kinase 4/6
FGFR	Fibroblast Growth Factor Receptor
MET	MET Proto-oncogene, Receptor Tyrosine Kinase
NGS	Next-Generation Sequencing
TNM	Tumor Node Metastasis
UICC	Union for International Cancer Control
dCDP	Deoxycytidine Diphosphate
CDP	Cytidine Diphosphate
UDP	Uridine Diphosphate
NAC	Neoadjuvant Chemotherapy

Part III

Introduction

1 Gastric Cancer and Lung Cancer

In this thesis, we select gastric cancer (GC) and lung squamous cell carcinoma (SCC) patient cohorts as research targets, and the choice of GC and SCC for spatial metabolomics investigation is driven by their clinical significance, unique metabolic characteristics, existence of inter-tumor heterogeneity, lack of effective biomarkers and treatments, and the potential to uncover insights that could lead to improved patient outcomes and therapeutic strategies. Firstly, GC and SCC are significant contributors to global cancer morbidity and mortality. GC is one of the leading causes of cancer-related deaths worldwide, and SCC is a major subtype of lung cancer, which is the leading cause of cancer-related deaths in many countries. Meanwhile, GC and SCC are clinically well-studied malignancies with substantial patient populations, making the findings from -omics studies more likely to have a meaningful impact on clinical practice and patient care [3]. Apart from their common characteristics, GC and SCC also show their unique metabolic characteristics. The primary site of cancer plays a significant role in determining its metabolic characteristics. GC arises from the cells lining the stomach, while SCC originates in the lung tissue, which has distinct physiological functions, such as oxygen exchange and respiratory support. These tissues have inherently different metabolic functions, leading to differences in their metabolic profiles [4, 5]. In addition, both tumor types exhibit unique inter-tumor heterogeneity, which can complicate treatment decisions and contribute to therapeutic resistance [6, 7].

The following chapters will first introduce the reader to the primary research background of GC and SCC biology and current therapeutic regimens. Next, a general picture of the current knowledge of the emerging molecular classification of GC and SCC and how the established subtypes benefit personalized therapy will be described. Finally, the spatial metabolomics by MALDI-IMS and clustering analysis method

applied in this thesis will be introduced. At the end of this part, I will conclude the aims of this dissertation based on the aforementioned. We assume that spatial metabolomics can stratify patients into metabolic subtypes, guiding the development of strategies to select subtypes for overcoming treatment resistance and improve patient responses.

1.1 Epidemiology

Gastric cancer (GC) develops from the lining of the stomach and is currently a leading cause of cancer-related deaths with the fourth highest mortality rate (7.7%) and fifth-most common diagnosed cancer (5.6%) worldwide (Fig. 1.1), which has 1,089,103 new cases in 2020 and an estimated 768,793 mortalities [3]. High-incidence areas are observed in East Asia, Eastern Europe, South America, Western Asia and Southern Europe. At the same time, low-incidence rates are observed in Middle Africa, Southern Africa, Western Africa, Eastern Africa, and Northern Africa [3].

Lung cancer is currently a leading cause of cancer-related deaths with the first highest mortality rate (18.0%) and second-most common diagnosed cancer (11.4%) worldwide (Figure 1.1) due to delayed diagnoses and few treatment interventions [3]. Lung cancer had 2,206,771 new cases in 2020 and an estimated 1,796,144 mortalities [3]. During the COVID pandemic, the diagnosis and treatment of lung cancer have been hampered; nevertheless, this has not been reflected in the 2022 predictions for incidence and death owing to the typical delays in gathering, calculating, and reporting the data [3]. Only 21.7% of all patients with lung cancer, including those with both non–small cell lung cancer (NSCLC) and small cell lung cancer, are still alive five years or more after diagnosis [8]. Adenocarcinoma and squamous cell carcinoma (SCC) are the most frequent histologic subtypes, accounting for 50% and 30% of NSCLC cases, respectively. Although the incidence of SCC is decreasing as a consequence of changes in tobacco consumption habits, SCC is still a major health issue.

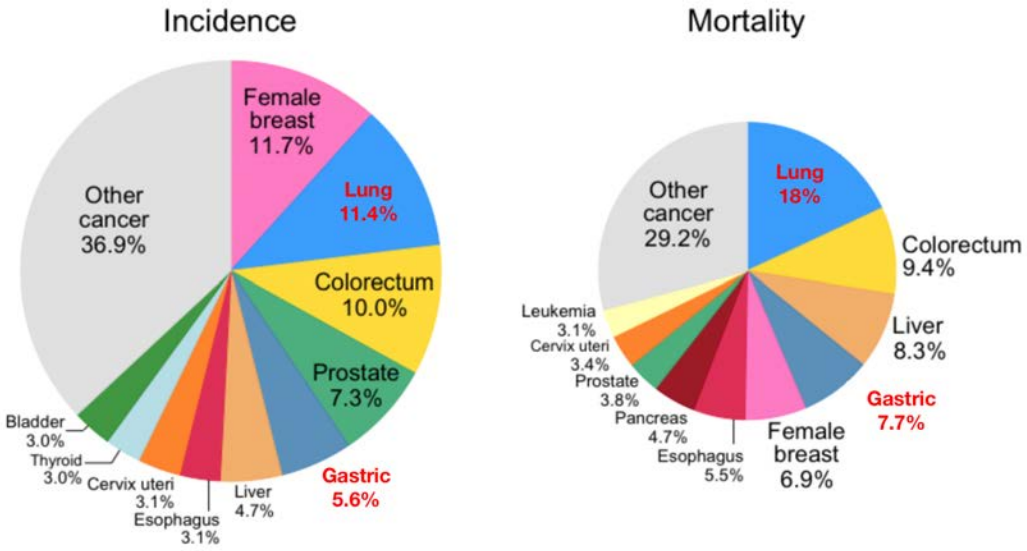

Fig. 1.1. Gastric cancer and lung cancer incidence and mortality in 2020. Request with permission from [3]. Copyright 2021, Sung, H., Ferlay, J., Siegel, R.L., Laversanne, M., Soerjomataram, I., Jemal, A. and Bray, F. Global cancer statistics 2020: GLOBOCAN estimates of incidence and mortality worldwide for 36 cancers in 185 countries. CA: a cancer journal for clinicians, 71(3), pp.209-249.

1.2 Clinical Therapy

1.2.1 Clinical therapy of gastric cancer

Gastric cancer (GC) is often diagnosed at an advanced stage [9]. The current algorithm for the treatment of GC is shown in Figure 1.2. Most patients with advanced GC are best treated with multimodality therapy, however, still results in a poor prognosis of 5-year survival in 6% of patients [10]. In addition, once GC is diagnosed as unresectable, metastatic, or recurrent disease, therapies are more limited and palliative, with the cure being extremely rare [10]. As a result, patients often do not receive systemic therapy despite the guideline recommendations in advanced GC.

Human epidermal growth factor recepter 2 (HER2) is a member of the HER family [11]. Trastuzumab is a humanized monoclonal antibody that targets the HER2 receptor, which inhibits downstream signal activation, and induces antibody-dependent cellular toxicity. It represents the first treatment option for approximately 20% of advanced GC patients with HER2 overexpression or amplification [11, 12]. The HER2 immunohistochemistry (IHC) scoring system categorizes HER2 protein expression into four levels, which ranges from Score 0 to Score 3+ [13]. An IHC score of 3+ is considered positive for HER2 overexpression. However, an IHC score of 2+ is considered equivocal. In these cases, additional Fluorescence In Situ Hybridization (FISH) testing is recommended to confirm HER2 gene amplification [13]. Trastuzumab showed benefit in patients with HER2-positive tumours enrolled in the pivotal phase 3 trial Trastuzumab for Gastric Cancer (ToGA) [14]. In this trial, trastuzumab plus chemotherapy improved median overall survival (OS) compared with chemotherapy alone (16.0 vs 11.8 months), particularly in a posthoc analysis of patients who had HER2 IHC scores of 3+ or FISH positivity and an IHC score of 2+, which was therefore defined as the standard of care in the first-line treatment in advanced HER2-positive gastric adenocarcinoma [14]. However, only a subgroup benefits from the addition of trastuzumab to

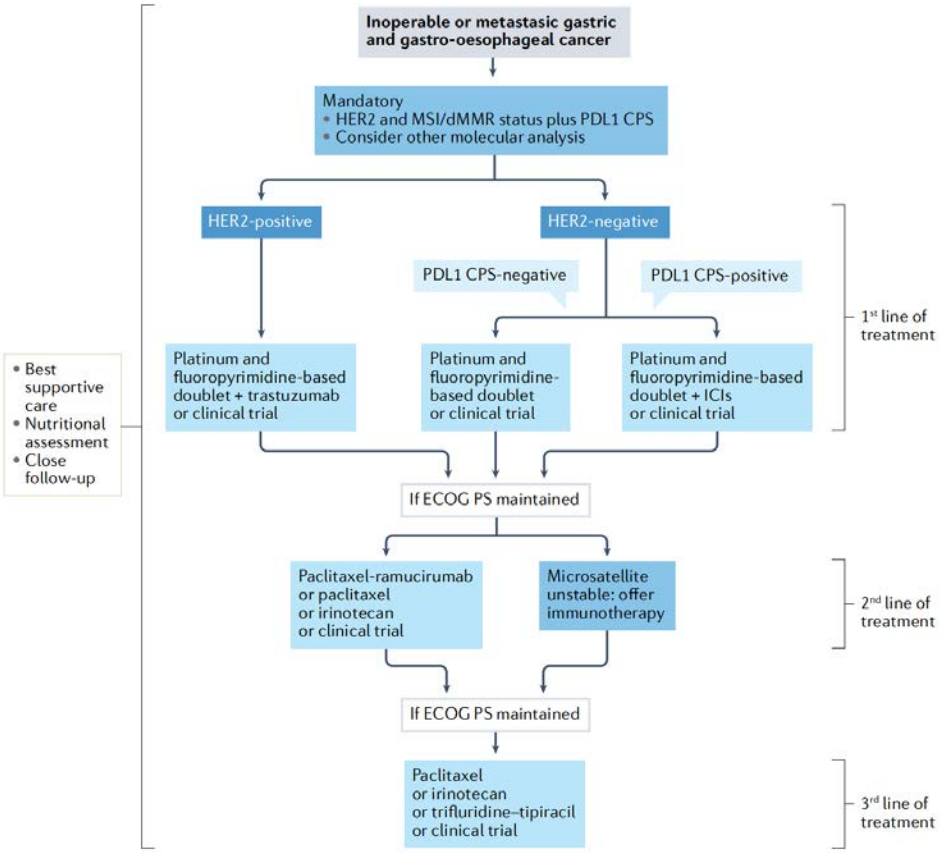

Fig. 1.2. Current algorithm for the treatment of gastric and gastro-oesophageal junction cancer [9]. Reproduced with permission from Springer Nature. Copyright 2023, Alsina, M., Arrazubi, V., Diez, M. and Tabernero, J. Current developments in gastric cancer: from molecular profiling to treatment strategy. Nature Reviews Gastroenterology Hepatology, 20(3), pp.155-170.

chemotherapy. Although some complete durable tumor responses in trastuzumab-treated patients were reported [15, 16], most patients experience initial or acquired resistance. The overall response rate of the combined therapy is below 50%, indicating a considerable proportion of HER2-positive cancers are resistant to HER2 inhibition [17, 18, 19]. Several issues have been addressed to account for the limited benefit of HER2 blockade. Among them, tumour molecular heterogeneity and molecular mechanisms responsible for anti-HER2 drug resistance are being considered and getting researchers' attention.

Programmed cell death protein 1 (PD–1), a T cell co-inhibitory receptor, plays an important role in cancer cell escape from the host's immune

system [20]. The programmed death-ligand 1/programmed cell death protein 1 (PD–L1/PD–1) axis can protect cancers from T-effector cells and help maintain an immunosuppressive microenvironment [21]. PD-L1 blockade has changed the direction of cancer care, and gastric cancer is no exception. Some subtypes, such as microsatellite instability high (MSI-H) tumours or Epstein-Barr Virus (EBV^+) GC, are especially sensitive to PD-L1 blockade [22, 23]. The post hoc analysis of the 84 patients with MSI-H tumours treated in the pembrolizumab trials KEYNOTE-059, KEYNOTE-061 and KEYNOTE-062 supported these findings [20]. Another novel approach to improving the treatment of GC patients is the combination of HER2-directed therapies with immunotherapy. The phase 3 KEYNOTE-811 trial recently showed that adding pembrolizumab to trastuzumab and chemotherapy effectively reduced tumor size, induced complete responses in some participants, and significantly improved objective response rate chemotherapy in HER2-positive, metastatic gastroesophageal adenocarcinoma [24]. However, the answer to the question regarding the best treatment line for immunotherapy remains uncertain. The prediction of response before therapy is an important issue in GC because the cost/benefit ratio for patients could be dramatically enhanced and overtreatment could be prevented.

1.2.2 Clinical therapy of lung squamous cell carcinoma

Progress in translating advances in our understanding of the molecular biology of GC into personalized treatments has lagged behind that achieved in certain other tumour types, such as NSCLC [25]. In NSCLC, unlike lung adenocarcinomas, no FDA-approved targeted therapy regimens available to benefit lung squamous cell carcinoma (SCC) patients [26], which will will serve as the central focus of my second study in the thesis. Given the emphasis of my second research on the SCC subtype in this thesis, the clinical therapy of SCC will accordingly be introduced in this part.

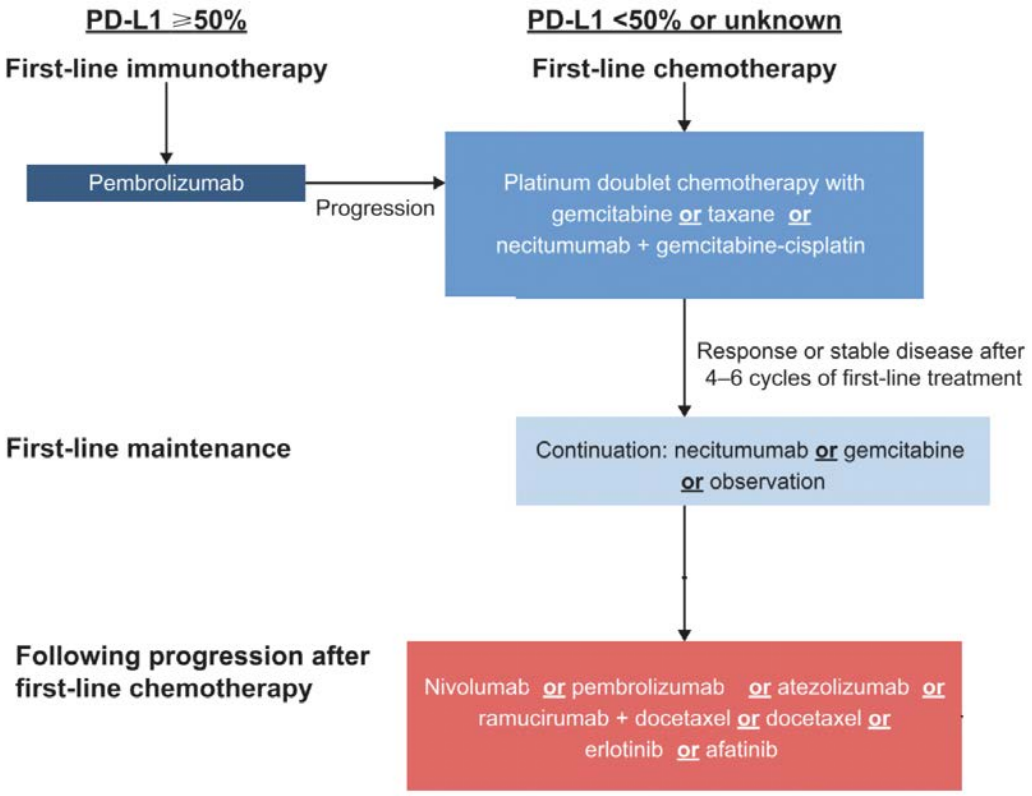

Fig. 1.3. Proposed treatment algorithm for advanced squamous cell lung cancer. Request with permission from [27]. Copyright 2018, Socinski, M.A., Obasaju, C., Gandara, D., Hirsch, F.R., Bonomi, P., Bunn Jr, P.A., Kim, E.S., Langer, C.J., Natale, R.B., Novello, S. and Paz-Ares, L. Current and emergent therapy options for advanced squamous cell lung cancer. Journal of Thoracic Oncology, 13(2), pp.165-183.

The clinical treatment of SCC is described in Fig. 1.3. For the patients with PD–L1 expression in less than 50%, treatment guidelines recommend first-line treatment with platinum-based doublet chemotherapy [27]. Pembrolizumab is the immunotherapeutic approved for use in the first-line, treatment-naive setting, but only for patients with PD–L1 expression in at least 50% of NSCLC cells [27, 28]. Pembrolizumab targets the PD–1/PD–L1 pathway, which has been shown to play a crucial role in mediating immune tolerance in NSCLC and producing durable responses [29]. Although pembrolizumab represents a major breakthrough for first-line treatment of SCC, only about 23% to 30% of the NSCLC population exhibits PD–L1 expression at this high level [30, 31, 32]. Consequently, most patients with SCC remain ineligible for first-line immunotherapy treatment. Thus,

identifying and validating additional predictive biomarkers for the new agents are also needed to enable their optimal use in clinical practice and improve patient outcomes.

2 Molecular Investigation for Personalized Therapy

2.1 Molecular classification systems

Given the high morbidity and mortality rate, the study of GC and SCC represents a critical area of clinical research, and much work is ongoing [33, 34, 35, 36, 37]. In GC, HER2 overexpression, HER2 amplification, MSI–H, and PD–L1^{+} are predictive biomarker [38]. In NSCLC, although a wealth of information on adenocarcinoma is available, only recently has information specifically focusing on SCC become available [39]. This is because SCC often lacks the targetable genetic alterations commonly found in adenocarcinoma, such ad epidermal growth factor receptor (EGFR), anaplastic lymphoma kinase (ALK), and ROS proto-oncogene 1 (ROS1) rearrangements. While SCC may have fewer targetable genetic alterations, it has shown responsiveness to immune checkpoint inhibitors like PD–1 inhibitors [39].

2.1.1 Molecular classifications of GC

Despite substantial histopathological evaluation systems, including tumor node metastasis (TNM) staging, Union for International Cancer Control (UICC) staging and Lauren classification system, have been well accepted as the current diagnostic reference, it is unable to identify actionable molecular targets and observed with a difference in treatment responsiveness of many therapeutic agents, which makes the development of an adjuvant molecular classifier a novel trend [40]. To have better GC stratification for clinical practice, researchers are now focusing on the development of classification systems based on multiple

molecular levels and the identification of predictive biomarkers to select patients for targeted modalities [33, 34, 35, 36].

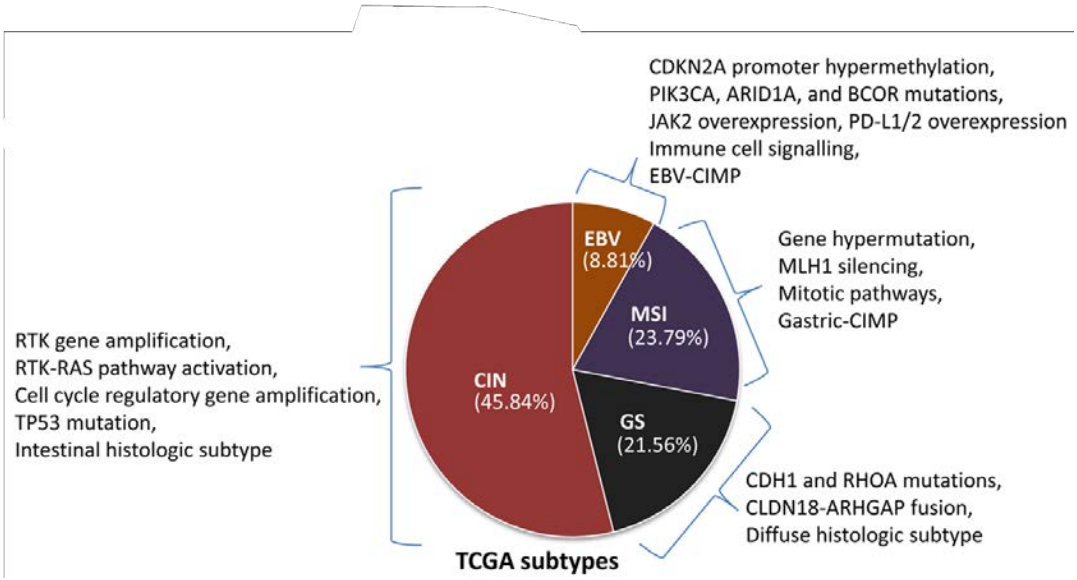

Fig. 2.1. Molecular subtypes established by TCGA. Request with permission from [41] without any changes. Copyright 2016, Chen, T., Xu, X.Y. and Zhou, P.H. Emerging molecular classifications and therapeutic implications for gastric cancer. Chinese journal of cancer, 35(1), pp.1-10.

Several recent studies have provided a molecular subtyping framework, including genomic, transcriptional, and proteomic features, to draw a roadmap for GC drug development and personalized therapy [33, 34]. Among these molecular classification systems, there are two comprehensive, large-scale studies from the Cancer Genome Atlas (TCGA) Research Network in 2014 and the Asian Cancer Research Group (ACRG) Network in 2015. The TCGA study characterized the GC genome and proteome using complex bioinformatics analysis of array-based somatic copy number, whole-exome sequencing, array-based DNA methylation profiling, messenger ribonucleic acid sequencing, microRNA sequencing and reverse-phase protein array data. It identified four genomic subtypes: EBV^{+} tumors (9% of the cases), MSI tumors (22% of the cases), genomically stable tumors (20% of the cases), and tumors with chromosomal instability (50% of the cases)

(Fig. 2.1) [40]. The original TCGA study did not investigate the relationship between tumour subtype and clinical outcome, although subsequent studies have. Among the four subtypes, MSI and EBV^{+} tumours have gained attention, as they are candidates for PD-1/PD-L1-based immune check-point inhibition, which has become a promising therapeutic option in advanced GC [42, 43]. Another large-scale study by the ACRG identified four subtypes which allows the stratification of GC patients into different prognostic and predictive groups, using the gene expression, genome-wide copy number microarray and targeted sequencing: Microsatellite stability/Epithelial–mesenchymal transition (MSS/EMT) subtype represent 15%, MSI subtype represent 23%, Microsatellite stability/Tumor protein p53-active (MSS/TP53-active) subtype represent 26%, and MSS/TP53-inactive subtype represent 36% (Fig. 2.2) [40, 44]. Survival analysis (median follow-up 86.4 months) indicated that the MSI subtype confers the best prognosis, followed by MSS/TP53^{+}, MSS/TP53^{-} and MSS/EMT.

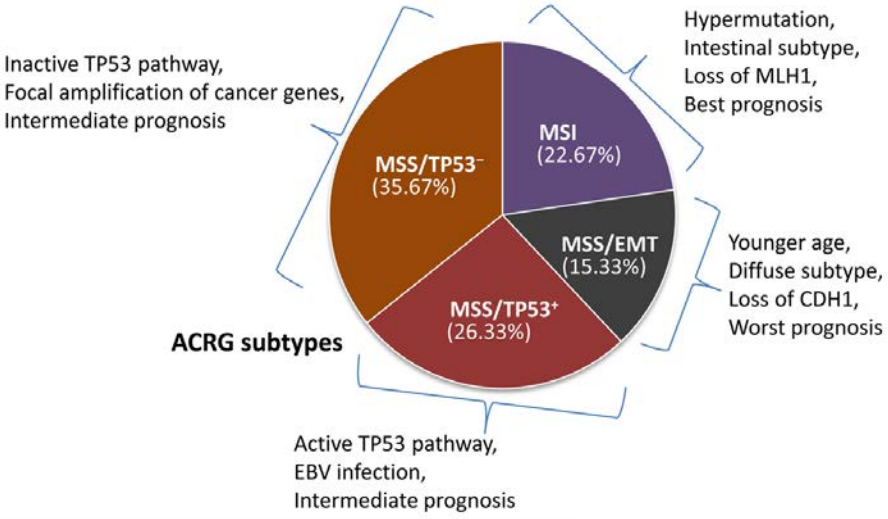

Fig. 2.2. Molecular subtypes established by ACRG. Request with permission from [41] without any changes. Copyright 2016, Chen, T., Xu, X.Y. and Zhou, P.H. Emerging molecular classifications and therapeutic implications for gastric cancer. Chinese journal of cancer, 35(1), pp.1-10.

2.1.2 Molecular classifications of SCC

Lung squamous cell carcinoma (SCC) has seen substantial progress in recent years, with efforts to classify subtypes based on molecular characteristics. Recent comprehensive surveys have defined the genomic and epigenomic alterations driving lung SCC [39, 45, 46]. Before these studies, little was known about SCC genomics. However, these reports using single-platform methods, such as gene expression profiling, SNP arrays, and focused DNA sequencing, showed that the genetic alterations defining lung adenocarcinomas and SCC were distinct, likely explaining the lack of efficacy of targeted therapeutic agents in SCC that had been applied successfully in lung adenocarcinomas.

Genomic and transcriptomic technologies have enabled important insights into the molecular underpinnings of SCC, leading to initial molecular classification strategies [39, 45, 46]. The Cancer Genome Atlas (TCGA) identified recurrent mutations in genes associated with cell cycle and apoptosis, including tumor protein p53 (TP53), cyclin dependent kinase inhibitor 2A (CDKN2A), and retinoblastoma 1 (RB1), antioxidant gene expression, including nuclear factor erythroid-derived 2-like 2 (NFE2L2) and kelch-like ECH-associated protein 1 (KEAP1), phosphatidylinositide 3-kinase signaling, including phosphatidylinositol-4,5-bisphosphate 3-kinase catalytic subunit alpha (PIK3CA) and phosphatase and tensin homolog (PTEN), and epigenetic signaling , including mixed lineage leukemia 2 (MLL2) [39]. Based on these results, studies such as the NCI's Molecular Analysis for Therapy Choice (MATCH) trial are attempting to capitalize on improved molecular knowledge of SCC to employ precision therapeutic medicine targeting phosphoinositide 3-kinases (PI3K), cyclin-dependent kinase 4/6 (CDK4/6), fibroblast growth factor receptor (FGFR), MET proto-oncogene, receptor tyrosine kinase (MET), and PD-L1 [47]. In addition, a recent study did a comprehensive proteogenomic characterization of SCC, which will aid in the understanding of SCC and in subsequently identifying therapeutic vulnerabilities and effective, biomarker-based patient stratification [37].

2.2 Molecular biomarkers and molecular subtypes could benefit personalized therapy

2.2.1 Molecular biomarkers of GC for personalized therapy

Classification of gastric cancer based on molecular subtypes provides an opportunity for personalized therapy. Specific agents recommended for the evaluation of distinct gastric cancer patient populations in clinical trials would be guided by these molecular subtypes. The subtypes-related molecular biomarkers, in particular microsatellite instability (MSI), programmed cell death ligand 1 (PD–L1), human epidermal growth factor receptor 2 (HER2), tumor infiltrating lymphocytes (TILs), and Epstein-Barr virus (EBV), are increasingly driving systemic therapy approaches and allowing for the identification of populations most likely to benefit from immunotherapy and targeted therapy [22, 44, 48, 49].

With the improved understanding of GC, a distinct and well recognized subset of gastric cancer patients infected with EBV has been identified. The EBV^+ subtype highlights the viral aetiology of GC; the TCGA characterization of this subtype suggests potential therapeutic targets for this subgroup of cancers [48]. EBV is a human herpes virus with a prevalence of around 10% of all GC, which is implicated in several malignancies, including gastric adenocarcinoma [50]. EBV^+ GC is associated with a rich $CD8^+$ T-cell infiltrate and increased PD–L1 expression, potentially making it more susceptible to PD–1 blockade. Several clinical studies have described robust responses of EBV-positivity to PD–1/PD–L1 blockade [22, 51, 52]. Recently, Panda et al. found EBV^+ gastric cancer with low mutation burden to be a subset of microsatellite stable (MSS) gastric cancer, which may respond to immune checkpoint therapy [53]. Thus, EBV^+ gastric cancer is now considered a unique molecular subtype of gastric cancer [54] and is

associated with good prognosis in patients. Several clinical studies have correlated MSI status with PD–1/PD-L1 blockade [23]. The high response and benefit of microsatellite instability-high (MSI-H) patient subtypes to PD-L1 blockade therapy is another example of how personalized treatment can benefit specific patient subgroups based on molecular features [20]. Identification of MSI tumours can be accomplished by using mismatch repair protein (MMR, including MLH1, PMS2, MSH2 and MSH6) immunohistochemistry. The concordance rate of MMR expression profiles by immunohistochemistry and microsatellite instability testing has been shown to be as high as 99% for GC [43, 55, 56]. Mismatch repair (MMR) genes are responsible for fixing errors that occur during deoxyribonucleic acid (DNA) replication. Tumors with defects in the mismatch repair system (MMR-deficient [dMMR]) harbor significantly more mutations than tumors with intact MMR machinery (MMR proficient). dMMR tumors are vulnerable to mutations in microsatellites, which are repetitive sequences of nucleotide bases found throughout the genome, leading to high levels of MSI [56]. Across tumor types, patients with dMMR cancers are more likely to respond to PD–1 blockade than those with MMR-proficient cancers. In part, this is because of high levels of neoantigens and PD–L1^{+} T-cell infiltration in dMMR tumors. Interestingly, the tendency to have a lymphocytic infiltrate, which is observed in MSI tumors, likely reflects immune activation of T cells that are associated with MSI [57, 58]. Further, one study extended to four surface markers of TILs, including PD–1, cluster of differentiation 8 (CD8), cluster of differentiation 4 (CD4) and forkhead box P3 (FOXP3) in patients with GC [49]. Thus, identification of these multiple molecular markers, together with their molecular classifications, opens novel perspectives to stratify patients who may benefit from immune and targeted therapies.

2.2.2 Molecular biomarkers of SCC for personalized therapy

The prognosis of SCC is not desirable due to the absence of reliable tumor biomarkers that can enhance the development of targeted therapies [39]. Consequently, there is an ongoing pursuit for new SCC biomarkers. Additionally, investigating additional predictive biomarkers to identify patients with SCC who are most likely to benefit from novel agents is of great interest.

The immune checkpoint pathway has been shown to play a crucial role in mediating immune tolerance in NSCLC, with antibody agents that block this pathway, such as agents against PD–1/PD–L1, producing durable responses [29, 59], and where expression of checkpoint markers correlates with treatment efficacy [31]. Some studies address the need by combining established molecular subtypes with multiple immunological markers, such as PD–1, PD–L1, CD3 and CD8, which can increase the predictive robustness and guide the implementation of NSCLC precision medicine [45]. Alternative markers for checkpoint blockade response, including T-cell and other immunological markers, are also being considered [60, 61, 62].

The Lung Master Protocol in SCC (Lung-MAP) project addresses the need by using a multi-substudy master protocol to facilitate the approval of targeted therapy-predictive biomarker combinations. This project consists of multiple ongoing phase II/III trials, capable of independently opening and closing without interfering with other substudies. Patients eligible for second-line therapy for SCC undergo genomic screening of their cancers using a next-generation sequencing (NGS) platform [63, 64]. Lung-MAP optimizes patient enrollment efficiency by employing a master protocol to screen patients and assigning each patient to a substudy based on biomarker identification. The Lung-MAP study is designed to adapt as new targeted agents become available for testing, and the results of this study are expected to have significant implications for the management of advanced SCC. However, targeting potentially

druggable genetic events in three primary pathways, which includes FGFR1, PI3K, or G1/S checkpoint genes such as CDKN2A, has largely failed in the Lung-MAP project [63, 64].

2.3 Metabolomics for predicting therapy response

As mentioned before, many important clinical advances in GC, SCC and other cancers have been driven by genomic profiling of bulk tumor material. The stratification of patients into appropriate treatment groups, and the prediction of response to treatment are all highly crucial for maximising survival rates of cancer patients [65]. In addition to the alterations in genomic or proteomic pathways, promising discoveries have been made with metabolomic studies. Thus we anticipate that the same will prove true of bulk metabolomic characterization. The metabolite profile may be considered as a factor in assessing a patient's initial response to treatment and selecting drug regimens to effectively increase tumor response rate in cancer patients [66]. Recently, the metabolomic approaches have been adopted in order to better understand the pathology and to search for novel diagnostic and therapeutic targets through the characterization of the metabolomic profile of cancer patients treated with therapy in GC and SCC [67, 68].

Metabolism reprogramming is a hallmark of cancer. Metabolomics provides in-depth information on metabolic perturbation between healthy and neoplastic states in the stomach and lung, and further help discovery disease-specific biomarkers [69]. In order to meet the increased energy demands necessary for cell proliferation, cancer cells exhibit a dysregulated metabolism that involves glucose, glutamine, fatty acids, amino acids, various nutrients and metabolites. This dysregulated metabolism encompasses processes such as glycolysis, suppressed aerobic respiration, and de novo fatty acid synthesis [69, 70, 71, 72]. Recent extensive investigations into the molecular changes

induced by rewired metabolism have resulted in the development of targeted therapies. [73, 74]. Indeed, a previous study has identified several metabolite-dependent subtypes among different cancer types [75]. Thus, unique metabolic characteristics in cancers may have potential as targets for cancer therapy.

Extensive research conducted in the field of GC and SCC has resulted in significant advances through targeted investigations of the mechanisms underlying altered metabolism and specific metabolic pathways. However, a comprehensive exploration of metabolite-level classification for therapy response prediction in GC and SCC is lacking. Therefore, our study aimed to assess the potential of metabolite profiles to stratify cancer patients and examine their association with clinical molecular features in GC and SCC individually.

3 MALDI-IMS Technology and Clustering Methods

Due to the interconnected nature of the studies within this dissertation, my initial emphasis will be on showcasing matrix-assisted laser desorption/ionization imaging mass spectrometry (MALDI–IMS) and introducing the developed immunophenotype-guided spatial metabolomics approach of tissue regions based on MALDI–IMS. Additionally, I will delve into the cutting-edge clustering techniques which are applied in my PhD thesis, including K–means clustering and hierarchical clustering analysis.

3.0.1 MALDI–IMS

High mass resolution MALDI–IMS is a technique that combines mass spectrometry with conventional histology, resulting in a new quality of data in biochemical research and diagnostics, which has emerged as an influential analytical tool in clinical research, such as being used to discover new predictive and prognostic markers in cancer research [76]. Apart from detecting new biomarkers, MALDI–IMS has been used to increase understanding of the patient response to therapy. A MALDI–IMS study of GC tumours highlights the possibility that MALDI–IMS would expand the understanding of patient response beyond histological and morphological appearance [77].

MALDI–IMS remains the most widely applied IMS owing to its capability to analyse a wide range of analyte classes [78]. The ability to simultaneously detect thousands of molecules within a single sample offers many advantages over traditional techniques that require labelling, such as immunoassays [79]. In addition, various mass spectrometry technologies allow for the detection of molecules which may not be easily labelled, for example, lipids, nucleotides, and other low molecular weight compounds [80].

In addition to its capability to analyze a wide range of analyte classes, MALDI–IMS technique directly enables the detection and localization of thousands of different molecules, including proteins, peptides, lipids and drugs in tissue sections [80]. The principle and application of MALDI—IMS is shown in Figure 3.1. A tissue or tissue microarray (TMA) block is cut into slices and placed onto a conductive glass side. The tissue section could be either from fresh frozen (FF) or archived material like formalin-fixed, paraffin-embedded (FFPE) tissues. Then, the section has to be coated with the matrix, including negative matrix and positive matrix. This is a crucial step because it determines the maximum spatial resolution, sensitivity, and reproducibility of a MALDI–IMS experiment. Next, the coated glass slide is introduced into the mass spectrometer and mass spectra are acquired in a raster process. Each individual measurement spot has an associated mass spectrum that will later constitute a pixel in the resulting MALDI image. The pixel size is technically limited by both the laser focus diameter and the average matrix droplet size. The spatial resolution typically ranges in the range of tens to hundreds of micrometers [80].

The MALDI images are subsequently correlated to histology, which allows the extraction of spectra generated from 'regions of interest', for example, the spectra from tumor or stroma tissue [81]. Tumor and stroma are distinct biological entities, and the same metabolites contribute differentially to the estimation of prognosis and treatment relevance in both tumor cells and the stroma [68, 82]. Assigning tumor tissues to specific molecular subtypes can be influenced by molecular expression profiles, giving rise to interpretive challenges. Subsequently, the extracted region-specific mass spectra can undergo additional bioinformatics processing to identify patterns, such as clustering similar spectra. Those advantages greatly facilitate the application of MALDI-IMS for tumor subtyping [81, 83, 84].

Recently, a new computational multimodal immunophenotype-guided in situ spatial metabolomics workflow, Spatial Correlation Image Analysis (SPACiAL), which designed to combine molecular imaging data with multiplex immunohistochemistry, facilitates the automated and objective

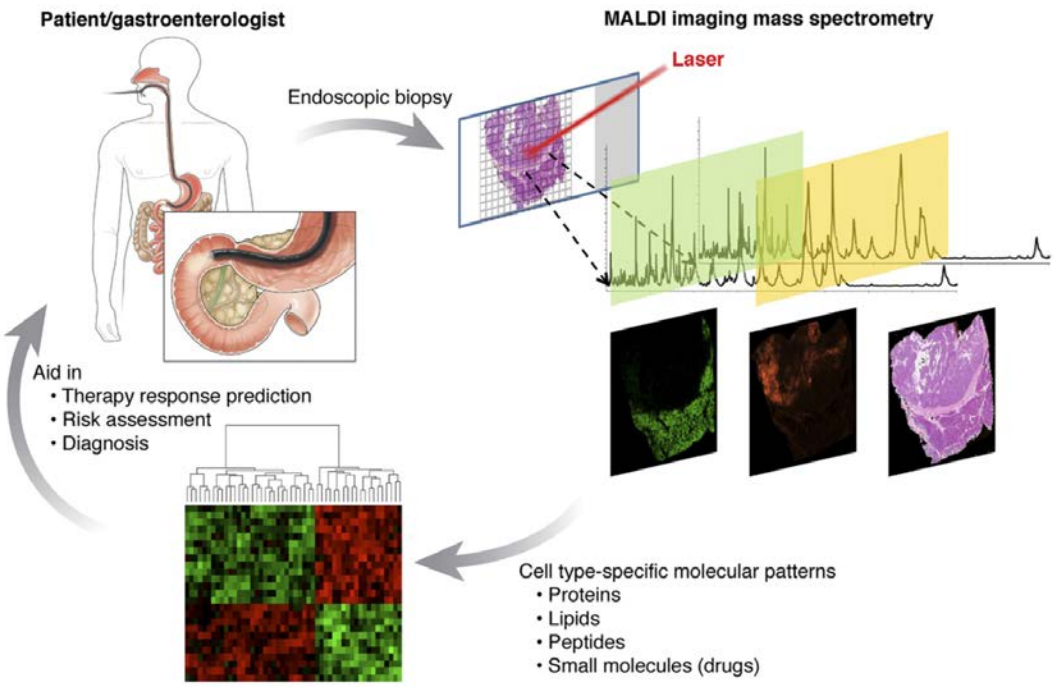

Fig. 3.1. The principle and application of MALDI–IMS. MALDI imaging is able to analyze even the smallest tissue samples from patients, such as endoscopic biopsies, which are readily collectable in a gastroenterological setting. The subsequent histology-directed and unlabeled analysis allows to extract spatially resolved, cell type-specific molecular signatures from a wide variety of molecule classes and to correlate them with clinical endpoints. These patterns may, therefore, directly support the clinician in relevant questions such as in tissue diagnostics, therapy response prediction, or disease outcome prediction. Request with permission from [80] without any changes. Copyright 2012, Balluff, B., Rauser, S., Ebert, M.P., Siveke, J.T., Höfler, H. and Walch, A. Direct molecular tissue analysis by MALDI imaging mass spectrometry in the field of gastrointestinal disease. Gastroenterology, 143(3), pp.544-549.

identification of histological and functional features in intact tissue sections and the comprehensive analyses of metabolic constitutions of tumor and the stroma regions from large-scale clinical cohort studies [85]. The workflow of immunophenotype-guided annotation of tissue regions for multi-omics analyses (SPACiAL pipeline) is shown in Fig. 3.2. This thesis will apply the immunophenotype-guided in situ spatial metabolomics workflow and focus on the separate extraction of tumor and stroma-based metabolite signatures in the patient stratification approach for both GC and SCC studies.

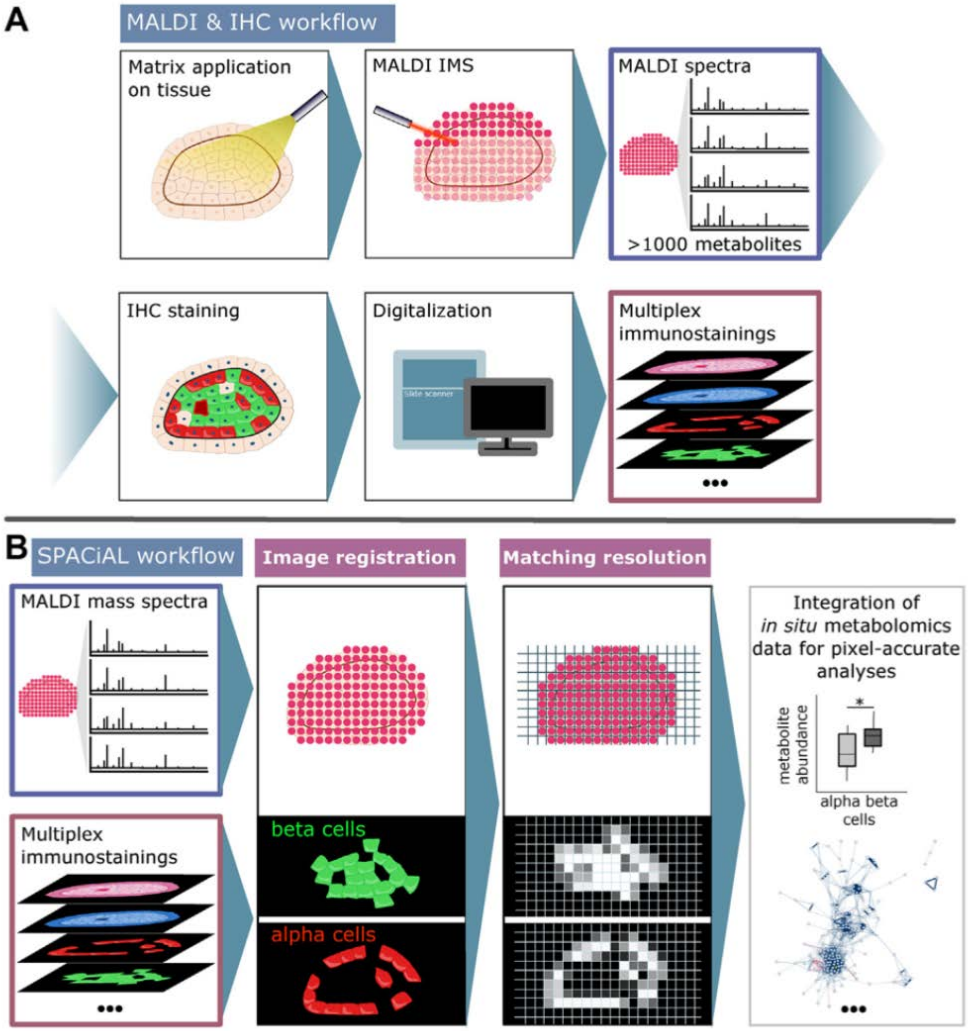

Fig. 3.2. Immunophenotype-guided in situ metabolomics workflow is exemplified using the islet of Langerhans. (A) MALDI and IHC workflow starting with matrix application on tissue sections, MALDI imaging and data processing which includes peak picking and annotation. Then, the matrix is removed for subsequent multiplex immunofluorescence staining. (B) The SPACiAL pipeline integrates molecular MALDI data and immunohistochemical data. The IHC images need to be co-registered to the coordinates of the mass spectra per pixel. Color values per pixel are used to define regions or to conduct pixel-precise metabolic analyses. Request with permission from [85] without any changes. Copyright 2020, Prade, V.M., Kunzke, T., Feuchtinger, A., Rohm, M., Luber, B., Lordick, F., Buck, A. and Walch, A. De novo discovery of metabolic heterogeneity with immunophenotype-guided imaging mass spectrometry. Molecular Metabolism, 36, p.100953.

3.0.2 Clustering methods

Clustering methods of ion images was proposed to investigate spatial similarities between ion images [86], and its usefulness for supervised analysis was recently demonstrated [87]. K–means is one of the commonly used clustering algorithms used in spatial metabolomics [88]. K–means analysis is a widely employed technique for segmenting and grouping spatially resolved metabolomic data into distinct clusters based on the similarities of metabolite profiles across different regions of interest, such as tumor and stroma-specific regions [89]. Hierarchical cluster analysis is another vital method in spatial metabolomics, which is one of the common used tree-based clustering algorithms [90]. Unlike K–means, hierarchical clustering doesn't require specifying the number of clusters beforehand. The advantage of this method is that it does not require prior knowledge about the number of expected clusters as it finds a whole cluster hierarchy [90]. Both K–means analysis and hierarchical cluster analysis contribute significantly to spatial metabolomics by revealing spatially dependent metabolic variations, distinct biochemical zones, and potential correlations between metabolites and spatial locations [89, 90]. The hierarchical clustering and K–means clustering of the tumour tissues were both applied in my PhD studies, which results in identifying molecular subtypes characterized by the abundance of identified metabolites in tumor and stroma-specific regions, making possible the formulation of hypotheses to account for their significance and the underlying biological heterogeneity between tumor and stroma sub-regions.

Aim of Thesis

4

This dissertation had the goal to investigate the association between metabolomics and the response to clinical therapy. To address this objective, a novel classification scheme was developed to stratify patients with gastric cancer (GC) and lung squamous cell carcinoma (SCC) based on their metabolic profiles. This classification scheme considered clinicopathological characteristics, molecular feature correlation, and importantly, assigned clinical treatment relevance to different patient subtypes. High mass resolution MALDI-IMS combined with unsupervised clustering analyses were utilized to establish metabolic subtypes using tumor- and stroma-specific tissue regions in GC and SCC patients separately. This approach enabled the monitoring and visualization of metabolites to understand their collective function and impact on therapy response. The validity of the results obtained from the GC study was confirmed in an independent validation cohort, demonstrating the predictive ability of metabolic subtypes for trastuzumab therapy. Similarly, the findings from the SCC study were also supported by results obtained from an independent cohort, indicating an association between metabolic subtypes and chemotherapy response. The use of metabolic profiling provides an alternative strategy for patient stratification in these two cancer types. These findings have implications for the development of personalized therapeutic approaches in clinical settings for patients with GC and SCC.

Part IV

Published Results

This chapter provides the first author publications that comprise my PhD work and makes this thesis eligible for credit as a cumulative dissertation. The first publication establishes three tumor-specific and stroma-specfic metabolic subtypes in a large series of 362 patients with GC. The results were validated in an independent validation cohort to demonstrate the ability of metabolic subtypes for trastuzumab therapy prediction. The second publication establishes four tumor-specific and stroma-specfic metabolic subtypes in a large series of 330 patients with SCC. The results were also confirmed in an independent cohort that metabolic subtypes had association with chemotherapy response. Taken together, our results suggest that distinct subtypes of GC and SCC as defined using metabolomics may show better responses to specific targeted therapies. Before each embedded publication, a short introduction resuming the respective work is given, and my individual contributions are mentioned.

Paper 1

5

Spatial Metabolomics Identifies Distinct Tumor-Specific Subtypes in Gastric Cancer Patients

The publication entitled "Spatial Metabolomics Identifies Distinct Tumor-Specific Subtypes in Gastric Cancer Patients" [1] represents the starting of my work to identify metabolic subtypes for therapy response prediction. We were interested in the idea of using spatial metabolomics to stratify patients and test the therapy response prediction ability of the established tumor-specific metabolic subtypes.

In this paper, I processed the data using R programming and calculated all statistics included in this manuscript. In addition, I interpreted the data, wrote the original draft of the manuscript, and prepared all figures. After peer-review, I was responsible for editing the manuscript and performing the new figures according to reviewers' suggestions. In addition, I co-designed this study together with Axel Walch and Na Sun.

Spatial Metabolomics Identifies Distinct Tumor-Specific Subtypes in Gastric Cancer Patients

Jun Wang[1], Thomas Kunzke[1], Verena M. Prade[1], Jian Shen[1], Achim Buck[1], Annette Feuchtinger[1], Ivonne Haffner[2], Birgit Luber[3], Drolaiz H.W. Liu[4,5], Rupert Langer[5], Florian Lordick[2,6], Na Sun[1], and Axel Walch[1]

ABSTRACT

Purpose: Current systems of gastric cancer molecular classification include genomic, molecular, and morphological features. Gastric cancer classification based on tissue metabolomics remains lacking. This study aimed to define metabolically distinct gastric cancer subtypes and identify their clinicopathological and molecular characteristics.

Experimental Design: Spatial metabolomics by high mass resolution imaging mass spectrometry was performed in 362 patients with gastric cancer. K−means clustering was used to define tumor and stroma-related subtypes based on tissue metabolites. The identified subtypes were linked with clinicopathological characteristics, molecular features, and metabolic signatures. Responses to trastuzumab treatment were investigated across the subtypes by introducing an independent patient cohort with HER2-positive gastric cancer from a multicenter observational study.

Results: Three tumor- and three stroma-specific subtypes with distinct tissue metabolite patterns were identified. Tumor-specific subtype T1($HER2^+MIB^+CD3^+$) positively correlated with HER2, MIB1, DEFA-1, CD3, CD8, FOXP3, but negatively correlated with MMR. Tumor-specific subtype T2($HER2^-MIB^-CD3^-$) negatively correlated with HER2, MIB1, CD3, FOXP3, but positively correlated with MMR. Tumor-specific subtype T3($pEGFR^+$) positively correlated with pEGFR. Patients with tumor subtype T1($HER2^+MIB^+CD3^+$) had elevated nucleotide levels, enhanced DNA metabolism, and a better prognosis than T2 ($HER2^-MIB^-CD3^-$) and T3($pEGFR^+$). An independent validation cohort confirmed that the T1 subtype benefited from trastuzumab therapy. Stroma-specific subtypes had no association with clinicopathological characteristics, however, linked to distinct metabolic pathways and molecular features.

Conclusions: Patient subtypes derived by tissue-based spatial metabolomics are a valuable addition to existing gastric cancer molecular classification systems. Metabolic differences between the subtypes and their associations with molecular features could provide a valuable tool to aid in selecting specific treatment approaches.

Introduction

Gastric cancer is a leading cause of cancer-related deaths with the fourth highest mortality rate worldwide (1). Treatment responsiveness of gastric cancer differs markedly among current therapeutic regimens (2). To improve gastric cancer stratification for clinical practice, research focuses on developing classification systems based on multiple molecular levels, such as genome, transcriptome, and proteome, to identify novel predictive biomarkers for personalized gastric cancer treatment (3, 4).

Several recent studies have provided a molecular subtyping framework, including morphological, genomic, and proteomic features, to draw a roadmap for gastric cancer drug development and personalized therapy (5, 6). Two comprehensive, large-scale studies from the Cancer Genome Atlas (TCGA) Research Network in 2014 and the Asian Cancer Research Group (ACRG) Network in 2015 are among these molecular classification systems. TCGA characterized the gastric cancer genome and proteome using complex bioinformatics analysis of array-based somatic copy number, whole-exome sequencing, array-based DNA methylation profiling, messenger ribonucleic acid sequencing, microRNA sequencing and reverse-phase protein array data. The TCGA study identified four genomic subtypes: Epstein–Barr virus–positive (EBV^+) tumors, microsatellite instable (MSI) tumors, genomically stable tumors, and tumors with chromosomal instability. Another large-scale study by the ACRG established four molecular subtypes using the gene expression, genome-wide copy-number microarray and targeted sequencing: MSS/EMT subtype, MSI subtype, MSS/TP53-active subtype, and MSS/TP53-inactive subtype (7, 8).

Gastric cancer could be considered potentially immunogenic. Several other studies characterized gastric cancer with immunological features (9, 10). Li and colleagues (9) identified three subtypes using a newly proposed pathway-based gastric cancer classification method: Immune-derived subtype (ImD), stroma-enriched subtype, and immune-enriched subtype and Zeng and colleagues (10) defined three gastric cancer subtypes based on patterns of immune cell infiltration into the tumor microenvironment.

The development of practical classification systems to predict treatment responses in patients with gastric cancer would be a valuable

[1]Research Unit Analytical Pathology, Helmholtz Zentrum München—German Research Center for Environmental Health, Neuherberg, Germany. [2]University Cancer Center Leipzig (UCCL), Leipzig University Medical Center, Leipzig, Germany. [3]Technische Universität München, Fakultät für Medizin, Klinikum rechts der Isar, Institut für Allgemeine Pathologie und Pathologische Anatomie, München, Germany. [4]Department of Pathology, GROW School for Oncology and Reproduction, Maastricht University Medical Center, Maastricht, the Netherlands. [5]Institute of Clinical Pathology and Molecular Pathology, Kepler University Hospital and Johannes Kepler University, Linz, Austria. [6]Department of Oncology, Gastroenterology, Hepatology, Pulmonology and Infectious Diseases, Leipzig University Medical Center, Leipzig, Germany.

Note: Supplementary data for this article are available at Clinical Cancer Research Online (http://clincancerres.aacrjournals.org/).

Corresponding Authors: Axel Walch, Ingolstädter Landstraße 1, Neuherberg, 85764, Germany. Phone: 49 89 3187-3349; E-mail: axel.walch@helmholtz-muenchen.de; and Na Sun, na.sun@helmholtz-muenchen.de

Clin Cancer Res 2022;28:2865–77

doi: 10.1158/1078-0432.CCR-21-4383

Translational Relevance

In recent years, several gastric cancer molecular classification systems have been established. However, gastric cancer classification based on metabolomics is still lacking. Here, we developed a novel tumor- and stroma-specific classification model to stratify a large series of patients with gastric cancer by applying tissue-based spatial metabolomics combined with K−means clustering analysis. Using this model, all of tumor- and stroma-specific subtypes were strongly associated with molecular features and distinctive metabolism pathways. Application of an independent validation cohort revealed that two tumor-specific subtypes were predictive of trastuzumab response. This is the first study to stratify patients with gastric cancer based on tissue metabolomics. Metabolic differences of the patient subtypes and their associations with molecular features could improve the personalization of therapeutic regimens.

addition to clinic settings. For example, trastuzumab represents the first option for approximately 20% of patients with HER2 overexpression (11). The MSS/TP53-inactive molecular subtype established by the ACRG study has been reported to potentially benefit from anti–HER2-directed therapy (8). The immunotherapeutic antibody, pembrolizumab, selectively binds to programmed cell death protein 1 (PD-1; ref. 12) and several clinical studies have correlated EBV infection and MSI status with PD1/PD-L1 blockade (13, 14). The high response and benefit of microsatellite instability-high (MSI-H) patient subtypes to PD-L1 blockade therapy is another example of how personalized treatment can benefit specific patient subgroups based on molecular features (15). Interestingly, the tendency to have a lymphocytic infiltrate, which is observed in MSI tumors, likely reflects immune activation of T cells that are associated with MSI (16, 17). Furthermore, one study extended to four surface markers of tumor-infiltrating lymphocytes (TIL), including cluster of differentiation 8 (CD8), cluster of differentiation 4 (CD4), PD-1, and forkhead box P3 (FOXP3) in patients with gastric cancer (18). Thus, identification of these multiple molecular markers, together with their molecular classifications, opens novel perspectives to stratify patients who may benefit from immune and targeted therapies.

Metabolism reprogramming is a hallmark of cancer. To meet the growing energy demands required for cell proliferation, gastric cancer cells have a unique metabolism comprising glucose, glutamine, fatty acids, amino acids, and many other nutrients and metabolites, such as glycolysis, repressed aerobic respiration, and *de novo* fatty acid synthesis (19–21). The recent deep exploration of molecular changes induced by rewired metabolism has led to the development of targeted therapies (22, 23). Indeed, a previous study identified several metabolite-dependent subtypes among 33 cancer types (24). Metabolite-level classification has not been comprehensively investigated in gastric cancer; hence, we assessed the ability of metabolite profiles to stratify patients with gastric cancer and explored the association with clinical molecular features.

High mass resolution Matrix-assisted laser desorption-ionization (MALDI) imaging mass spectrometry (IMS) directly enables detection and localization of thousands of different molecules within a routinely preserved tissue section, and thus greatly facilitates the application of MALDI-IMS for tumor subtyping (25–27). Recently, a new computational multimodal workflow, Spatial Correlation Image Analysis (SPACiAL), which designed to combine molecular imaging data with multiplex IHC, was developed for an objective analysis of high-throughput data from large-scale clinical cohort studies (28).

This study aimed to derive a novel classification scheme to stratify patients with gastric cancer by their metabolic profiles, encompass clinicopathological characteristics and molecular feature correlation, and more importantly, assign clinical treatment relevance to patient subtypes. High mass resolution MALDI-IMS combined with K−means clustering analysis was applied to establish metabolic classification based on tumor- and stroma-specific tissue regions in patients with gastric cancer. The results were validated in an independent validation cohort to demonstrate the predictive metabolic constitution of the subtypes for the trastuzumab therapy. The metabolic constitution in gastric cancer provided an alternative for patient stratification.

Materials and Methods

Collection of tissue samples and clinical characteristics data

Primary resected gastric cancer samples were obtained from 362 patients who had not received prior chemotherapy, trastuzumab therapy, or immunotherapy. Tissue microarrays (TMA) were analyzed in triplicates (three tissue cores from each patient; **Table 1**). All samples used in this study were obtained from patients who underwent gastrectomy between 1995 and 2005 at the Surgery Department at the Technical University Munich. This study was conducted in accordance with the Declaration of Helsinki, and approved by the local Ethics Committee of the Faculty of Medicine at Technical University Munich with informed written consent from all patients. **Table 1** describes the clinical characteristics of the gastric cancer participants. Pathological TNM-staging was performed according to the Union Internationale Contre le Cancer (UICC) system 7th edition (29) and histopathological grading was classified in accordance to the World Health Organization (30). Parameter variables were categorized as follows: Sex into female versus male; tumor node metastasis classification, pT1–pT4 for primary tumor, pN0–pN3 for primary lymph nodes, M0 and M1 category for distant metastasis; UICC classification into stage I–stage IV; resection state into R0–R2; Lauren classification into diffuse, intestinal, and mixed type; and primary tumor grading into scores of G1–G3.

Patients and tissue samples for the independent validation cohort (VARIANZ cohort)

A previous publication established a metabolomic classifier to predict trastuzumab therapy response in patients with HER2-positive advanced gastric cancer (VARIANZ cohort; ref. 31). The VARIANZ cohort data were integrated here as a validation study for predicting trastuzumab therapy response of the metabolic subtypes. The VARIANZ cohort ($n = 42$) was divided into therapy-resistant ($n = 17$) and therapy-sensitive ($n = 25$) patients (31). This study was conducted in accordance with the Declaration of Helsinki, and approved by the Ethics Committee of the Leipzig University Medical Faculty with informed written consent from all patients (32). The patients were centrally reviewed, and their HER2 status was fully characterized by the application of IHC staining and ISH. All patients included in this analysis belonged to UICC stage IV, were HER2-positive and underwent trastuzumab therapy and chemotherapy (platin-fluoropyrimidine; Supplementary Table S1).

Sample acquisition and preparation

Sample preparation was performed as previously described (26). Briefly, formalin-fixed paraffin-embedded sections (3 μm, Microm,

Table 1. Summary of patient characteristics.

Characteristic	Numbers
Number of patients	362
Age, y	
Median	68
Range	17–100
Sex	
Male	219
Female	123
NA	20
Survival time (mo)	
Median	20
Range	0–344
NA	108
Lauren classification	
Intestinal	178
Diffuse	146
Mixed	15
NA	23
Primary tumor extension	
pT1	40
pT2	140
pT3	134
pT4	28
NA	20
Regional lymph nodes	
pN0	93
pN1	100
pN2	107
pN3	35
NA	27
Distant metastasis	
M0	193
M1	82
NA	87
UICC stage	
Stage I	87
Stage II	71
Stage III	77
Stage IV	105
NA	22
Primary resection state	
R0	203
R1	78
R2	29
NA	52
Grade	
G1	2
G2	48
G3	285
NA	27

Note: Distant metastasis was defined as metastasis in any lymph node other than regional. Samples with insufficient data to make a conclusion were set to "NA."

HM340E, Thermo Fisher Scientific) were mounted onto indium–tin–oxide-coated glass slides (Bruker Daltonik) pretreated with 1:1 poly-L-lysine (Sigma-Aldrich) and 0.1% Nonidet P-40 (Sigma). Deparaffinized tissue sections were spray-coated with 10 mg/mL of 9-aminoacridine hydrochloride monohydrate matrix (Sigma-Aldrich) in 70% methanol using a SunCollect sprayer (Sunchrom).

High mass resolution MALDI-Fourier transforms ion cyclotron resonance IMS

High mass resolution MALDI-IMS was conducted as previously described (26). MALDI-IMS was performed in negative ion mode using a Bruker Solarix 7.0 T FT-ICR (Fourier transforms ion cyclotron resonance) MS (Bruker Daltonik) equipped with a dual ESI-MALDI source and a SmartBeam-II Nd: YAG (355 nm) laser. Data acquisition parameters were specified in ftmsControl software 2.2 and flexImaging (v. 5.0; Bruker Daltonik). Mass spectra were acquired covering m/z 50–1100. The laser operated at a frequency of 1000 Hz, using 100 laser shots per pixel, and with a pixel resolution of 60 μm. Non-tissue regions were measured as a background control to differentiate between tissue and matrix-associated peaks. L-Arginine was used for external calibration in the ESI mode. After MALDI-IMS analysis, the matrix was removed with 70% ethanol, and the samples were stained with hematoxylin and eosin (H&E), coverslipped, and scanned with an AxioScan.Z1 digital slide scanner (Zeiss) equipped with a ×20 magnification objective.

Multiplex fluorescent IHC staining

TMAs were analyzed by double staining for pan-cytokeratin [monoclonal mouse pan-cytokeratin plus (AE1/AE3þ8/18; 1:75), catalog no. CM162, Biocare Medical, RRID: AB_10582491] and vimentin [recombinant anti-vimentin antibody (EPR3776; 1:500), catalog no. ab92547, Abcam, RRID: AB_10562134]. Signal was detected using fluorescence-labeled secondary antibodies [goat anti-rabbit IgG (H + L)-cross-adsorbed secondary antibody-DyLight 633 (1:200), catalog no. 35563; and goat anti-mouse IgG (H + L)-cross-adsorbed secondary antibody-Alexa Fluor 750 (1:100), catalog no. A-21037, RRID: AB_2535708, both Thermo Fisher Scientific]. Nuclei were identified with Hoechst 33342 in all stains. Fluorescence stains were scanned with an AxioScan.Z1 digital slide scanner (Zeiss) equipped with a ×20 magnification objective and visualized with ZEN 2.3 blue edition software (Zeiss).

IHC and ISH

Protein expression of molecular features, including HER2, DNA mismatch repair (MMR), phospho-EGFR (pEGFR), E3 ubiquitin-protein ligase (MIB1), cluster of differentiation 3 (CD3), CD8, FOXP3, and human alpha defensin 1 (DEFA-1), *HER2* ISH status and Epstein–Barr virus (EBV) positivity, were performed as previously described (33, 34). In short, IHC with anti-HER2/neu (A0785; 1:300, DAKO), anti-pEGFR (36-9700; 1:100, Invitrogen, RRID: AB_2533287), anti-CD3 (RM-9107-S; 1:200; Thermo Fisher Scientific, RRID: AB_149922), anti-CD8 (ab178089; 1:50, Abcam, RRID: AB_2756374), anti–DEFA-1 (T1034; 1:400, Dioanova), anti-FOXP3 (12653; 1:100, Cell Signaling Technology), and anti-MIB1 (M7240; 1:100, DAKO, RRID: AB_2142367) were performed on consecutive 3-μm sections using an automated stainer (Ventana DISCOVERY XT System, Ventana Medical Systems, Inc.) according to the manufacturer's instructions. Antibodies mutL homolog 1 (MLH1; clone ES05, Agilent Dako, RRID: AB_2631352) and mutS homolog 2 (MSH2; clone FE11, Biocare Medical) of the DNA MMR proteins were stained on consecutive 3-μm sections (BenchMark ULTRA System). An assay with fluorescence-labeled locus-specific DNA probes for *HER2* and chromosome-17 (CEP17) centromeric α-satellite was hybridized onto TMAs for ISH analysis. The TMAs were incubated with an EBV-encoded small RNA probe (DAKO Cytomations) for EBV-encoded small RNA ISH analysis.

Immunophenotype-guided IMS and data processing

In situ tissue cores were processed using the SPACiAL pipeline for immunophenotype-guided MALDI-IMS analysis, which includes a series of MALDI data and image-processing steps to automatically annotate tumor and stroma regions as previously described (28). First, H&E staining was removed by incubating tissue sections with 70% ethanol for 5 minutes followed by IHC. Tumor and stroma regions were distinguished by multiplex fluorescent IHC staining with epithelial cell–specific cytokeratin antibody [(AE1/AE3þ8/18; 1:75), catalog no. CM162, Biocare Medical, US, RRID: AB_10582491] and stroma cell–specific vimentin antibody [recombinant anti-vimentin antibody (EPR3776; 1:500), catalog no. ab92547, Abcam, UK, RRID: AB_10562134] on the same tissue section. Immunostaining images were then co-registered with the MALDI measurement region to define 347 tumor region samples and 339 stroma region samples by SPACiAL workflow. Specification of tumor and stroma regions and exportation of each patient's spectral data were finally managed using the SPACiAL pipeline (28).

Consensus clustering

Consensus clustering was conducted using the "ConcensusClusterPlus" package in R to explore gastric cancer subtypes based on the cancer patient sample matrix. The consensus matrix was used to check cluster co-occurrence, find intrinsic groupings over variation in different numbers of clusters, and use K−means on the distance matrix. The matrix is arranged so that samples belonging to the same cluster are adjacent to each other.

Pathway enrichment analysis

Metabolites were annotated with the Kyoto Encyclopedia of Genes and Genomes (KEGG, RRID: SCR_012773; www.genome.jp/kegg/), allowing M−H, M−H_2O, M+K−2H, M+Na−2H, and M+Cl as negative adducts with a mass tolerance of 4 ppm. Significance analysis of tumor- or stroma-specific subtypes was performed by a Kruskal–Wallis test with subsequent Benjamini–Hochberg correction ($P < 0.05$). The enriched metabolites in each subtype were identified by comparing with every other subtype using the Dunn's test with a cutoff P value of <0.05 and a fold change of >1 based on the significant metabolites. The feature matrix of enriched metabolites was then normalized by the 0–1 normalization method, which scaled the minimum of each row to zero and maximum to one as visualized by the abundance heatmap. Pathway enrichment analysis was performed via the KEGG database (RRID: SCR_012773) using the MetaboAnalyst online tool (RRID: SCR_015539; www.metaboanalyst.ca; Fisher's exact test, $q < 0.05$ for FDR correction).

Statistical analysis

Correlations were calculated using pairwise Spearman's rank-order correlation and P values were adjusted with Benjamini–Hochberg correction. The clinicopathological characteristics differences among tumor- and stroma-specific subtypes was evaluated by the χ^2 test or Fisher's exact test, and P values in the pairwise comparison between subtypes were adjusted with FDR correction. To determine the intensity differences of representative metabolites, the Kruskal–Wallis and *post hoc* Dunn's multiple comparison tests were used in conjunction with Benjamini–Hochberg correction. The Mann–Whitney U test was used for testing intensity differences in the validation cohort. Further statistical differences and comparison in patient survival were determined using the Kaplan–Meier curve and the Log–Rank test. Multivariate survival analysis was performed using Cox proportional hazard regression model. All statistical tests were conducted using R (R version 4.0.0, RRID: SCR_001905).

Data availability

The data generated in this study are available upon reasonable request from the corresponding author.

Results

Identification of gastric cancer patient subtype based on metabolite profiling

The study workflow is shown in **Fig. 1**. From a total of 362 patient samples, 347 could be automatically annotated with tumor regions and 339 could be annotated with stroma regions using immuno-guided spatial metabolomics. The annotatable patient cases form the basis for our calculations. To determine whether tumor and stroma regions had significantly different metabolite compositions, we performed a tumor and stroma region-specific unsupervised K−means clustering analysis. A total of 9,278 ion features were identified and selected as the basis of K−means clustering.

Consensus matrix heatmaps and cumulative distribution function (CDF) plots were drawn to determine the optimal number of K clusters. Optimal cluster numbers for tumor-specific and stroma-specific data were both set to 3, which led to a lesser increase in CDF difference following the consensus index (**Fig. 2A** and **B**). Color-coded heatmaps corresponding to the consensus matrix were obtained by applying consensus clustering to tumor- and stroma-specific datasets (**Fig. 2C** and **D**). The selected blocks were almost disjointed in the heatmap, indicating that the three clusters could be distinguished on tumor-specific spectra. The three clusters also had relatively clean separation and displayed a well-defined three-block structure for stroma-specific data. The sharp and crisp boundaries further validated stable and robust clustering of the tumor- and stroma-specific dataset. Both datasets were subsequently processed by unsupervised K−means centroid clustering. Of the 347 tumor regions, 161 were assigned to subtype T1 (46%), 55 to T2 (16%), and 131 to T3 (38%), respectively. Furthermore, of the 339 stroma regions, 125 were assigned to subtype S1 (37%), 50 to subtype S2 (15%), and 164 to subtype S3 (48%).

To estimate the ability of MALDI-IMS data to distinguish gastric cancer subtypes and validate subtype assignments without referring to clustering, we additionally assessed the variance among molecular subtypes using a t-distributed stochastic neighbor embedding-based approach. Results showed that both tumor- and stroma-specific subtypes were clearly separated, indicating that they could be readily distinguished on the basis of metabolite levels (**Fig. 2E** and **F**).

Correlation of tumor- and stroma-specific subtypes with molecular features

To explore differences in tumor- and stroma-specific subtypes, we investigated their association with protein expression of molecular features, including DNA MMR, HER2, pEGFR, E3 ubiquitin-protein ligase (MIB1), CD3, CD8, FOXP3, and human alpha defensin 1 (DEFA-1), *HER2* ISH status, and EBV positivity. All associations between molecular features and patient subtypes are shown in **Fig. 2G–H** and Supplementary Tables S2 and S3. Among the three tumor-specific subtypes, gastric cancer molecular features, including HER2 ($P = 0.00017$), CD3 ($P = 0.005$), CD8 ($P = 0.02$), FOXP3 ($P = 0.0011$), MIB1 ($P = 0.0012$), and DEFA-1 ($P = 0.014$) positively correlated with tumor-specific subtype T1. Conversely, pEGFR ($P = 0.012$) and MMR ($P = 0.0033$) negatively correlated with T1. Tumor-specific subtype T2 negatively

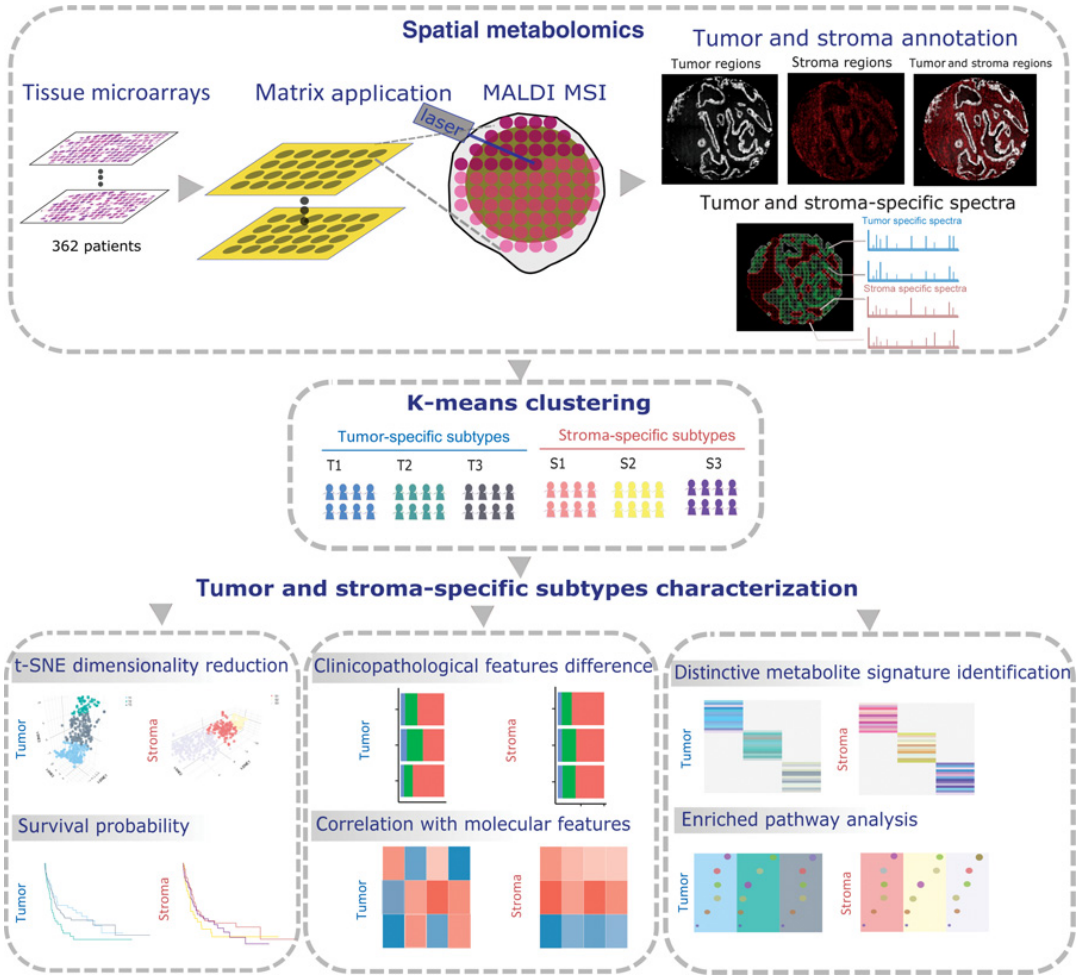

Figure 1.

Spatial metabolomics pipeline scheme and subtype characterization process. The workflow begins with immunophenotype-guided spatial metabolomics, including matrix application, immunophenotype-guided MALDI-IMS assessment, and data processing. For the immunophenotype-guided MALDI-IMS approach, tumor and stroma cells were annotated using multiplex fluorescent IHC staining. Tumor and stroma region-specific mass spectra were then subjected to further the K−means clustering and statistical analysis.

correlated with HER2 ($P = 0.0076$), CD3 ($P = 0.017$), FOXP3 ($P = 0.0013$), and MIB1 ($P = 0.00009$). Meanwhile, T2 showed no significant correlation with CD8 ($P = 0.13$), DEFA-1 ($P = 0.080$), and pEGFR ($P = 0.89$). Conversely, MMR ($P = 0.047$) positively correlated with T2. Tumor-specific subtype T3 positively correlated with pEGFR ($P = 0.013$) and showed no significant correlation with HER2 ($P = 0.082$), MMR ($P = 0.17$), CD3 ($P = 0.23$), CD8 ($P = 0.23$), FOXP3 ($P = 0.36$), MIB1 ($P = 0.71$), and DEFA-1 ($P = 0.26$). The metabolic subtypes significantly correlated with HER2 IHC status, but showed no correlation with *HER2* ISH status. As shown in Supplementary Table S4, EBV positivity was observed in 14 patients. Of these, 9 and 5 EBV-positive tumors were the T1 and T2 subtype, whereas no EBV-positive tumor samples were the T2 subtype. On the basis of these results, we categorized tumor-specific subtypes based on HER2, MIB1, and CD3-positive correlation as T1($HER2^+MIB^+CD3^+$), those based on negative HER2, MIB1, and CD3 correlation, as T2($HER2^-MIB^-CD3^-$), and the remaining tumor subtype based on elevated pEGFR protein expression, as T3($pEGFR^+$).

Stroma-specific subtype S1 did not significantly correlate with HER2 ($P = 0.098$), MMR ($P = 0.572$), pEGFR ($P = 0.49$), MIB1 ($P = 0.21$), DEFA-1 ($P = 0.20$), CD3 ($P = 0.22$), or CD8 ($P = 0.51$), and indeed had a negative correlation with FOXP3 ($P = 0.028$). Stroma-specific subtype S2 was negatively associated with HER2 ($P = 0.028$), MIB1 ($P = 0.002$), FOXP3 ($P = 0.002$), and CD3 ($P = 0.019$). Meanwhile, S2 did not significantly correlate with MMR ($P = 0.0847$), pEGFR ($P = 0.14$), DEFA-1 ($P = 0.47$), or CD8 ($P = 0.22$). Stroma-specific subtype S3 had a positive correlation with HER2 ($P = 0.0019$), MIB1 ($P = 0.00079$), FOXP3 ($P = 0.000013$), and CD3 ($P = 0.008$), and had no significant correlation with MMR ($P = 0.5$), pEGFR ($P = 0.11$), DEFA-1 ($P = 0.082$), and CD8 ($P = 0.14$). Of the 14

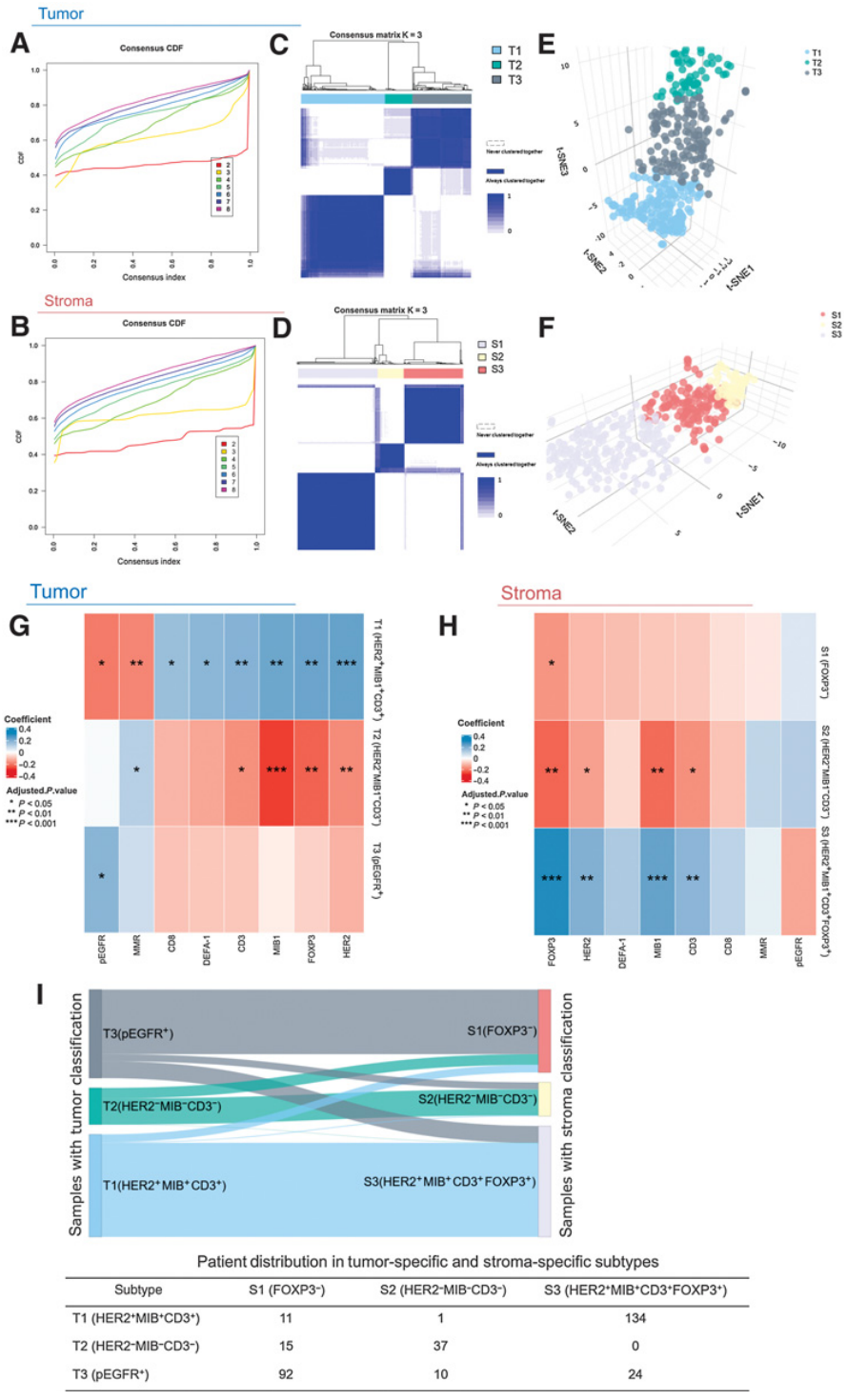

Patient distribution in tumor-specific and stroma-specific subtypes

Subtype	S1 (FOXP3⁻)	S2 (HER2⁻MIB⁻CD3⁻)	S3 (HER2⁺MIB⁺CD3⁺FOXP3⁺)
T1 (HER2⁺MIB⁺CD3⁺)	11	1	134
T2 (HER2⁻MIB⁻CD3⁻)	15	37	0
T3 (pEGFR⁺)	92	10	24

Figure 2.

Tumor- and stroma-specific subtypes identification and their association with molecular features. The relative change in the area under CDF curve of (**A**) tumor and (**B**) stroma datasets. The number of cluster K changed from 2 to 8. $K = 3$ led to a lesser increase in CDF difference following the consensus index and thus was selected as the optimal number of cluster. Consensus matrix heatmap of the chosen optimal number of cluster $K = 3$ of (**C**) tumor and (**D**) stroma-specific datasets. A color gradient of 0–1 is used, blue = consensus score of 1, meaning that patients were always clustered together; white = consensus score of 0, meaning that patients were never clustered together. Three-dimensional t-SNE analysis supported that patients could be stratified into three subtypes in both tumor- (**E**) and stroma-specific datasets. **F,** Points represented samples colored according to the metabolic patient subtypes. Statistical association of molecular features (HER2, MMR, pEGFR, MIB1, CD3, CD8, FOXP3, and DEFA-1) with tumor- (**G**) and stroma-specific subtypes (**H**). **I,** Alluvial diagram depicted the relationship of tumor- and stroma-specific subtypes. Detailed patient numbers in each subtype were shown in the table; *, $P < 0.05$; **, $P < 0.01$; and ***, $P < 0.001$.

EBV-positive tumors, 3 and 11 EBV-positive tumors were the S1 and S3 subtype, whereas no EBV-positive tumor samples were the S2 subtype (Supplementary Table S4). Hence, stroma-specific subtypes were accordingly named S1(FOXP3$^-$), S2(HER2$^-$MIB$^-$CD3$^-$), and S3(HER2$^+$MIB$^+$CD3$^+$FOXP3$^+$). The alluvial diagram shown in **Fig. 2I** indicated the distribution of patients between tumor- and stroma-specific subtypes. Subtype similarities were observed between T1(HER2$^+$MIB$^+$CD3$^+$) and S3(HER2$^+$MIB$^+$CD3$^+$FOXP3$^+$),

T2(HER2$^-$MIB$^-$CD3$^-$) and S2(HER2$^-$MIB$^-$CD3$^-$), and T3(pEGFR$^+$) and S1(FOXP3$^-$).

Tumor-specific subtypes have different clinicopathological features

We next tested whether consensus clustering subtypes had striking differences in the most common gastric cancer clinicopathological characteristics. Our results showed that the proportion of samples in pT ($P = 0.022$), pN ($P = 0.0043$), M ($P = 0.00017$), and UICC stage ($P = 0.00026$) was significantly different in distinct tumor-specific subtypes (Supplementary Fig. S1D–S1F and S1H). Particularly, T1 (HER2$^+$MIB$^+$CD3$^+$) subtype had a significantly different proportion of samples in the "M stage" in comparison with the T2 (HER2$^-$MIB$^-$CD3$^-$) and T3(pEGFR+) subtypes. No associations of tumor-specific subtypes with age, sex, grade, or Lauren classification were found (Supplementary Fig. S1A, S1B, S1G, and S1I). Stroma-specific subtypes were not significantly associated with clinicopathological characteristics (Supplementary Fig. S1).

Association between tumor-specific subtypes and patient prognosis

We next compared potential differences in prognosis among tumor- and stroma-specific subtypes. The Kaplan–Meier survival analysis indicated better outcomes for subtype T1(HER2$^+$MIB$^+$CD3$^+$) than T2(HER2$^-$MIB$^-$CD3$^-$; $P = 0.022$; **Fig. 3B**). No statistically significant differences were observed in other pairwise tumor-specific subtype comparisons or overall, in three tumor-specific subtype comparisons (**Fig. 3A**, **C**, and **D**). In stroma-specific subtypes, survival was not statistically different in pairwise subtype comparisons or in an overall comparison of the three subtypes (**Fig. 3E–H**). The T1 (HER2$^+$MIB$^+$CD3$^+$) and T2(HER2$^-$MIB$^-$CD3$^-$) subtypes, which have significant survival differences, were included in the multivariate Cox regression analysis, and showed that tumor-specific subtypes do not serve as independent prognostic subtypes with regard to the UICC classification system [T1(HER2$^+$MIB$^+$CD3$^+$): $P = 0.323$; hazard ratio (HR), 1.244; T2(HER2$^-$MIB$^-$CD3$^-$): $P = 0.481$; HR, 1.184; UICC stage: $P = 5.38 \times 10^{-12}$; HR, 1.970].

Gastric cancer patient subtypes with distinct metabolites and related metabolism pathways

To gain a deeper insight into the underlying metabolism differences among tumor- and stroma-specific subtypes, a differential analysis was conducted on 277 annotated metabolites, and significant enriched metabolites for each of tumor- and stroma-specific subtypes were identified. Enriched metabolites for each subtype were visualized by a heatmap as shown in **Fig. 4A** and Supplementary Fig. S2A. **Figure 4B–D** and Supplementary Fig. S2B–S2D separately demonstrated distinct subtype-specific pathway patterns of tumor and stroma. T1 (HER2$^+$MIB$^+$CD3$^+$) had 45 significantly upregulated metabolic pathways, 13 of which were related to carbohydrate metabolism, as opposed to 10 that were related to amino acid metabolism (**Fig. 4B**). Notably, nucleotide metabolism and ascorbate and aldarate metabolism were upregulated exclusively in T1(HER2$^+$MIB$^+$CD3$^+$). At the same time, T2(HER2$^-$MIB$^-$CD3$^-$) had 17 significantly upregulated metabolic pathways, 7 of which were related to carbohydrate metabolism and 4 were related to amino acid metabolism, respectively (**Fig. 4C**). T3 (pEGFR$^+$) was found to be related to biotin metabolism and the cytosolic DNA-sensing pathway (**Fig. 4D**). Concerning stroma-specific subtypes, S3(HER2$^+$MIB$^+$CD3$^+$FOXP3$^+$) had 32 specific upregulated metabolism pathways, in comparison with 2 and 17 in S1(FOXP3$^-$) and S2(HER2$^-$MIB$^-$CD3$^-$), respectively (Supplementary Fig. S2B–S2D). S1(FOXP3$^-$) was related to the pentose phosphate pathway and cysteine and methionine metabolism (Supplementary Fig. S2B). Furthermore, some amino acid-related pathways were elevated in S3(HER2$^+$MIB$^+$CD3$^+$FOXP3$^+$; Supplementary Fig. S2D). **Figure 4E** and Supplementary Fig. S2E showed the spatial distribution of one representative metabolite selected from each tumor- and stroma subtype-specific pathway. The above results demonstrate that tumor- and stroma-specific subtypes were enriched with diverse metabolites and metabolism pathways.

T1(HER2$^+$MIB$^+$CD3$^+$) and T2(HER2$^-$MIB$^-$CD3$^-$) subtypes correlate with trastuzumab therapy efficiency in an independent validation cohort (VARIANZ cohort)

Response to trastuzumab therapy in gastric cancer has been linked to a metabolomic classifier in our recent study (**Fig. 5A** and **B**; ref. 31). This metabolomic classifier was established by applying spatial metabolomics and machine learning. The metabolomic classifier could stratify patients diagnosed with HER2-positive gastric cancer into trastuzumab-sensitive and trastuzumab-resistant, and thus predict those patients' response to trastuzumab. HER2-positive tumor patients from the study were used as an independent validation cohort (VARIANZ cohort), and the metabolomic classifier was applied to predict trastuzumab responses in T1(HER2$^+$MIB$^+$CD3$^+$) and T2(HER2$^-$MIB$^-$CD3$^-$) subtypes, due to their specific correlation with HER2 protein expression. As shown in **Fig. 5C** and **D**, the metabolomic classifier can distinguish T1(HER2$^+$MIB$^+$CD3$^+$) and T2(HER2$^-$MIB$^-$CD3$^-$) subtypes in our discovery cohort. In the VARIANZ cohort ($n = 42$), patients treated with trastuzumab therapy were classified into the T1(HER2$^+$MIB$^+$CD3$^+$) and T2(HER2$^-$MIB$^-$CD3$^-$) subtypes, which significantly correlated with a response to trastuzumab (**Fig. 5E**). The percentage of trastuzumab-sensitive patients was significantly higher in the T1(HER2$^+$MIB$^+$CD3$^+$) subtype (82%) than in the T2 (HER2$^-$MIB$^-$CD3$^-$) subtype (44%; **Fig. 5F**). In addition, trastuzumab-treated patients in the T1(HER2$^+$MIB$^+$CD3$^+$) subtype also had a better prognosis than patients in the T2(HER2$^-$MIB$^-$CD3$^-$) subtype (**Fig. 5G**). Spearman correlation analysis revealed no correlation between patient subtypes T1(HER2$^+$MIB$^+$CD3$^+$) and T2(HER2$^-$MIB$^-$CD3$^-$) with HER2 IHC status or ISH gene amplification rate (Supplementary Table S5). Overall, these analyses demonstrate the correlation of these tumor-specific subtypes with survival and reveal their potential as a biomarker across trastuzumab therapy. Particularly, Spearman correlation analysis showed no correlation between any of these metabolites and HER2 protein (Supplementary Table S6). Moreover, multivariate analysis showed that HER2 did not show an independent prognostic value of either the T1(HER2$^+$MIB$^+$CD3$^+$) subtype [$P = 0.26$; HR, 0.68; 95% confidence interval (CI), 0.34–1.34] or the T2(HER2$^-$MIB$^-$CD3$^-$) subtype ($P = 0.26$; HR, 1.48; 95% CI, 0.75–2.93; Supplementary Table S7), further confirming that patient response to trastuzumab depends on tumor-specific subtype variables irrespective of HER2 expression.

Discussion

This study describes a novel tumor- and stroma-specific classification model in a large series of patients with gastric cancer based on metabolites. We defined three distinct tumor-specific subtypes: T1 (HER2$^+$MIB$^+$CD3$^+$), T2(HER2$^-$MIB$^-$CD3$^-$), and T3(pEGFR$^+$), and three stroma-specific subtypes: S1(FOXP3$^-$), S2(HER2$^-$MIB$^-$CD3$^-$) and S3(HER2$^+$MIB$^+$CD3$^+$FOXP3$^+$). The characteristics

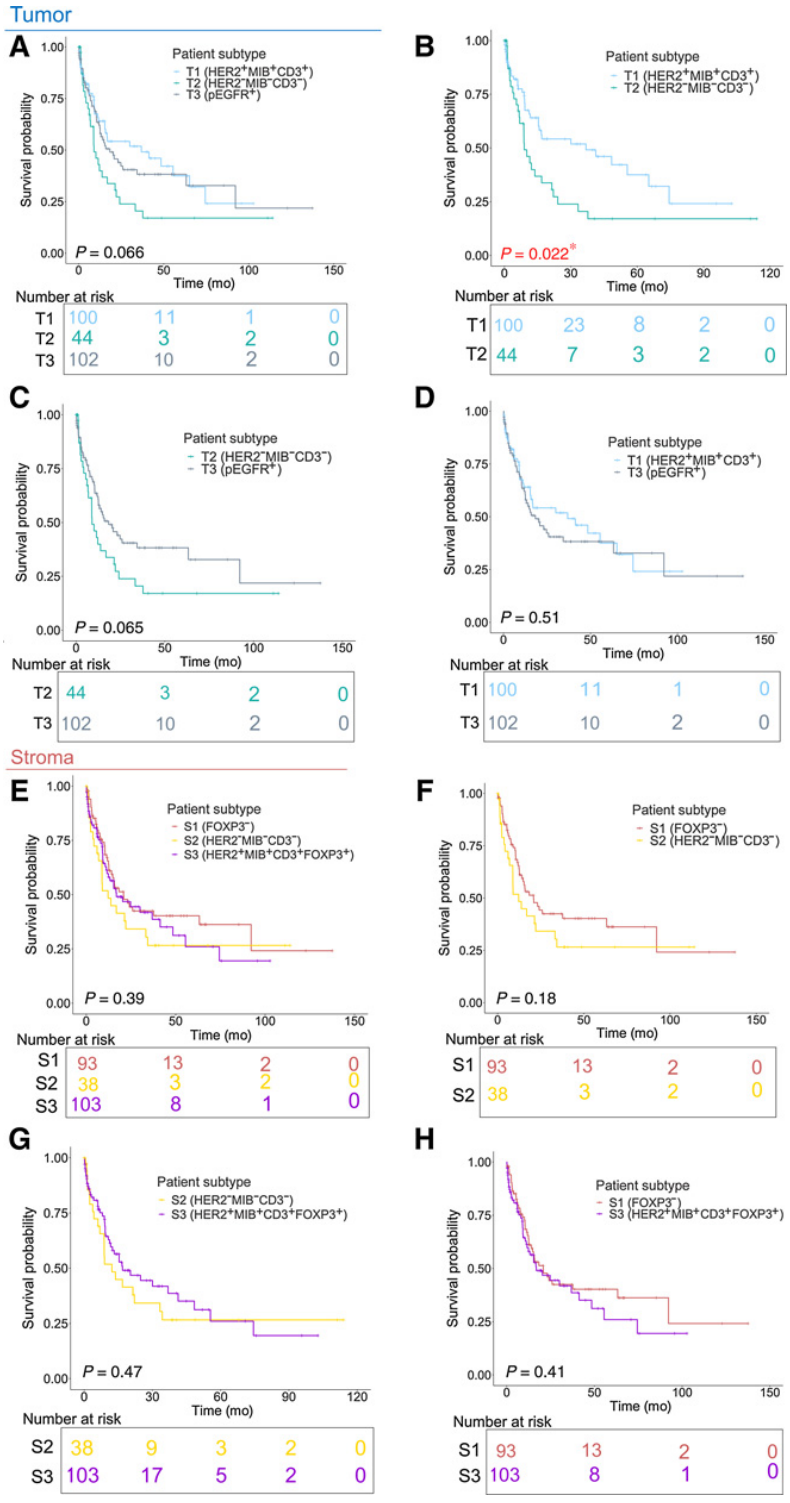

Figure 3.

Metabolic patient subtypes and their prognosis. Survival analysis of (**A**) three tumor-specific subtypes and (**B–D**) pairwise subtype comparison in Kaplan–Meier curves. Survival analysis of (**E**) three stroma-specific subtypes and (**F–H**) pairwise subtype comparison. The *x*-axis represented the survival time, and the *y*-axis represented the probability of survival. The log-rank test was used to assess the statistical significance of the prognostic differences among the subtypes; *, $P < 0.05$.

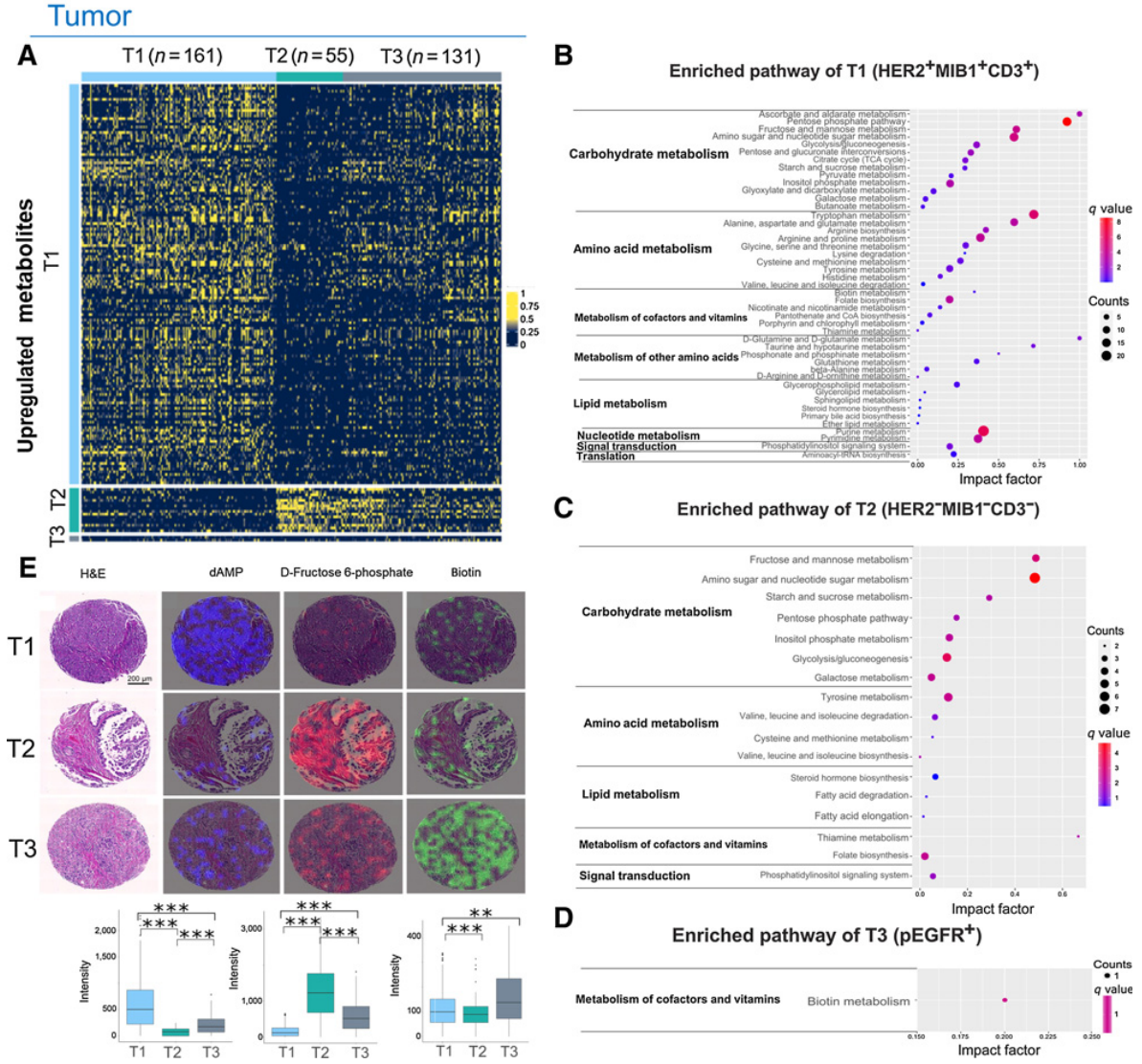

Figure 4.

Tumor subtype-specific metabolite characteristics and pathways enrichment. **A,** Upregulated metabolites of each tumor-specific subtype. Each row represented one metabolite. Colored bars at the top indicated tumor-specific subtypes. **B–D,** Pathways enriched in each tumor-specific subtype were represented by scatter plots. The *x*-axis indicated the pathway impact factor, and the *y*-axis indicated the pathway term. Dot color indicated the *q* value. Dot size indicated the counts of metabolites. **E,** Representative upregulated metabolite distribution and its intensities in the tumor-specific subtypes. Deoxyadenosine monophosphate (dAMP), a nucleotide metabolism member; D-Fructose 6-phosphate, carbohydrate metabolism member; Biotin, biotin metabolism member. The statistic differences were evaluated with the Kruskal–Wallis test. **, $P < 0.01$; ***, $P < 0.001$.

of tumor-specific subtypes are summarized in **Fig. 6**. T1 ($HER2^+MIB^+CD3^+$) was characterized by high immune cell infiltration, presence of EBV, MSI-H, earlier UICC stage, nucleotide metabolism, and good prognosis. By contrast, T2($HER2^-MIB^-CD3^-$) was characterized by low immune cell infiltration, absence of EBV, low MSI, later UICC stage and poor prognosis; Finally, T3($pEGFR^+$) was characterized by high pEGFR. Stroma-specific subtypes were linked to distinct metabolic pathways and molecular features. An independent validation cohort confirmed that the T1($HER2^+MIB^+CD3^+$) subtype had predictive power for a trastuzumab benefit. Identification of these tumor- and stroma-specific subtypes would be a valuable addition to current molecular classification by maximizing the use of established therapy in proper patient populations and reducing the use of costly drugs.

In recent years, molecular methods, such as next-generation sequencing, including deoxyribonucleic acid sequencing, ribonucleic acid sequencing, whole-exome sequencing, copy-number variation analysis, and DNA methylation arrays, have been used for the classification of gastric cancer into molecular subtypes (7–10, 35). Our subtype classification drew from these stratification approaches and

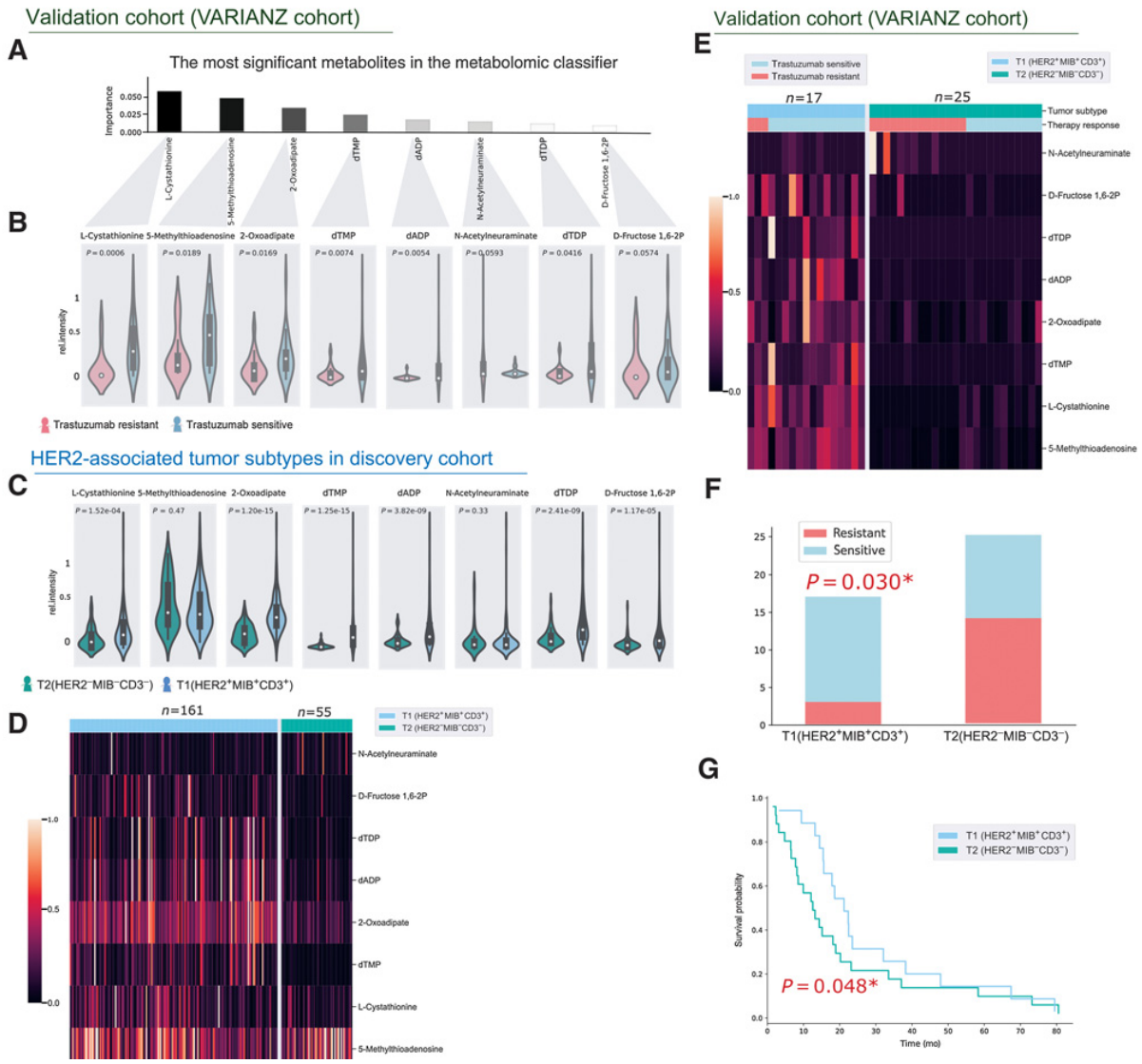

Figure 5.

Association with trastuzumab therapy response in HER2-associated tumor-specific subtypes T1(HER2$^+$MIB$^+$CD3$^+$) and T2(HER2$^-$MIB$^-$CD3$^-$). **A,** Importance plot, including the most significant metabolites, which represented an unequal distribution of trastuzumab-sensitive and -resistant patients in the metabolomic classifier from the VARIANZ cohort. **B,** Abundance difference of metabolites in trastuzumab-sensitive and trastuzumab-resistant patients with gastric cancer using the Mann–Whitney *U* test. **C,** The abundance difference of metabolites in T1(HER2$^+$MIB$^+$CD3$^+$) and T2(HER2$^-$MIB$^-$CD3$^-$) subtypes using the Mann–Whitney *U* test. **D,** Heatmap illustrating the abundance of metabolites showed tumor-specific subtype classification in our discovery cohort. **E,** Heatmap of the abundance of metabolites showed tumor-specific subtype classification in the VARIANZ cohort. **F,** Numbers of trastuzumab-sensitive and trastuzumab-resistant patients in T1(HER2$^+$MIB$^+$CD3$^+$) and T2(HER2$^-$MIB$^-$CD3$^-$) subtypes. The *P* value was calculated by using the Fisher's exact test. **G,** Survival difference of patients with T1(HER2$^+$MIB$^+$CD3$^+$) and T2 (HER2$^-$MIB$^-$CD3$^-$) subtypes treated with trastuzumab therapy using the log-rank test; *, $P < 0.05$.

supplemented them using tissue metabolomics to stratify patients with gastric cancer. The T1(HER2$^+$MIB$^+$CD3$^+$) subtype shared similarity to the EBV$^+$ and MSI subtypes established by TCGA study (7) for the presence of EBV and high MSI. The T2(HER2$^-$MIB$^-$CD3$^-$) subtype was similar to the ImD in immune cell absence and showed consistently poor survival (9). Good prognosis in T1(HER2$^+$MIB$^+$CD3$^+$) and poor prognosis in T2(HER2$^-$MIB$^-$CD3$^-$) subtypes may be due to the combined effects of high CD3, CD8, and FOXP3 expression. Previous studies support our observation that high T-cell density was associated with improved gastric cancer clinical outcomes (14, 36).

Only a subset of patients benefit from trastuzumab therapy (32). However, effective prediction of treatment response to trastuzumab could dramatically enhance this benefit ratio while preventing overtreatment. Several response predictors have been proposed. However, at present, neither HER2 IHC (11) nor *HER2* ISH (37) provides a robust prediction of trastuzumab therapy benefit in patients with

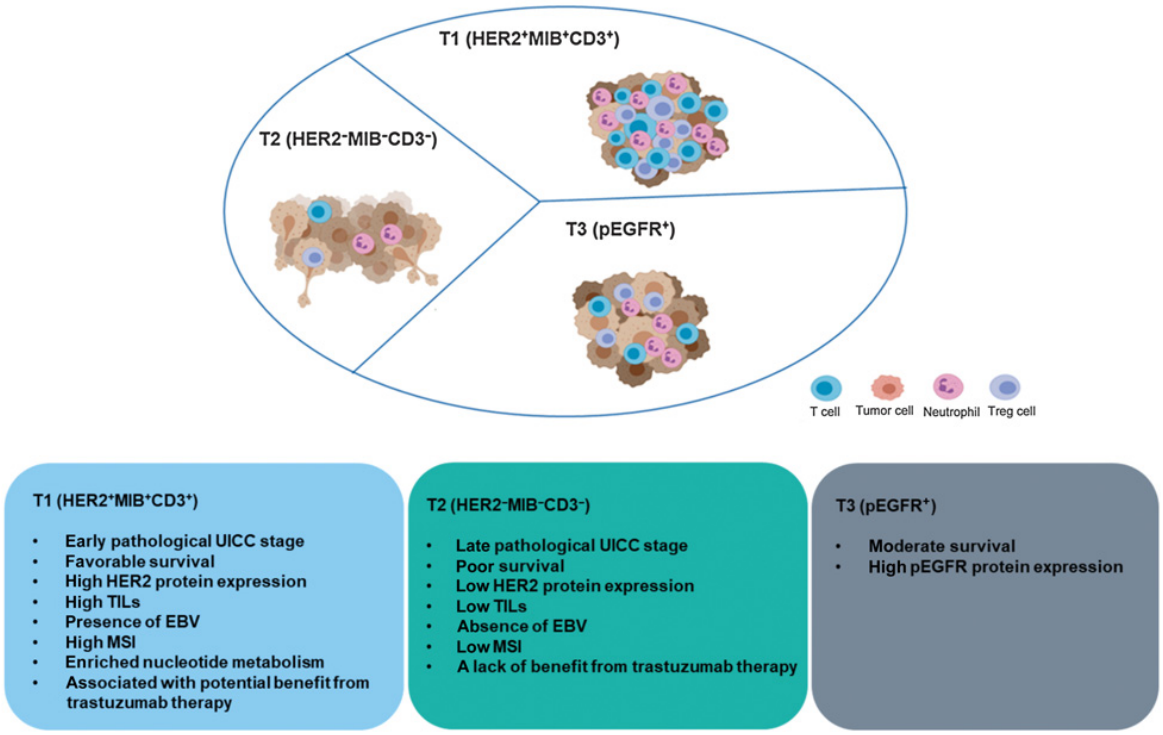

Figure 6.
Summary of clinicopathological and molecular characteristics of three tumor-specific gastric cancer patient subtypes. The three tumor-specific subtypes displayed significantly distinct metabolites and molecular features. EBV, Epstein–Barr virus; HER2, human epidermal growth factor receptor 2; MSI, microsatellite instability; pEGFR, phosphoepidermal growth factor receptor; TIL, tumor-infiltrating lymphocytes.

gastric cancer. Therefore, *a priori* identification of responders is critically needed as it would improve treatment outcomes. A metabolomic classifier involving DNA metabolism molecules was built in our previous study, and could predict trastuzumab response in patients with HER2-positive gastric cancer (31). Patients with HER2-positive tumor from this recent study were used as the validation cohort, and the same metabolomic classifier was applied in the current study. We successfully confirmed that our tumor-specific subtypes can further stratify HER2-positive patient responses to trastuzumab therapy, with patients with gastric cancer possessing T1($HER2^+MIB^+CD3^+$) experiencing better outcomes to trastuzumab therapy than T2 ($HER2^-MIB^-CD3^-$) patients. Strikingly, nucleotides were elevated in sensitive patients, and DNA metabolism in gastric cancer tumor cells has been reported as a crucial factor that affects the response to trastuzumab therapy in our previous study (31). The current study consistently showed a higher abundance of nucleotides and DNA metabolism in the T1 ($HER2^+MIB^+CD3^+$) subtype. Together, this evidence suggests that the T1($HER2^+MIB^+CD3^+$) subtype assignment predicts a benefit when initiating trastuzumab therapy.

In addition, response to trastuzumab therapy has been reported to improve when combined with bifunctional HER2/CD3 CART-like human T-cell treatment (38). Significant inhibition in drug-resistant solid tumors has been exhibited in other HER2-targeted bispecific antibodies undergoing clinical investigation, including ertumaxomab-targeting HER2 and CD3 on T cells and activated T-cell armed with HER2-targeted bispecific antibody (HER2Bi-aATC; ref. 39). In our study, HER2 and CD3 protein expressions were found to be positively correlated with the T1($HER2^+MIB^+CD3^+$) subtype. Hence, we expect the T1($HER2^+MIB^+CD3^+$) subtype to be predisposed with the trastuzumab therapy combined with HER2-targeted bispecific antibodies.

Pioneering studies in this field revealed a close correlation between TILs and PD-L1 overexpression in gastric cancer (16, 40). The expression of PD-1 is found not only on $CD8^+$-infiltrated cells but also on $FOXP3^+$ Treg cells (18). Tumors with elevated immune infiltration often have a more active response to immunotherapy (41). Patients with these characteristics had better clinical outcomes in response to immune checkpoint therapy. Thus, TILs can be considered a potentially important predictive marker in a broad variety of gastric cancer and other tumor types (14, 42). Some previous studies have demonstrated that PD-1 blockade could be effective in patients with elevated $CD8^+$ TILs, even with low PD-L1 expression (43–45). In addition, several recent studies found a close relationship of immune checkpoints with EBV-positive and MSI-high gastric cancer (14, 15). Thus, we expect T1($HER2^+MIB^+CD3^+$) to be predisposed with immune checkpoint inhibitors, such as PD-1 blockade, because of its higher frequency of EBV positivity, MSI and positive correlation with $CD8^+$ T-cell infiltration and FOXP3-positive Treg cells.

Immunotherapy has also been successfully added to HER2-directed therapy. The phase 3 KEYNOTE-811 trial recently showed that adding pembrolizumab to trastuzumab and chemotherapy markedly reduced tumor size, induced complete responses in some participants, and significantly improved objective response rate chemotherapy in HER2-positive, metastatic gastroesophageal adenocarcinoma (46). Notably, there was an impressive 74.4% response rate, which was

significantly higher than the 47% response rate achieved with chemotherapy plus trastuzumab, suggesting that T1($HER2^+MIB^+CD3^+$) treatment responsiveness may be increased by combining checkpoint blockade with standard trastuzumab plus chemotherapy.

The distinct metabolite networks and biochemical processes in tumor- and stroma-specific subtypes revealed by enriched pathway analysis were consistent with previously known features of gastric cancer. For instance, previous studies suggested that metabolic alteration was typically characterized by repression of the Warburg effect aerobic respiration and increased glycolysis for glucose metabolism (19, 47, 48). The association between glucose metabolism and gastric cancer has been confirmed and discussed in several studies (19, 48). One proposed explanation why the Warburg effect is advantageous for tumor growth is that through increased glycolysis, glycolytic intermediates can funnel into anabolic side pathways to support de novo synthesis of nucleotides, lipids, and amino acids needed to support cell proliferation (47, 49). This evidence robustly supports our observation that carbohydrate metabolism and amino acid metabolism pathways are enriched among T1($HER2^+MIB^+CD3^+$), T2($HER2^-MIB^-CD3^-$), S2($HER2^-MIB^-CD3^-$), and S3($HER2^+MIB^+CD3^+FOXP3^+$) subtypes. Apart from commonly enriched metabolism, T1 ($HER2^+MIB^+CD3^+$) and S3($HER2^+MIB^+CD3^+FOXP3^+$) specifically exhibited upregulation of nucleotide metabolism. Accumulation of nucleotide metabolism end products is also found in patients with gastric cancer (50).

Molecular expression profiles of tumor tissues may influence their assignment to specific molecular categories, creating interpretative challenges. Novel, distinctive, stroma-based signatures have been proposed for predominant cancer phenotypes (35). In this study, we successfully performed the classification of tumor epithelial cells and stromal cells, whereas no well-established large-scale classification research has considered the influence of active, nonmalignant stromal cells. As we found, T1($HER2^+MIB^+CD3^+$) and S3($HER2^+MIB^+CD3^+FOXP3^+$) share similar metabolic pathways but different correlations with pathological parameters and molecular features. This result shows that tumor- and stroma-specific metabolite patterns from the same patient may convey different information, and the same patient cohort may have different subtype patterns in tumor- and stroma-specific regions. Thus, identification of subtypes must be more precise to individual tumor or stroma regions rather than mixed tissue regions.

In conclusion, our results increase the understanding of the metabolic subtypes of gastric cancer. With the further development of image mass spectrometry tools, the metabolic classification of gastric cancer will become more precise. If confirmed and extended in future studies, the association between metabolic subtypes reported here and therapy responses might refine patient selection for personalized therapy.

Authors' Disclosures

F. Lordick reports grants, personal fees, and other support from BMS, as well as personal fees from AstraZeneca, Astellas, Eli Lilly, MSD, Merck Serono, Roche, Amgen, BioNTech, MedUpdate, StreamedUp!, and Novartis outside the submitted work. No disclosures were reported by the other authors.

Authors' Contributions

J. Wang: Conceptualization, formal analysis, visualization, methodology, writing–original draft, writing–review and editing. **T. Kunzke:** Conceptualization, methodology. **V.M. Prade:** Conceptualization, methodology. **J. Shen:** Visualization, writing–review and editing. **A. Buck:** Conceptualization, writing–review and editing. **A. Feuchtinger:** Methodology, writing–review and editing. **I. Haffner:** Resources, methodology, writing–review and editing. **B. Luber:** Methodology, writing–review and editing. **D.H.W. Liu:** Methodology, writing–review and editing. **R. Langer:** Methodology, writing–review and editing. **F. Lordick:** Resources, methodology, writing–review and editing. **N. Sun:** Conceptualization, resources, supervision, methodology, writing–review and editing. **A. Walch:** Conceptualization, resources, supervision, project administration, writing–review and editing.

Acknowledgments

The authors thank Ulrike Buchholz, Claudia-Mareike Pflüger, Cristina Hübner Freitas, Andreas Voss, and Elenore Samson for excellent technical assistance. The study was supported by the Ministry of Education and Research of the Federal Republic of Germany (BMBF; 01ZX1610B and 01KT1615; to A. Walch); the Deutsche Forschungsgmeinschaft SFB 824 C4, CRC/Transregio 205/1; to A. Walch); and the China Scholarship Council (CSC; No. 201906210076; to J. Wang).

The costs of publication of this article were defrayed in part by the payment of page charges. This article must therefore be hereby marked *advertisement* in accordance with 18 U.S.C. Section 1734 solely to indicate this fact.

Received December 14, 2021; revised March 1, 2022; accepted April 6, 2022; published first April 8, 2022.

References

1. Sung H, Ferlay J, Siegel RL, Laversanne M, Soerjomataram I, Jemal A, et al. Global cancer statistics 2020: GLOBOCAN estimates of incidence and mortality worldwide for 36 cancers in 185 countries. CA Cancer J Clin 2021;71:209–49.
2. Joshi SS, Badgwell BD. Current treatment and recent progress in gastric cancer. CA Cancer J Clin 2021;71:264–79.
3. Shah MA, Khanin R, Tang L, Janjigian YY, Klimstra DS, Gerdes H, et al. Molecular classification of gastric cancer: a new paradigm. Clin Cancer Res 2011; 17:2693–701.
4. Lin X, Zhao Y, Song WM, Zhang B. Molecular classification and prediction in gastric cancer. Comput Struct Biotechnol J 2015;13:448–58.
5. Lei Z, Tan IB, Das K, Deng N, Zouridis H, Pattison S, et al. Identification of molecular subtypes of gastric cancer with different responses to PI3-kinase inhibitors and 5-fluorouracil. Gastroenterology 2013;145:554–65.
6. Liu Z, Zhang J, Gao Y, Pei L, Zhou J, Gu L, et al. Large-scale characterization of DNA methylation changes in human gastric carcinomas with and without metastasis. Clin Cancer Res 2014;20:4598–612.
7. Cancer Genome Atlas Research N. Comprehensive molecular characterization of gastric adenocarcinoma. Nature 2014;513:202–9.
8. Cristescu R, Lee J, Nebozhyn M, Kim KM, Ting JC, Wong SS, et al. Molecular analysis of gastric cancer identifies subtypes associated with distinct clinical outcomes. Nat Med 2015;21:449–56.
9. Li L, Wang X. Identification of gastric cancer subtypes based on pathway clustering. NPJ Precis Oncol 2021;5:46.
10. Zeng D, Li M, Zhou R, Zhang J, Sun H, Shi M, et al. Tumor microenvironment characterization in gastric cancer identifies prognostic and immunotherapeutically relevant gene signatures. Cancer Immunol Res 2019;7:737–50.
11. Bang YJ, Van Cutsem E, Feyereislova A, Chung HC, Shen L, Sawaki A, et al. Trastuzumab in combination with chemotherapy versus chemotherapy alone for treatment of HER2-positive advanced gastric or gastro-oesophageal junction cancer (ToGA): a phase 3, open-label, randomised controlled trial. Lancet 2010; 376:687–97.
12. Muro K, Chung HC, Shankaran V, Geva R, Catenacci D, Gupta S, et al. Pembrolizumab for patients with PD-L1–positive advanced gastric cancer (KEYNOTE-012): a multicentre, open-label, phase 1b trial. Lancet Oncol 2016;17:717–26.
13. Fuchs CS, Doi T, Jang RW, Muro K, Satoh T, Machado M, et al. Safety and efficacy of pembrolizumab monotherapy in patients with previously treated advanced gastric and gastroesophageal junction cancer: phase 2 clinical KEYNOTE-059 trial. JAMA Oncol 2018;4:e180013.
14. Dai C, Geng R, Wang C, Wong A, Qing M, Hu J, et al. Concordance of immune checkpoints within tumor immune contexture and their prognostic significance in gastric cancer. Mol Oncol 2016;10:1551–8.

15. Chao J, Fuchs CS, Shitara K, Tabernero J, Muro K, Van Cutsem E, et al. Assessment of pembrolizumab therapy for the treatment of microsatellite instability-high gastric or gastroesophageal junction cancer among patients in the KEYNOTE-059, KEYNOTE-061, and KEYNOTE-062 clinical trials. JAMA Oncol 2021;7:895–902.
16. Yi M, Jiao D, Xu H, Liu Q, Zhao W, Han X, et al. Biomarkers for predicting efficacy of PD-1/PD-L1 inhibitors. Mol Cancer 2018;17:129.
17. Kwon M, An M, Klempner SJ, Lee H, Kim KM, Sa JK, et al. Determinants of response and intrinsic resistance to PD-1 blockade in microsatellite instability-high gastric cancer. Cancer Discov 2021;11:2168–85.
18. Morihiro T, Kuroda S, Kanaya N, Kakiuchi Y, Kubota T, Aoyama K, et al. PD-L1 expression combined with microsatellite instability/CD8$^+$ tumor-infiltrating lymphocytes as a useful prognostic biomarker in gastric cancer. Sci Rep 2019; 9:4633.
19. Yuan LW, Yamashita H, Seto Y. Glucose metabolism in gastric cancer: the cutting-edge. World J Gastroenterol 2016;22:2046–59.
20. Cluntun AA, Lukey MJ, Cerione RA, Locasale JW. Glutamine metabolism in cancer: understanding the heterogeneity. Trends Cancer 2017;3:169–80.
21. Huang S, Guo Y, Li Z, Zhang Y, Zhou T, You W, et al. A systematic review of metabolomic profiling of gastric cancer and esophageal cancer. Cancer Biol Med 2020;17:181–98.
22. Wei Q, Qian Y, Yu J, Wong CC. Metabolic rewiring in the promotion of cancer metastasis: mechanisms and therapeutic implications. Oncogene 2020; 39:6139–56.
23. Andre F, Trinh A, Balayssac S, Maboudou P, Dekiouk S, Malet-Martino M, et al. Metabolic rewiring in cancer cells overexpressing the glucocorticoid-induced leucine zipper protein (GILZ): activation of mitochondrial oxidative phosphorylation and sensitization to oxidative cell death induced by mitochondrial targeted drugs. Int J Biochem Cell Biol 2017;85:166–74.
24. Peng X, Chen Z, Farshidfar F, Xu X, Lorenzi PL, Wang Y, et al. Molecular characterization and clinical relevance of metabolic expression subtypes in human Cancers. Cell Rep 2018;23:255–69.
25. Norris JL, Caprioli RM. Analysis of tissue specimens by matrix-assisted laser desorption/ionization imaging mass spectrometry in biological and clinical research. Chem Rev 2013;113:2309–42.
26. Ly A, Buck A, Balluff B, Sun N, Gorzolka K, Feuchtinger A, et al. High-mass-resolution MALDI mass spectrometry imaging of metabolites from formalin-fixed paraffin-embedded tissue. Nat Protoc 2016;11:1428–43.
27. Buck A, Ly A, Balluff B, Sun N, Gorzolka K, Feuchtinger A, et al. High-resolution MALDI-FT-ICR MS imaging for the analysis of metabolites from formalin-fixed, paraffin-embedded clinical tissue samples. J Pathol 2015;237:123–32.
28. Prade VM, Kunzke T, Feuchtinger A, Rohm M, Luber B, Lordick F, et al. De novo discovery of metabolic heterogeneity with immunophenotype-guided imaging mass spectrometry. Mol Metab 2020;36:100953.
29. Sobin LHGM, Wittekind C. TNM classification of malignant tumors. 7th ed. Oxford: Wiley-Blackwell; 2009.
30. Bosman FT, Carneiro F, Hruban RH, Theise ND. World Health Organization, International Agency for Research on Cancer. WHO classification of tumours of the digestive system. Lyon: International Agency for Research on Cancer; 2010. p. 417.
31. Kunzke T, Holzl FT, Prade VM, Buck A, Huber K, Feuchtinger A, et al. Metabolomic therapy response prediction in pretherapeutic tissue biopsies for trastuzumab in patients with HER2-positive advanced gastric cancer. Clin Transl Med 2021;11:e547.
32. Haffner I, Schierle K, Raimundez E, Geier B, Maier D, Hasenauer J, et al. HER2 expression, test deviations, and their impact on survival in metastatic gastric cancer: results from the Prospective Multicenter VARIANZ Study. J Clin Oncol 2021;39:1468–78.
33. Genitsch V, Novotny A, Seiler CA, Kroll D, Walch A, Langer R. Epstein-barr virus in gastro-esophageal adenocarcinomas—single center experiences in the context of current literature. Front Oncol 2015;5:73.
34. Berezowska S, Novotny A, Bauer K, Feuchtinger A, Slotta-Huspenina J, Becker K, et al. Association between HSP90 and Her2 in gastric and gastroesophageal carcinomas. PLoS One 2013;8:e69098.
35. Ren Q, Zhu P, Zhang H, Ye T, Liu D, Gong Z, et al. Identification and validation of stromal-tumor microenvironment-based subtypes tightly associated with PD-1/PD-L1 immunotherapy and outcomes in patients with gastric cancer. Cancer Cell Int 2020;20:92.
36. Arigami T, Uenosono Y, Ishigami S, Matsushita D, Hirahara T, Yanagita S, et al. Decreased density of CD3$^+$ tumor-infiltrating lymphocytes during gastric cancer progression. J Gastroenterol Hepatol 2014;29:1435–41.
37. Gomez-Martin C, Plaza JC, Pazo-Cid R, Salud A, Pons F, Fonseca P, et al. Level of HER2 gene amplification predicts response and overall survival in HER2-positive advanced gastric cancer treated with trastuzumab. J Clin Oncol 2013; 31:4445–52.
38. Luo F, Qian J, Yang J, Deng Y, Zheng X, Liu J, et al. Bifunctional alphaHER2/CD3 RNA-engineered CART-like human T cells specifically eliminate HER2(+) gastric cancer. Cell Res 2016;26:850–3.
39. Yu S, Li A, Liu Q, Yuan X, Xu H, Jiao D, et al. Recent advances of bispecific antibodies in solid tumors. J Hematol Oncol 2017;10:155.
40. Thompson ED, Zahurak M, Murphy A, Cornish T, Cuka N, Abdelfatah E, et al. Patterns of PD-L1 expression and CD8 T-cell infiltration in gastric adenocarcinomas and associated immune stroma. Gut 2017;66:794–801.
41. Haanen J. Converting cold into hot tumors by combining immunotherapies. Cell 2017;170:1055–6.
42. Motz GT, Coukos G. Deciphering and reversing tumor immune suppression. Immunity 2013;39:61–73.
43. Sun JY, Zhang D, Wu S, Xu M, Zhou X, Lu XJ, et al. Resistance to PD-1/PD-L1 blockade cancer immunotherapy: mechanisms, predictive factors, and future perspectives. Biomark Res 2020;8:35.
44. Tumeh PC, Harview CL, Yearley JH, Shintaku IP, Taylor EJ, Robert L, et al. PD-1 blockade induces responses by inhibiting adaptive immune resistance. Nature 2014;515:568–71.
45. Nowicki TS, Hu-Lieskovan S, Ribas A. Mechanisms of resistance to PD-1 and PD-L1 blockade. Cancer J 2018;24:47–53.
46. Janjigian YY, Kawazoe A, Yanez P, Li N, Lonardi S, Kolesnik O, et al. The KEYNOTE-811 trial of dual PD-1 and HER2 blockade in HER2-positive gastric cancer. Nature 2021;600:727–30.
47. Vander Heiden MG, Cantley LC, Thompson CB. Understanding the Warburg effect: the metabolic requirements of cell proliferation. Science 2009;324: 1029–33.
48. Leiting JL, Grotz TE. Advancements and challenges in treating advanced gastric cancer in the West. World J Gastrointest Oncol 2019;11:652–64.
49. Vander Heiden MG, DeBerardinis RJ. Understanding the intersections between metabolism and cancer biology. Cell 2017;168:657–69.
50. Yu L, Aa J, Xu J, Sun M, Qian S, Cheng L, et al. Metabolomic phenotype of gastric cancer and precancerous stages based on gas chromatography time-of-flight mass spectrometry. J Gastroenterol Hepatol 2011;26:1290–7.

Paper 2

6

Spatial Metabolomics Identifies Distinct Tumor-specific and Stroma-specific Subtypes in Patients with Lung Squamous Cell Carcinoma

The second publication, entitled "Spatial Metabolomics Identifies Distinct Tumor-specific and Stroma-specific Subtypes in Patients with Lung Squamous Cell Carcinoma" [2], reveals the alternative option of SCC patient stratification based on spatial metabolomics. This publication applies high-mass-resolution MALDI-IMS combined with hierarchical clustering analysis to establish metabolic subtypes based on tumor- and stroma-specific tissue regions in SCC patients. The results were tested in an independent cohort to demonstrate the ability of metabolic subtypes to associate with the response to chemotherapy.

In this paper, I processed the data using python and R programming and calculated all statistics included in this manuscript. Additionally, I interpreted the data, wrote the original draft of the manuscript, and prepared all figures. After peer-review, I was responsible for editing the manuscript and performing the new figures according to reviewers' suggestions. In addition, I co-designed this study together with Axel Walch and Na Sun.

npj | precision oncology

www.nature.com/npjprecisiononcology

ARTICLE OPEN

Check for updates

Spatial metabolomics identifies distinct tumor-specific and stroma-specific subtypes in patients with lung squamous cell carcinoma

Jun Wang[1,5], Na Sun[1,5], Thomas Kunzke[1], Jian Shen[1], Philipp Zens[2,3], Verena M. Prade[1], Annette Feuchtinger[1], Sabina Berezowska[2,4]✉ and Axel Walch[1]✉

Molecular subtyping of lung squamous cell carcinoma (LUSC) has been performed at the genomic, transcriptomic, and proteomic level. However, LUSC stratification based on tissue metabolomics is still lacking. Combining high-mass-resolution imaging mass spectrometry with consensus clustering, four tumor- and four stroma-specific subtypes with distinct metabolite patterns were identified in 330 LUSC patients. The first tumor subtype T1 negatively correlated with DNA damage and immunological features including CD3, CD8, and PD-L1. The same features positively correlated with the tumor subtype T2. Tumor subtype T4 was associated with high PD-L1 expression. Compared with the status of subtypes T1 and T4, patients with subtype T3 had improved prognosis, and T3 was an independent prognostic factor with regard to UICC stage. Similarly, stroma subtypes were linked to distinct immunological features and metabolic pathways. Stroma subtype S4 had a better prognosis than S2. Subsequently, analyses based on an independent LUSC cohort treated by neoadjuvant therapy revealed that the S2 stroma subtype was associated with chemotherapy resistance. Clinically relevant patient subtypes as determined by tissue-based spatial metabolomics are a valuable addition to existing molecular classification systems. Metabolic differences among the subtypes and their associations with immunological features may contribute to the improvement of personalized therapy.

npj Precision Oncology (2023)7:114 ; https://doi.org/10.1038/s41698-023-00434-4

INTRODUCTION

Lung squamous cell carcinoma (LUSC) and lung adenocarcinoma (LUAD) are the most common histological subtypes of non-small cell lung cancer (NSCLC), which accounts for almost 85% of all human lung cancers[1]. Unlike LUAD, patients with LUSC have not benefited from targeted therapies[2–4], and there are substantial differences of LUSC treatment responses among current therapeutic options[5]. There continues to be great interest in investigating additional predictive biomarkers to facilitate the selection of those patients with LUSC who are most likely to benefit from chemotherapy, immunotherapy, targeted therapy, and other novel agents. To address this issue, research is now focusing on the development of classification systems based on multiple molecular levels, including genomics, transcriptomics, and proteomics, which would aid in understanding LUSC and in subsequently identifying therapeutic vulnerabilities and achieving effective, biomarker-based patient stratification.

Genomic and transcriptomic technologies have provided important insights into the molecular underpinnings of LUSC, leading to preliminary patient stratification strategies[6–10]. The Cancer Genome Atlas established four LUSC-related gene subtypes associated with cell cycle and apoptosis, antioxidant gene expression, phosphatidylinositide 3-kinase signaling, and epigenetic signaling[6]. In addition, two recent studies performed comprehensive proteogenomic characterization of LUSC[11,12]. One of these identified five distinct molecular subtypes by multiomic clustering analysis: the basal-inclusive subtype, classical subtype, EMT-enriched subtype, inflamed-secretory subtype, and proliferative-primitive subtype[12]. Based on these molecular classification results, research such as the NCI's Molecular Analysis for Therapy Choice trial is attempting to capitalize on improved molecular knowledge of LUSC to employ precision therapy[13].

Combining multiple immunological markers, such as programmed cell death protein 1 (PD1), programmed death ligand 1 (PD-L1), cluster of differentiation 3 (CD3), and cluster of differentiation 8 (CD8), with established molecular subtypes may increase the predictive robustness and guide the implementation of NSCLC precision medicine[7]. The genomic and transcriptomic alterations in LUSC shape the functional proteome, control the infiltration of immune cells, and present potential vulnerabilities that can be exploited therapeutically. The immune checkpoint pathway has been shown to play a crucial role in mediating immune tolerance in NSCLC, with antibody agents that block this pathway (e.g., agents against PD1/PD-L1) producing durable responses[14,15], and where expression of checkpoint markers correlates with treatment efficacy[5]. Alternative markers for checkpoint blockade response, including T-cell immunohistochemistry and other immunological markers, are also being considered[16–18].

Many important clinical advances in LUSC have been driven by genomic and proteomic profiling of bulk tumor material, and thus we anticipate that the same will prove true of bulk metabolomic characterization in the LUSC tissues. Recently, one study demonstrates the feasibility of an ensemble machine learning approach to accurately predict NSCLC patient survival from tumor core biopsy metabolomic data[19], while another study suggests

[1]Research Unit Analytical Pathology, Helmholtz Zentrum München–German Research Center for Environmental Health, Neuherberg 85764, Germany. [2]Institute of Tissue Medicine and Pathology, University of Bern, Murtenstrasse 31, 3008 Bern, Switzerland. [3]Graduate School for Health Sciences, University of Bern, Mittelstrasse 43, Bern 3012, Switzerland. [4]Department of Laboratory Medicine and Pathology, Institute of Pathology, Lausanne University Hospital and University of Lausanne, Lausanne 1011, Switzerland. [5]These authors contributed equally: Jun Wang, Na Sun. ✉email: sabina.berezowska@chuv.ch; axel.walch@helmholtz-muenchen.de

Published in partnership with The Hormel Institute, University of Minnesota

npj THE HORMEL INSTITUTE UNIVERSITY OF MINNESOTA

that metabolomic analysis of lung tumor core biopsies can differentiate patients into low- and high-risk groups based on survival events and probability[20]. The two studies applied liquid chromatography-tandem mass spectrometry (LC-MS/MS) and showed great promise of metabolomics in identifying diagnostic and prognostic biomarkers for NSCLC patients in clinical practice[19,20]. High-mass-resolution matrix-assisted laser desorption-ionization (MALDI) imaging mass spectrometry (IMS) directly enables the detection and localization of thousands of different molecules within a routinely preserved tissue section, allowing for the discrimination of tumor and stroma regions in NSCLC tissues[21] and tumor subtyping[22–24]. The metabolic compositions of both tumor and stroma regions were able to provide rich molecular information and may contribute to estimating prognosis in patients diagnosed with NSCLC. Spatial metabolomics enables immunophenotype-guided in situ metabolomics, facilitating the automated and objective identification of histological and functional features in intact tissue sections and the comprehensive analyses of metabolic constitutions of tumor and the stroma regions from large-scale clinical cohort studies[25].

This is the first large-scale study to stratify LUSC patients based on their tissue metabolic profiles. High-mass-resolution MALDI-IMS combined with consensus clustering analysis was applied to establish metabolic classification based on tumor- and stroma-specific tissue regions in LUSC patients. The results were tested in an independent cohort to demonstrate the ability of metabolic subtypes to associate with the response to chemotherapy. The metabolic constitution in LUSC provides an alternative option with which to stratify LUSC patients.

RESULTS

Identification of LUSC patient subtype based on metabolite profiling

A schematic overview of the conceptual methodology in this study is shown in Fig. 1. To determine whether tumor and stroma regions in the primary resected patient cohort had significant differences in metabolite composition, we performed tumor and stroma region-specific unsupervised consensus clustering analysis. Consensus matrix heatmaps and cumulative distribution function (CDF) plots were drawn to determine the optimal number of clusters. The delta area plot shown in Fig. 2a, b reflects the relative changes in the area under the CDF curve. The largest changes in area for tumor-specific and stroma-specific data occurred when the number of clusters was set to 4, at which point the relative increase in area became noticeably smaller. Thus, the optimal cluster numbers for both tumor-specific and stroma-specific data were set to 4. Color-coded consensus heatmaps were obtained by applying consensus clustering to tumor- and stroma-specific datasets (Fig. 2c, d). As shown in Fig. 2c, the blocks are barely overlap in the heatmap, indicating that the four clusters could be distinguished on tumor-specific spectra. The four stroma-specific clusters also have clean boundaries, indicating good cluster stability over repeated iteration (Fig. 2d). Of the 313 tumor regions, 91 were assigned to subtype T1 (29%), 64 to T2 (20%), 81 to T3 (26%), and 77 to T4 (25%). Furthermore, of the 268 stroma regions, 100 were assigned to subtype S1 (37%), 71 to subtype S2 (27%), 22 to subtype S3 (8%), and 75 to subtype S4 (28%).

To estimate the ability of MALDI-IMS data to distinguish LUSC subtypes, we additionally assessed the variance among molecular subtypes using sparse partial least-squares discriminant analysis (sPLSDA). The results revealed clear separation of both tumor- and stroma-specific subtypes, indicating that they could be readily distinguished based on metabolite levels (Fig. 2e, f). The alluvial diagram shown in Fig. 2g indicates the distribution of patients between tumor- and stroma-specific subtypes. Subtype similarities are observed between T1 and S2.

Correlation of tumor- and stroma-specific subtypes with immunological features and DNA damage

To explore differences in tumor- and stroma-specific subtypes, we investigated their associations with DNA damage (γH2AX expression) and immunological features including cluster of differentiation 3 (CD3), cluster of differentiation 8 (CD8), and programmed death ligand 1 (PD-L1). All associations of those features with tumor-specific subtypes and stroma-specific subtypes are shown in Fig. 3a, b (left) and Supplementary Tables 2 and 3. Among the four tumor-specific subtypes (Fig. 3a), PD-L1 ($p = 0.0012$), CD3 ($p = 0.0002$), CD8 ($p = 0.0001$), and γH2AX ($p = 0.0016$) are positively correlated with tumor-specific subtype T1. Conversely, tumor-specific subtype T2 is negatively correlated with PD-L1 ($p = 0.0390$), CD3 ($p = 0.0071$), CD8 ($p = 0.0080$), and γH2AX ($p = 0.0933$). No significant correlation is found between T3 and these features. Tumor-specific subtype T4 is positively correlated with PD-L1 ($p = 0.0004$) and γH2AX ($p = 0.0333$). Meanwhile, T4 shows no significant correlation with CD3 ($p = 0.9919$) or CD8 ($p = 0.1755$). Based on these results, we categorize the tumor-specific subtype with negative associations with PD-L1, CD3, and CD8 as T1(PD-L1$^-$CD3$^-$CD8$^-$), that with positive associations with PD-L1, CD3, and CD8 as T2(PD-L1$^+$CD3$^+$CD8$^+$), that with elevated PD-L1 protein expression as T4(PD-L1$^+$), and the remaining tumor subtype as T3. The distribution of the expression of all immunological features and DNA damage in the tumor-specific subtypes is shown as boxplots in Fig. 3a (right).

As shown in Fig. 3b, stroma-specific subtype S2 is negatively associated with PD-L1 ($p = 0.0058$), CD3 ($p = 0.0041$), CD8 ($p = 0.3660$), and γH2AX ($p = 0.1242$). In contrast, stroma-specific subtype S4 is positively associated with PD-L1 ($p = 0.0056$), CD3 ($p = 0.0019$), CD8 ($p = 0.0017$), and γH2AX ($p = 0.1242$). No significant correlations with these features are found in S1 and S3. Thus, stroma-specific subtypes are accordingly renamed S1, S2(PD-L1$^-$CD3$^-$CD8$^-$), S3, and S4(PD-L1$^+$CD3$^+$CD8$^+$). The distribution of the expression of all immunological features and DNA damage in stroma-specific subtypes is shown as boxplots in Fig. 3b (right).

Association of tumor-specific and stroma-specific subtypes with patient prognosis and clinicopathological features

The potential differences in prognosis among the tumor- and stroma-specific subtypes were analyzed. The Kaplan–Meier curve and log-rank test indicate better outcomes for subtype T3 than for T1(PD-L1$^-$CD3$^-$CD8$^-$) ($p = 0.0158$) and T4 (PD-L1$^+$) ($p = 0.0404$) (Fig. 3c). No statistically significant differences are observed in other pairwise tumor-specific subtype comparisons or overall in the four tumor-specific subtype comparisons. The multivariate Cox regression analysis shows that T3 can serve as a subtype with an independent effect on prognosis with regard to the UICC classification system ($p = 0.021$, HR = 0.439) (Fig. 3d). In the stroma-specific subtypes, S4(PD-L1$^+$CD3$^+$CD8$^+$) has a better prognosis than S2(PD-L1$^-$CD3$^-$CD8$^-$) ($p = 0.0394$). Survival does not differ significantly in other pairwise subtype comparisons or in an overall comparison of the four subtypes (Fig. 3e). None of the stroma-specific subtypes is found to serve as independent predictors of prognosis with regard to the UICC classification system (Fig. 3f).

We next investigated whether tumor-specific and stroma-specific subtypes differed in the most common clinicopathological characteristics. In all tumor-specific and stroma-specific subtypes, no associations were found with age, sex, resection status, grade, UICC stage, or TNM stage (Supplementary Fig. 1).

Tumor- and stroma-specific metabolic subtypes with distinct metabolites and related metabolic pathways

To obtain a deeper insight into the underlying differences in metabolites among the metabolic subtypes, a correlation network analysis and quantitative enrichment analysis were conducted

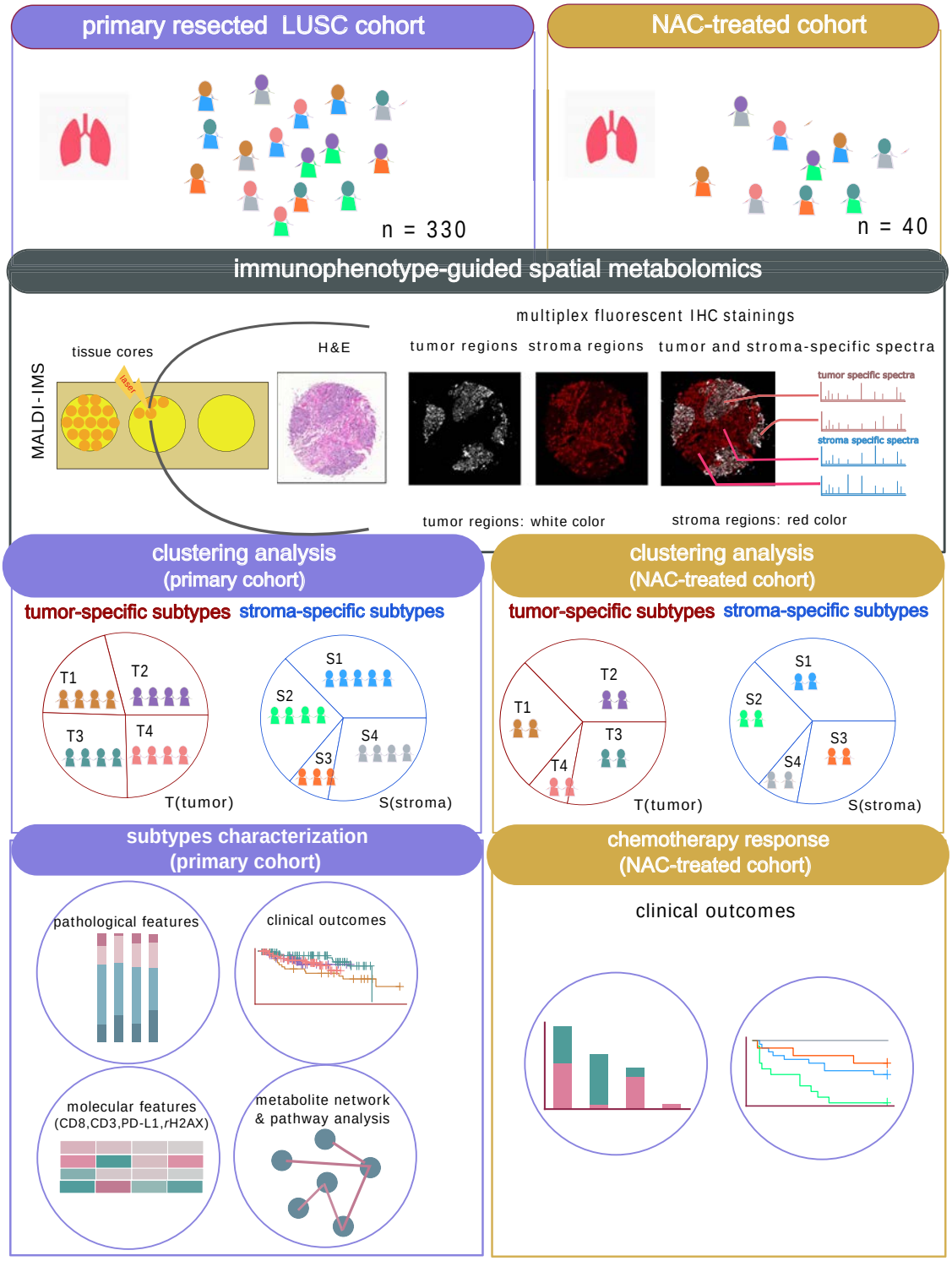

Fig. 1 Study design for combining spatial metabolomics with consensus clustering analysis to stratify LUSC patients. LUSC patients were analyzed with spatial metabolomics by MALDI–IMS. The pipeline includes immunophenotype-guided spatial metabolomics, data preprocessing, and data analysis. Separate consensus clustering analyses were performed using the metabolic features evaluated in tumors and the stroma, resulting in tumor and stroma-specific subtypes. The tumor and stroma-specific subtypes of the primary resected cohort were then characterized by clinicopathological features, clinical outcomes, molecular features (immunological features and DNA damage marker), and specific metabolic pathways. The independent NAC-treated cohort was applied to associate chemotherapy responses with the established metabolic subtypes.

based on each of the tumor- and stroma-specific subtypes, and significantly correlated metabolites of each subtype were identified and visualized as networks and pathways as shown in Fig. 4a and Supplementary Fig. 2. As shown in Fig. 4a, the dense cluster and enriched pathways in T1(PD-L1^{-}CD3^{-}CD8^{-}) indicates a correlation of lipid metabolism and pyrimidine metabolism. For the T2(PD-L1^{+}CD3^{+}CD8^{+}) subtype, there are correlations of metabolites involved in amino acid metabolism and nucleotide

Table 1. Summary of patient characteristics.

Characteristic	Numbers
Number of patients	330
Age [years]	
Median	69
Range	43–85
Sex	
Male	281 (85%)
Female	49 (15%)
pT stage	
T1	72 (22%)
T2	157 (48%)
T3	75 (22%)
T4	26 (8%)
pN stage	
N0	187 (57%)
N1	105 (32%)
N2	38 (11%)
M	
M0	321 (97%)
M1	9 (3%)
UICC stage	
I	98 (30%)
II	113 (34%)
III	110 (33%)
IV	9 (3%)
Primary resection status	
R0	287 (87%)
R1	40 (12%)
R2	3 (1%)
Grade	
G1	6 (2%)
G2	163 (49%)
G3	161 (49%)

M: distant metastases (M0: absent; M1: present).

metabolism. For the T3 subtype, there are multiple correlations of metabolites involved in nucleotide metabolism. T4(PD-L1$^+$) is representatively characterized by amino acid metabolism. As shown in Supplementary Fig. 2, the most representative pathways are amino acid metabolism and nucleotide metabolism in S1 subtype. Similar to the T1(PD-L1$^-$CD3$^-$CD8$^-$) subtype, S2(PD-L1$^-$CD3$^-$CD8$^-$) demonstrates a correlation of lipid metabolism and pyrimidine metabolism. S3 is representatively characterized by lipid metabolism. For the S4 subtype, there are correlations of metabolites involved in nucleotide metabolism. Figure 4b showed the spatial distribution of representative metabolites selected from correlated networks of tumor-specific subtypes. The above results demonstrate that tumor- and stroma-specific subtypes are correlated with diverse metabolites and metabolic pathways. Specifically, the subtype similarities of enriched metabolic pathways are observed between T1(PD-L1$^-$CD3$^-$CD8$^-$) and S2(PD-L1$^-$CD3$^-$CD8$^-$).

Three stroma-specific subtypes correlate with chemotherapy efficiency in an independent neoadjuvant chemotherapy-treated cohort (NAC-treated cohort)

A previous study established a metabolomic classifier which comprises 100 metabolites to evaluate the response to chemotherapy in patients with non-small cell lung cancer[26]. This metabolomic classifier was established by applying spatial metabolomics and machine learning. The metabolomic classifier could stratify NSCLC patients into chemotherapy-sensitive and chemotherapy-resistant groups, and thus assess those patients' response to chemotherapy. The metabolomic classifier of tumor and stroma were separately applied to associate chemotherapy responses in the established tumor- and stroma-specific subtypes. As shown in Fig. 5a, the stroma metabolomic classifier can distinguish the stroma-specific subtypes in our discovery cohort. In the NAC-treated cohort ($n = 40$), patients treated with chemotherapy were classified into the four stroma-specific subtypes (Fig. 5b). The proportion of chemotherapy-resistant patients was significantly higher in the S2(PD-L1$^-$CD3$^-$CD8$^-$) subtype (92%) than in the S1 subtype (44%) ($p = 0.018$) and S3 subtype (22%) ($p = 0.002$) (Fig. 5c). In addition, chemotherapy-treated patients in the S2(PD-L1$^-$CD3$^-$CD8$^-$) subtype also had a worse prognosis than patients in the S1 ($p = 0.005$) and S3 subtypes ($p = 0.006$) (Fig. 5d). Multivariate analysis shows that stroma-specific subtypes S1 and S2(PD-L1$^-$CD3$^-$CD8$^-$) can serve as subtypes that are independently predictive of prognosis with regard to the major pathological response (MPR) and UICC classification system [S1: $p = 0.024$, HR = 0.381; S2(PD-L1$^-$CD3$^-$CD8$^-$): $p = 0.002$, HR = 4.187] (Fig. 5e). No association of tumor-specific subtypes with chemotherapy response is found (Supplementary Fig. 3). Overall, these analyses demonstrate the correlation of these stroma-specific subtypes with survival and reveal their potential as biomarkers reflecting the response to chemotherapy.

DISCUSSION

This study establishes metabolic subtypes in a large series of 330 patients with lung squamous cell carcinoma (LUSC). We define four distinct tumor-specific subtypes: T1(PD-L1$^-$CD3$^-$CD8$^-$), T2(PD-L1$^+$CD3$^+$CD8$^+$), T3, and T4(PD-L1$^+$), and four stroma-specific subtypes: S1, S2(PD-L1$^-$CD3$^-$CD8$^-$), S3, and S4(PD-L1$^+$CD3$^+$CD8$^+$). The characteristics of these subtypes are summarized in Fig. 6. T1(PD-L1$^-$CD3$^-$CD8$^-$) is characterized by low immune cell infiltration, low PD-L1 expression, low DNA damage (γH2AX expression), and poor prognosis. By contrast, T2(PD-L1$^+$CD3$^+$CD8$^+$) is characterized by high immune cell infiltration, high PD-L1 expression, and good prognosis; meanwhile, T3 has a favorable prognosis. Finally, T4(PD-L1$^+$) is characterized by high PD-L1 expression. Stroma-specific subtypes are linked to immunological features and prognosis. An independent neoadjuvant chemotherapy-treated cohort (NAC-treated cohort) confirms that the S2(PD-L1$^-$CD3$^-$CD8$^-$) subtype has an association with chemotherapy resistance. Taken together, our results suggest that distinct subtypes of LUSC as defined using metabolomics may show better responses to specific targeted therapies.

In recent years, molecular methods have been used for the classification of cancer into molecular subtypes[2–4,6–8,27]. Our subtype classification drew from these stratification approaches and supplemented them using tissue metabolomics to stratify LUSC patients. However, previous metabolomics stratification studies on patients with lung cancer focused largely on a mixture of tumor and stroma regions, analyzing few stromal regions from tumors and matching nonmalignant tissue. One study recently proposed distinctive stroma-based lung cancer subtypes by using single-cell RNA-sequencing[28]. In this study, we successfully separately performed the classification of tumor epithelial cells and stromal cells based on tissue-based spatial metabolomics. We found that the metabolic profiles of tumor and stroma tissues can be used to assign them to specific metabolic categories. Both tumor and stroma regions play important roles in the LUSC stratification, which could be confirmed by the tumor-specific subtype associations for several immune-related markers,

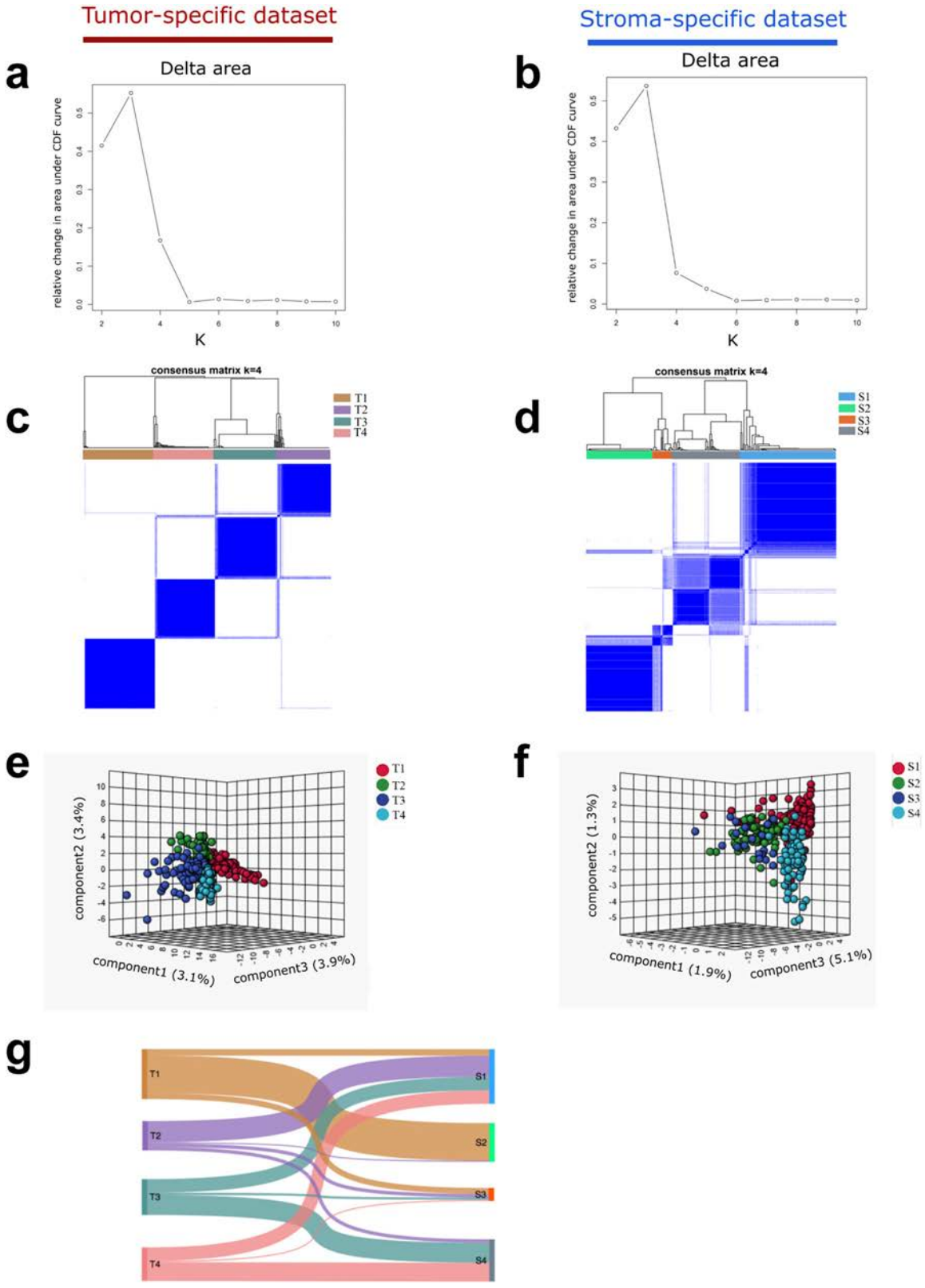

Fig. 2 Identification of tumor- and stroma-specific subtypes and their association with molecular features. The relative change in the area under CDF curve of **a** tumor and **b** stroma datasets. The number of clusters is changed from 2 to 10. Delta area plot reflecting the relative changes in the area under the CDF curve. Setting the number of clusters to 4 leads to the relative increase in area became noticeably smaller; this number was thus selected as the optimal number of clusters. Consensus matrix heatmap of the chosen four clusters of **c** tumor- and **d** stroma-specific datasets. A color gradient ranging between 0 and 1 is defined as the average consensus value for all pairs of individuals. A value closer to 1 indicates better cluster stability. Three-dimensional sPLSDA analysis suggests that patients could be stratified into four subtypes in both **e** tumor- and **f** stroma-specific datasets. Points representing samples are colored according to the metabolic subtypes of patients. **g** Alluvial diagram depicts the relationship of tumor- and stroma-specific subtypes. CDF cumulative distribution function, sPLSDA sparse partial least-squares discriminant analysis.

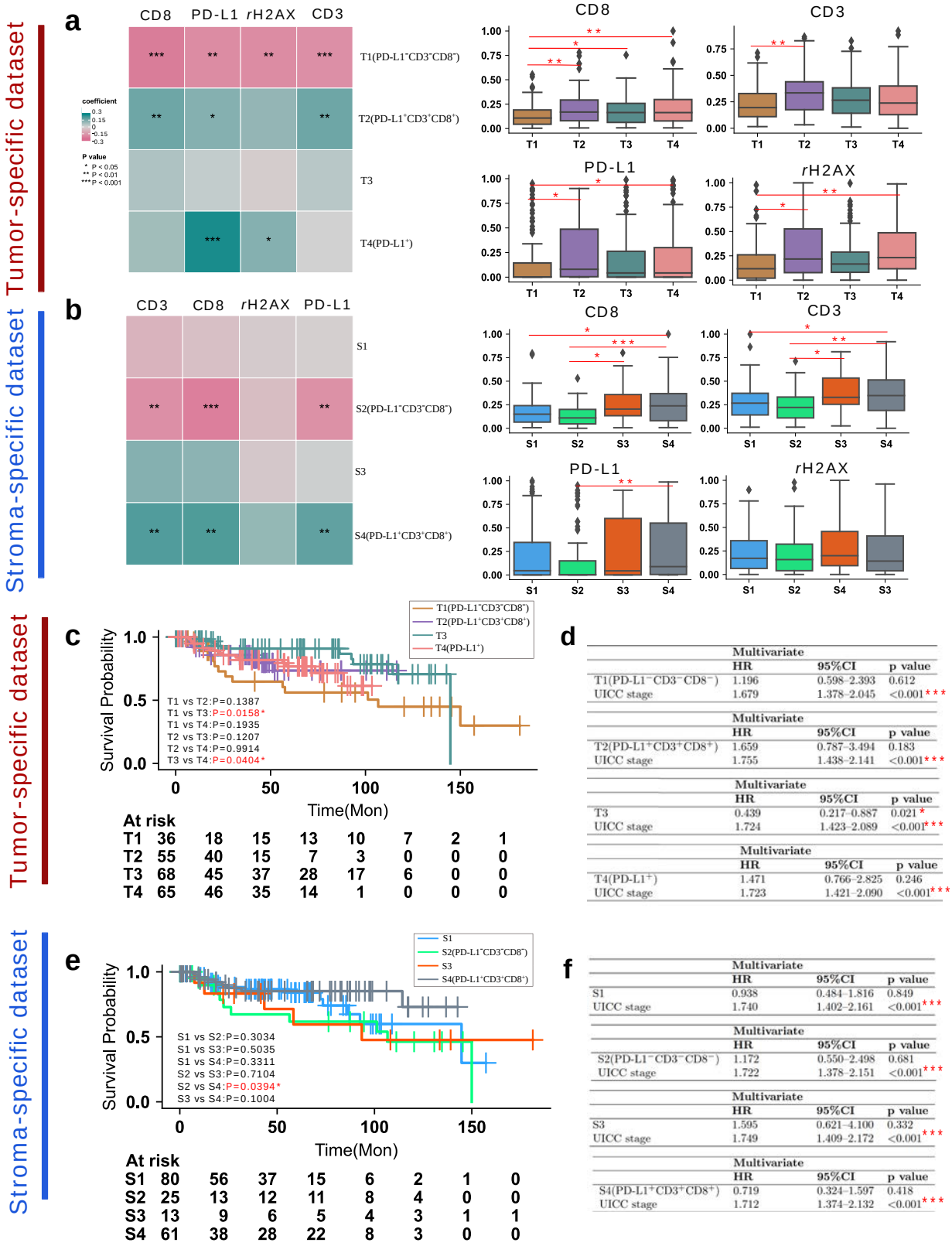

including PD-L1, CD3, and CD8, being retained in the stroma-specific subtypes. However, stroma-specific subtypes were confirmed to be associated with chemotherapy response, while tumor metabolite signatures were not. This shows that tumor- and stroma-specific metabolite patterns from the same patient may convey different information, and the same patient cohort may have different subtype patterns in tumor- and stroma-specific regions. Thus, subtypes must be more precisely identified for individual tumor or stroma regions, rather than regions containing a mixture of tissues.

Fig. 3 Association of metabolic subtypes with molecular features and prognosis. Molecular features (CD8, CD3, PD-L1, and γH2AX) significantly associated with tumor- (**a**, left) and stroma-specific (**b**, left) subtypes by Spearman's rank-order correlation analysis and the distribution of expression per molecular feature in each subtype as shown by boxplots (**a** and **b**, right). Each box plot displays the interquartile range (IQR), with the lower boundary representing the 25th percentile and the upper boundary representing the 75th percentile. The line within the box displays the median, and the whiskers extend to ±1.5 × IQR. Two-sided *p* value was calculated by Kruskal–Wallis test and post hoc Dunn's multiple comparison test. **c** Survival analysis of tumor-specific subtypes using Kaplan–Meier curves by log-rank test and **d** multivariate Cox proportional hazard analysis of tumor-specific subtypes as well as UICC stage. T3 remains significant in multivariate analysis, indicating that it is a factor independently predictive of patient survival. **e** Survival analysis of stroma-specific subtypes using Kaplan–Meier curves by log-rank test and **f** multivariate Cox proportional hazard analysis of stroma-specific subtypes as well as UICC stage. * represents two-sided $p < 0.05$, ** represents two-sided $p < 0.01$, *** represents two-sided $p < 0.001$.

Several predictors of response to chemotherapy have been proposed in small cell lung cancer[29]. However, none yet provides a robust prediction of the benefit of chemotherapy in LUSC patients. There is thus an urgent need for a priori identification of responders to improve treatment outcomes. A metabolomic classifier was established in a previous study, and could assess the response to chemotherapy in patients with non-small cell lung cancer[26]. In the current study, LUSC patients from this recent study were used as an independent cohort and the identical metabolomic classifier was applied. Key metabolomic patterns distinguishing the LUSC stroma-specific subtypes, as first observed in the discovery cohort, were confirmed from the independent NAC-treated LUSC cohort. We successfully confirmed that our stroma-specific subtypes can further stratify patient responses to chemotherapy, with LUSC patients possessing S1 and S3 exhibiting better clinical responses to chemotherapy than S2(PD-L1$^-$CD3$^-$CD8$^-$) patients. This evidence suggests that those assigned to the S1 and S3 subtypes are associated with a benefit from chemotherapy. In addition, the LUSC patients analyzed from the independent cohort could be classified into one of the four stroma-specific subtypes in the discovery cohort, raising the realistic possibility that prospective subtyping could be performed in a single trial, wherein patients are assigned to other treatment arms on the basis of their LUSC subtype [e.g., T2(PD-L1$^+$CD3$^+$CD8$^+$) to PD-L1 immune checkpoint inhibitor].

To date, only immunotherapy has evolved into a successful therapeutic strategy for patients with LUSC[30,31], but differences in patients' responses to PD-1/PD-L1 inhibitors hinder its clinical application[32]. Effective prediction of the response to immunotherapy could dramatically enhance the proportion of patients who benefit while preventing overtreatment. T2(PD-L1$^+$CD3$^+$CD8$^+$) captures several immunological features that are predictive of response to immunotherapy. The predictive biomarker for this immunotherapeutic class is PD-L1 overexpression[14,15]. Apart from this, the rate of tumor-infiltrating lymphocytes (TILs) is considered a potentially important predictive marker in a broad variety of tumor types[33–35]. In addition, pioneering studies in this field have confirmed a close correlation between TILs and PD1 overexpression in NSCLC[36–39]. Consequently, we expect T2(PD-L1$^+$CD3$^+$CD8$^+$) to be susceptible to immune checkpoint inhibitors, such as PD-1/PD-L1 blockade, because of its positive association with PD-L1 expression, and CD3 and CD8$^+$ T-cell infiltration. Besides the low expression of PD-L1, the T1(PD-L1$^-$CD3$^-$CD8$^-$) subtype also shows low expression of CD3 and CD8. If confirmed in future studies, molecular classification might potentially be used to identify tumors of the T1(PD-L1$^-$CD3$^-$CD8$^-$) subtype in order to select optimal treatment, particularly as these cases appear to represent an "immunologically ignorant" group unlikely to respond to immune checkpoint inhibitors.

To investigate the metabolites' processes and events that play a role in the established tumor or stroma subtypes, we performed metabolic network analysis determining the correlations between endogenous metabolites. The metabolites that are correlated within each subtype comprise different classes of biomolecules, such as nucleotides and amino acids. These are involved in various pathways contributing to cancer cell growth and survival[40]. Cancer cells exhibit the deactivation of crucial DNA damage response signaling routes and have often undergone rewiring of their metabolism and energy production networks[41,42]. In addition, amino acids play a role in energy generation, maintaining cellular redox homeostasis and driving the synthesis of nucleic acids. Typically, alongside its association with the DNA damage-related protein γH2AX, T1(PD-L1$^-$CD3$^-$CD8$^-$) also 2′-demonstrates a dense cluster which strongly involves 2'-deoxycytidine diphosphate, cytidine diphosphate (CDP), uridine diphosphate (UDP), 2′-Deoxyinosine 5′-phosphate and cytidine in the metabolite network, which can be interpreted as an involvement in nucleotide metabolism occurring in response to DNA damage.

One major advantage of using FFPE TMAs in this study is the ability to directly detect and visualize metabolites, assigning them to specific tumor or stroma types in their native histological context. Compared to fresh frozen samples, FFPE TMAs offer superior morphological integrity[23], enabling better tumor and stroma classification of metabolite content. A major limitation of using FFPE TMAs is the reduced or removed intensity of hydrophobic molecules. In a previous study, it was found that although metabolite peaks in the low mass range (*m/z* 50–400) were comparable to those in fresh frozen tissue, several peak intensities were decreased in the mass range above *m/z* 600[24]. The loss of hydrophobic molecules, for example, lipids, from the sample is a general limitation with FFPE patient samples due to the tissue embedding process and removal of paraffin wax via solvents, but there were classes of robust metabolites both chemically and spatially preserved in FFPE tissue specimens[23]. Moreover, many mass spectrometry studies, including those based on liquid- and gas-chromatography MS, have demonstrated that metabolites are reliably retained in FFPE tissue samples[43,44]. A recently published protocol for metabolomic and lipidomic profiling in FFPE kidney tissue by LC-MS with subsequent detection of selected lipid species by an independent in situ MS imaging approach demonstrates the complementary use of both techniques[45].

In summary, our approach presented in this paper was successfully applied to reveal the ability of metabolomics to stratify LUSC patients. Such studies should aid in connecting metabolic profiles to clinical immunological features and in subsequently identifying therapeutic vulnerabilities and achieving effective, biomarker-based patient stratification.

METHODS

Patients and tissue samples for the primary resected squamous cell lung carcinoma (LUSC) cohort

This study includes two retrospective single-center patient cohorts of primary resected and neoadjuvant chemotherapy-treated LUSC cases (Fig. 1). We analyzed 330 consecutive patients with primary resected LUSC[46], diagnosed at the Institute of Tissue Medicine and Pathology, University of Bern, without previous or concomitant diagnosis of LUSC of other organs, to reliably exclude metastatic lung disease. The cohort of primary resected LUSC was resected and diagnosed during 2000–2013. The study was performed in

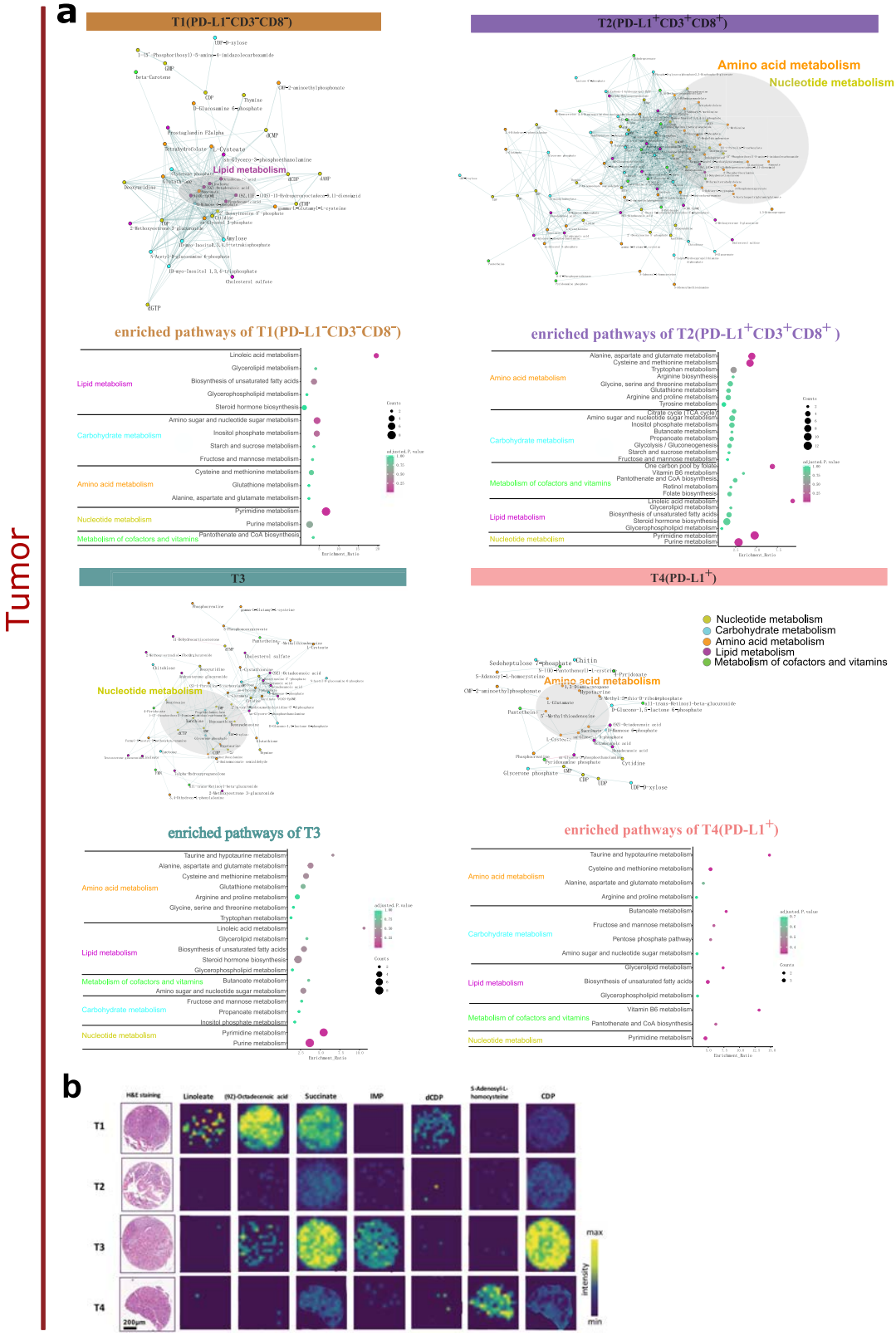

accordance with the Declaration of Helsinki, and the local Ethics Committee of the Canton of Bern approved the study and waived the requirement for written informed consent (KEK 200/14). In this study, we used only tissue material from the archives of the Institute of Pathology which is left after the diagnostic process has been finalized. Due to the retrospective nature of the study and reusage of left-over or already collected material, and also due to the significant number of patients already deceased, the requirement for informed consent was waived by the local ethics committee. It was argued that contacting the relatives and the

Fig. 4 Metabolite characteristics and enriched pathways of tumor subtypes. a (top) Correlation networks of endogenous metabolites within each of the four tumor-specific subtypes. Correlations between metabolites were calculated and filtered (adjusted two-sided $p < 0.001$). Edges represent positive (green) and negative (pink) correlations between metabolites. Node color in the network indicates metabolic pathways. **a** (bottom) Quantitative enrichment pathway analysis within each of the four tumor-specific subtypes. Pathways enriched in each of the tumor-specific subtypes are represented by scatter plots. The x-axis indicates the pathway enrichment ratio, and the y-axis indicates the pathway term. Dot color indicates the adjusted *p* value. Dot size indicates the counts of metabolites. **b** Ion distribution maps of representative metabolites in the tumor-specific subtypes. Linoleate and (9Z)-Octadecenoic acid are selected from the correlation network T1(PD-L1$^-$CD3$^-$CD8$^-$). dCDP is selected from the correlation network T1(PD-L1$^-$CD3$^-$CD8$^-$) and T2(PD-L1$^+$CD3$^+$CD8$^+$). Succinate shows in the correlation networks T1(PD-L1$^-$CD3$^-$CD8$^-$) and T3. CDP and IMP are selected from the correlation network T3. S-Adenosyl-L-homocysteine is selected from the correlation network T4(PD-L1$^+$). IMP inosine monophosphate, CDP cytidine diphosphate, dCDP 2′-deoxycytidine diphosphate.

associated stress this would cause them would be disproportionate. Patients with documented refusal to participate in research, i.e., patients who refused that their tissue and data is used in retrospective research, had been excluded from the study. The cohort was assembled according to pathology files and validated according to clinical files. The histology of all cases was reassessed in accordance with current World Health Organization guidelines for the diagnosis of LUSC[47]. All tumors were restaged in accordance with the Union for International Cancer Control (UICC) 2017, 8th edition, tumor–node–metastasis (TNM) classification[48]. Disease-specific survival was defined as the duration from the date of diagnosis until death due to LUSC other than other causes. For patient characteristics, see Table 1. A tissue microarray was constructed from formalin-fixed, paraffin-embedded (FFPE) tissue blocks, as described previously[49]. Representative tissue blocks were selected for each tumor after reviewing all available slides per case (hematoxylin and eosin stained), and eight tumor cores were randomly selected from the block by placing digital annotations on the scanned slide. The eight cores were placed on tissue microarray blocks to exclude technical assessment bias.

Patients and tissue samples for the independent neoadjuvant chemotherapy-treated cohort

The NAC-treated cohort comprises 40 cases[26] diagnosed at the Institute of Pathology of the University of Bern between 2000 and 2016. All eligible patients had a pathology-confirmed diagnosis. The NAC-treated cohort was separated into long-term ($n = 19$) and short-term survivors ($n = 21$) according to median overall survival[26]. The cohort included consecutive patients who received at least one cycle of platinum-based chemotherapy prior to resection (Supplementary Table 1). The study was approved by the Cantonal Ethics Commission of the Canton of Bern (KEK 2017-00830), which waived the requirement for a written informed consent from patients. Due to the retrospective nature of the study and reusage of left-over or already collected material, and also due to the significant number of patients already deceased, the requirement for informed consent was waived by the local ethics committee. It was argued that contacting the relatives and the associated stress this would cause them would be disproportionate. Patients with documented refusal to participate in research, i.e., patients who refused that their tissue and data is used in retrospective research, had been excluded from the study. A tissue microarray was constructed from FFPE tissue blocks. The NAC-treated cohort was integrated for an independent study for evaluating the response to chemotherapy of the metabolic subtypes.

High-mass-resolution MALDI-Fourier transform ion cyclotron resonance (FT-ICR) IMS

Data for spatial metabolomics of the primary resected LUSC cohort and NAC-treated cohort were obtained from previous studies[26,46]. High-mass-resolution MALDI FT-ICR IMS was performed as previously described[23]. In brief, FFPE sections (4 µm) were mounted onto indium–tin–oxide (ITO)-coated glass slides (Bruker Daltonik). The air-dried tissue sections were spray-coated with 10 mg/mL 9-aminoacridine hydrochloride monohydrate matrix (Sigma-Aldrich) in methanol (70%) using the SunCollect sprayer (Sunchrom). Spray-coating of the matrix was conducted in eight passes, utilizing a line distance of 2 mm and a spray velocity of 900 mm/min.

Metabolites were detected in negative-ion mode on a 7 T Solarix XR FT-ICR mass spectrometer (Bruker Daltonik) equipped with a dual electrospray ionization MALDI (ESI-MALDI) source and a SmartBeam-II Nd:YAG (355 nm) laser. The SCiLS Lab software 2020b was used to export the selected peaks of the mass spectra as processed and root mean square-normalized imzML files. Peak annotations were based on accurate mass matching with the Human Metabolome Database (HMDB) (https://hmdb.ca/) and Kyoto Encyclopedia of Genes and Genomes (KEGG) database (https://www.genome.jp/kegg/).

Immunophenotype-guided IMS and data processing

The SPACiAL workflow was used as previously described[25] to automatically annotate tumor and stroma regions in LUSC tissues in the primary resected cohort and NAC-treated cohort (Supplementary Fig. 4). SPACiAL is a computational multimodal workflow that includes a series of image and MALDI data processing steps to combine molecular imaging data with multiplex immunofluorescence. First, after MALDI–IMS analysis, the 9-aminoacridine matrix was removed from tissue sections, followed by immunofluorescence staining. Double staining of the TMA was performed using the epithelial marker pan-cytokeratin [monoclonal mouse pan-cytokeratin plus (AE1/AE3þ8/18), 1:75, catalog no. CM162; Biocare Medical] and vimentin (Abcam, clone ab92547, 1:500). Second, single-channel images of pan-cytokeratin and vimentin were used to annotate and separate tumor and stroma using fluorescence imaging. Regions positive for pan-cytokeratin were defined as tumor. Regions negative for pan-cytokeratin but positive for vimentin were defined as stroma; third, the digitized and co-registered fluorescence images were scaled to match the exact MALDI resolution and converted into numerical matrices comprised of values corresponding to the lightness values for each pixel; fourth, objective tissue annotations were assigned based on semantics and function. The annotatable patient cases formed the basis of our calculations. The entire workflow is applied to the same tissue section, allowing for the automatic integration of morphological and spatial metabolomics data for thousands of molecules.

Immunohistochemistry (IHC)

IHC staining for cluster of differentiation 3 (CD3), cluster of differentiation 8 (CD8), and programmed death ligand 1 (PD-L1) was performed as previously described[49] on consecutive sections. In brief, an automated immunostainer (Bond III, Leica Bio-systems) with anti-CD3 (Abcam Cambridge; clone SP7, 1:400, RRID: AB_443425), anti-CD8 (Dako, clone C8/144B, 1:100, RRID: AB_2075537), and anti-PD-L1 (Cell Signaling Technology, clone E1L3N, 1:400, RRID: AB_2687655) was used. CD3 and CD8

Stroma-specific dataset

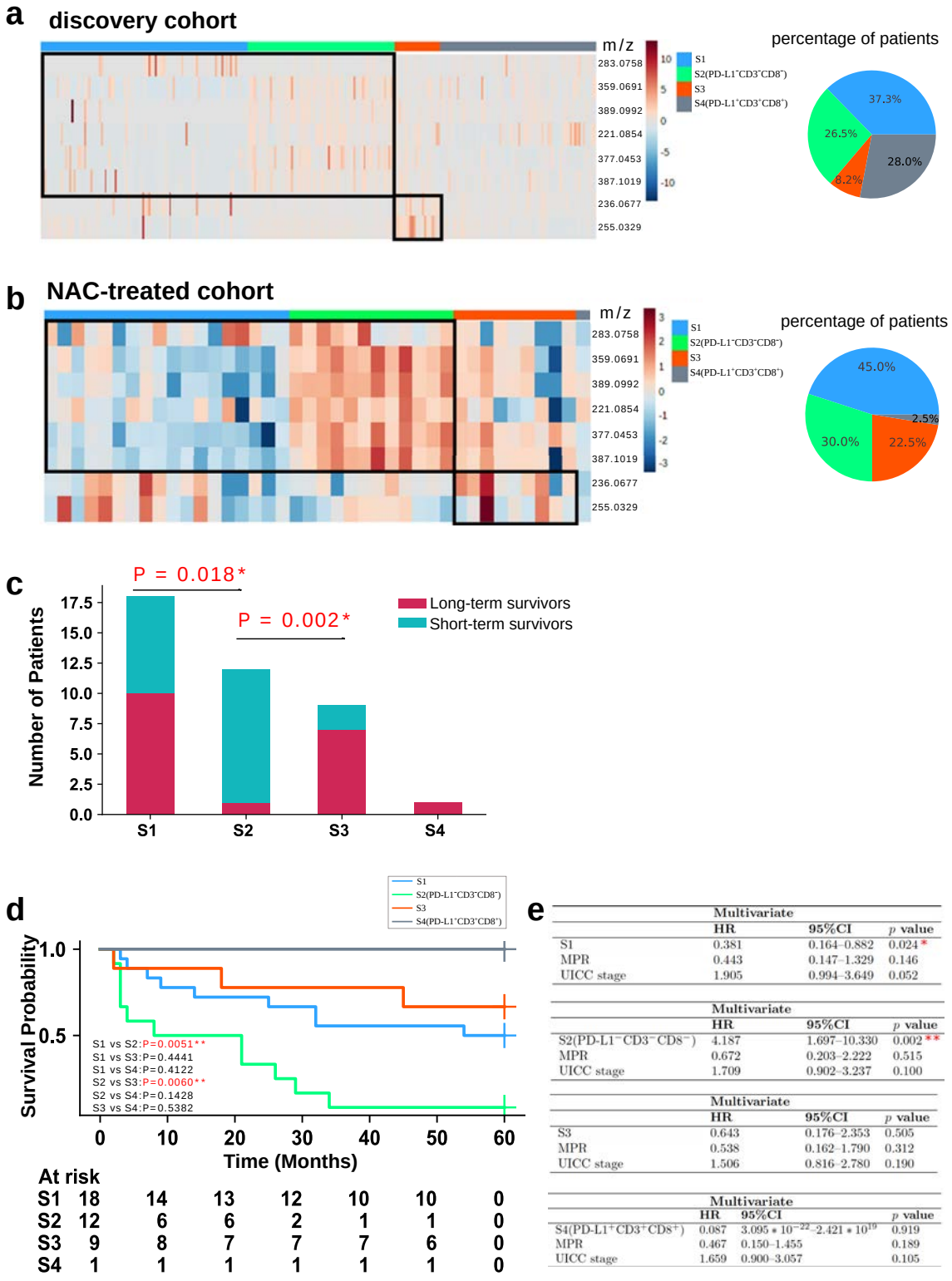

e

Multivariate			
	HR	95%CI	*p* value
S1	0.381	0.164–0.882	0.024 *
MPR	0.443	0.147–1.329	0.146
UICC stage	1.905	0.994–3.649	0.052

Multivariate			
	HR	95%CI	*p* value
S2(PD-L1⁻CD3⁻CD8⁻)	4.187	1.697–10.330	0.002 **
MPR	0.672	0.203–2.222	0.515
UICC stage	1.709	0.902–3.237	0.100

Multivariate			
	HR	95%CI	*p* value
S3	0.643	0.176–2.353	0.505
MPR	0.538	0.162–1.790	0.312
UICC stage	1.506	0.816–2.780	0.190

Multivariate			
	HR	95%CI	*p* value
S4(PD-L1⁺CD3⁺CD8⁺)	0.087	$3.095 * 10^{-22}$–$2.421 * 10^{19}$	0.919
MPR	0.467	0.150–1.455	0.189
UICC stage	1.659	0.900–3.057	0.105

Fig. 5 Association with chemotherapy response in the stroma-specific subtypes. Heatmap illustrating the abundance of metabolites shows stroma-specific subtype classification (**a**, left) in the discovery cohort and (**b**, left) NAC-treated cohort. The percentage of patients in the stroma-specific subtypes in the discovery cohort (**a**, right) and NAC-treated cohort (**b**, right). **c** Numbers of long-term survivors (chemotherapy-sensitive patients) and short-term survivors (chemotherapy-resistant patients) in the stroma-specific subtypes. Two-sided *p* value was calculated by Fisher's exact test. **d** Survival comparison using log-rank test between overall and pairwise subtypes. **e** Multivariate Cox proportional hazard analysis for each of the stroma-specific subtypes, MPR as well as UICC stage. S1 and S2(PD-L1⁻CD3⁻CD8⁻) remain significant in multivariate analysis. * represents two-sided $p < 0.05$, ** represents two-sided $p < 0.01$, *** represents two-sided $p < 0.001$.

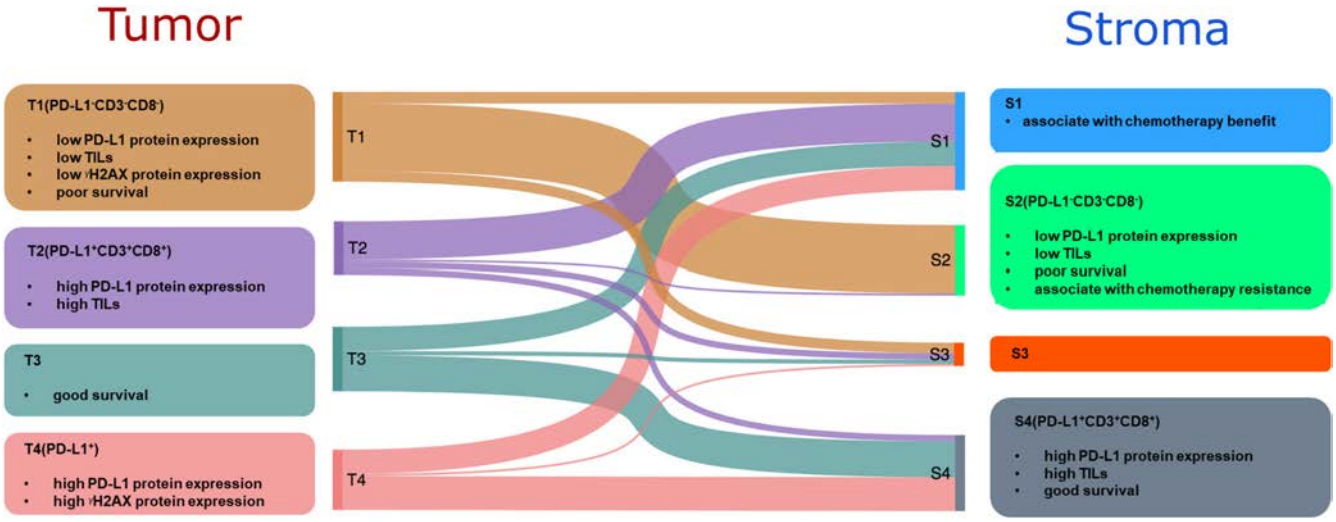

Fig. 6 Summary of characteristics of the four tumor-specific and four stroma-specific LUSC patient subtypes. CD3: cluster of differentiation 3, CD8: cluster of differentiation 8, PD-L1: programmed death ligand 1, γH2AX: DNA damage marker.

expression was determined using image analysis (Aperio Image Scope) and adjusted for core completeness. PD-L1 expression was assessed by a pathologist (S. Berezowska) as the proportion of positive tumor cells.

Immunofluorescence analysis of γH2AX

Immunofluorescence analysis of γH2AX expression was achieved using primary antibodies against pH2A.X (Cell Signaling Technology; catalog no. 2577, 1:400, RRID: AB_2118010) and pan-cytokeratin [monoclonal mouse pan-cytokeratin plus (AE1/AE3þ8/18), 1:75, catalog no. CM162; Biocare Medical] on consecutive sections. Slides were digitized at ×20 objective magnification using an Axio Scan.Z1 (Zeiss). Quantification was performed by digital image analysis in Definiens Developer XD2, following a previously published procedure[50]. The quantified parameter was the proportion of γH2AX- and pan-cytokeratin-positive cells to the total number of pan-cytokeratin-positive cells.

Consensus clustering

Consensus clustering was conducted using the 'ConcensusClusterPlus' package in R using HMDB-annotated metabolites to explore LUSC subtypes based on the patient sample matrix. The consensus matrix was used to check cluster co-occurrence, find intrinsic groupings over variation in different numbers of clusters, and use hierarchical clustering on the distance matrix. We used a prespecified subsampling parameter of 80% with 1000 iterations and assigned the number of potential clusters (K) to range from 2 to 10 in order to avoid producing an excessive number of clusters that would not be clinically useful. The matrix was arranged so that samples belonging to the same cluster were adjacent to each other.

Correlation network analysis and quantitative pathway analysis

Correlation networks were created using Cytoscape (v. 3.8.0). All networks were visualized using the absolute value of the correlation coefficient calculated by Spearman's rank-order correlation. Metabolites with at least one significant correlation are shown ($p < 0.001$). Quantitative pathway analysis was performed via the KEGG database using the MetaboAnalyst online tool (www.metaboanalyst.ca) based on the correlated metabolites.

Statistical analysis

All statistical tests were conducted using Python or R. Correlations were calculated using Spearman's rank-order correlation. The significance of differences in clinicopathological characteristics among tumor- and stroma-specific subtypes was evaluated by chi-squared test or Fisher's exact test. To determine the intensity of differences of representative metabolites, Kruskal–Wallis test and post hoc Dunn's multiple comparison test were used in conjunction with Benjamini–Hochberg correction. Further comparisons to identify the statistical significance of differences in patient survival were performed using the Kaplan–Meier curve and the log-rank test. Multivariate survival analysis was performed using Cox proportional hazard regression model. A two-sided p value of <0.05 was considered statistically significant.

Reporting summary

Further information on research design is available in the Nature Research Reporting Summary linked to this article.

DATA AVAILABILITY

The datasets generated during and/or analyzed during the current study are available from the corresponding author on reasonable request. Full microscopy image datasets are deposited in BioStudies under the accession number S-BIAD814 at https://www.ebi.ac.uk/biostudies/bioimages/studies/S-BIAD814.

Received: 5 January 2023; Accepted: 8 August 2023;
Published online: 02 November 2023

REFERENCES

1. Bade, B. C. & Dela Cruz, C. S. Lung cancer 2020: epidemiology, etiology, and prevention. *Clin. Chest Med.* **41**, 1–24 (2020).
2. Rizvi, N. A. et al. Nivolumab in combination with platinum-based doublet chemotherapy for first-line treatment of advanced non-small-cell lung cancer. *J. Clin. Oncol.* **34**, 2969–2979 (2016).
3. Hirsch, F. R. et al. Lung cancer: current therapies and new targeted treatments. *Lancet* **389**, 299–311 (2017).
4. Kulasingam, V. & Diamandis, E. P. Strategies for discovering novel cancer biomarkers through utilization of emerging technologies. *Nat. Clin. Pr. Oncol.* **5**, 588–599 (2008).
5. Garon, E. B. et al. Pembrolizumab for the treatment of non-small-cell lung cancer. *N. Engl. J. Med.* **372**, 2018–2028 (2015).
6. Cancer Genome Atlas Research, N. Comprehensive genomic characterization of squamous cell lung cancers. *Nature* **489**, 519–525 (2012).

7. Chen, F. et al. Multiplatform-based molecular subtypes of non-small-cell lung cancer. *Oncogene* **36**, 1384–1393 (2017).
8. Wilkerson, M. D. et al. Lung squamous cell carcinoma mRNA expression subtypes are reproducible, clinically important, and correspond to normal cell types. *Clin. Cancer Res.* **16**, 4864–4875 (2010).
9. Fu, D., Zhang, B., Yang, L., Huang, S. & Xin, W. Development of an immune-related risk signature for predicting prognosis in lung squamous cell carcinoma. *Front. Genet.* **11**, 978 (2020).
10. Li, X. S. et al. Molecular subtypes based on DNA methylation predict prognosis in lung squamous cell carcinoma. *BMC Cancer* **21**, 96 (2021).
11. Stewart, P. A. et al. Proteogenomic landscape of squamous cell lung cancer. *Nat. Commun.* **10**, 3578 (2019).
12. Satpathy, S. et al. A proteogenomic portrait of lung squamous cell carcinoma. *Cell* **184**, 4348–4371.e4340 (2021).
13. Flaherty, K. T. et al. Molecular landscape and actionable alterations in a genomically guided cancer clinical trial: National Cancer Institute Molecular Analysis for Therapy Choice (NCI-MATCH). *J. Clin. Oncol.* **38**, 3883–3894 (2020).
14. Paik, P. K., Pillai, R. N., Lathan, C. S., Velasco, S. A. & Papadimitrakopoulou, V. New treatment options in advanced squamous cell lung cancer. *Am. Soc. Clin. Oncol. Educ. Book* **39**, e198–e206 (2019).
15. Shien, K., Papadimitrakopoulou, V. A. & Wistuba, I. I. Predictive biomarkers of response to PD-1/PD-L1 immune checkpoint inhibitors in non-small cell lung cancer. *Lung Cancer* **99**, 79–87 (2016).
16. Chae, Y. K. et al. Biomarkers for PD-1/PD-L1 blockade therapy in non-small-cell lung cancer: is PD-L1 expression a good marker for patient selection? *Clin. Lung Cancer* **17**, 350–361 (2016).
17. Newman, A. M. et al. Robust enumeration of cell subsets from tissue expression profiles. *Nat. Methods* **12**, 453–457 (2015).
18. Kamphorst, A. O. et al. Proliferation of PD-1+ CD8 T cells in peripheral blood after PD-1-targeted therapy in lung cancer patients. *Proc. Natl Acad. Sci. USA* **114**, 4993–4998 (2017).
19. Miller, H. A., van Berkel, V. H. & Frieboes, H. B. Lung cancer survival prediction and biomarker identification with an ensemble machine learning analysis of tumor core biopsy metabolomic data. *Metabolomics* **18**, 57 (2022).
20. Miller, H. A. et al. Lung cancer metabolomic data from tumor core biopsies enables risk-score calculation for progression-free and overall survival. *Metabolomics* **18**, 31 (2022).
21. Neumann, J. M. et al. Subtyping non-small cell lung cancer by histology-guided spatial metabolomics. *J. Cancer Res. Clin. Oncol.* **148**, 351–360 (2022).
22. Norris, J. L. & Caprioli, R. M. Analysis of tissue specimens by matrix-assisted laser desorption/ionization imaging mass spectrometry in biological and clinical research. *Chem. Rev.* **113**, 2309–2342 (2013).
23. Ly, A. et al. High-mass-resolution MALDI mass spectrometry imaging of metabolites from formalin-fixed paraffin-embedded tissue. *Nat. Protoc.* **11**, 1428–1443 (2016).
24. Buck, A. et al. High-resolution MALDI-FT-ICR MS imaging for the analysis of metabolites from formalin-fixed, paraffin-embedded clinical tissue samples. *J. Pathol.* **237**, 123–132 (2015).
25. Prade, V. M. et al. De novo discovery of metabolic heterogeneity with immunophenotype-guided imaging mass spectrometry. *Mol. Metab.* **36**, 100953 (2020).
26. Shen, J. et al. Spatial metabolomics for evaluating response to neoadjuvant therapy in non-small cell lung cancer patients. *Cancer Commun.* **42**, 517–535 (2022).
27. Wang, J. et al. Spatial metabolomics identifies distinct tumor-specific subtypes in gastric cancer patients. *Clin. Cancer Res.* **28**, 2865–2877 (2022).
28. Lambrechts, D. et al. Phenotype molding of stromal cells in the lung tumor microenvironment. *Nat. Med.* **24**, 1277 (2018).
29. Gay, C. M. et al. Patterns of transcription factor programs and immune pathway activation define four major subtypes of SCLC with distinct therapeutic vulnerabilities. *Cancer Cell* **39**, 346 (2021).
30. Kelly, R. J. et al. A phase I/II study of sepantronium bromide (YM155, survivin suppressor) with paclitaxel and carboplatin in patients with advanced non-small-cell lung cancer. *Ann. Oncol.* **24**, 2601–2606 (2013).
31. Karachaliou, N., Fernandez-Bruno, M. & Rosell, R. Strategies for first-line immunotherapy in squamous cell lung cancer: are combinations a game changer? *Transl. Lung Cancer R.* **7**, S198–S201 (2018).
32. Xu-Monette, Z. Y., Zhang, M. Z., Li, J. Y. & Young, K. H. PD-1/PD-L1 blockade: have we found the key to unleash the antitumor immune response? *Front. Immunol.* **8**, 1597 (2017).
33. Motz, G. T. & Coukos, G. Deciphering and reversing tumor immune suppression. *Immunity* **39**, 61–73 (2013).
34. Teng, M. W. L., Ngiow, S. F., Ribas, A. & Smyth, M. J. Classifying cancers based on T-cell infiltration and PD-L1. *Cancer Res.* **75**, 2139–2145 (2015).
35. Mazzaschi, G. et al. Low PD-1 expression in cytotoxic CD8(+) tumor-infiltrating lymphocytes confers an immune-privileged tissue microenvironment in NSCLC with a prognostic and predictive value. *Clin. Cancer Res.* **24**, 407–419 (2018).
36. Velcheti, V. et al. Programmed death ligand-1 expression in non-small cell lung cancer. *Lab Invest* **94**, 107–116 (2014).
37. Zhang, Y., Huang, S. D., Gong, D. J., Qin, Y. H. & Shen, Q. A. Programmed death-1 upregulation is correlated with dysfunction of tumor-infiltrating CD8(+) T lymphocytes in human non-small cell lung cancer. *Cell Mol. Immunol.* **7**, 389–395 (2010).
38. Konishi, J. et al. B7-h1 expression on non-small cell lung cancer cells and its relationship with tumor-infiltrating lymphocytes and their PD-1 expression. *Clin. Cancer Res.* **10**, 5094–5100 (2004).
39. Cui, S. H., Dong, L. L., Qian, J. L., Ye, L. & Jiang, L. Y. Classifying non-small cell lung cancer by status of programmed cell death ligand 1 and tumor-infiltrating lymphocytes on tumor cells. *J. Cancer* **9**, 129–134 (2018).
40. Vettore, L., Westbrook, R. L. & Tennant, D. A. New aspects of amino acid metabolism in cancer. *Br. J. Cancer* **122**, 150–156 (2020).
41. Lord, C. J. & Ashworth, A. The DNA damage response and cancer therapy. *Nature* **481**, 287–294 (2012).
42. Dang, C. V. Links between metabolism and cancer. *Gene Dev.* **26**, 877–890 (2012).
43. Wojakowska, A. et al. Detection of metabolites discriminating subtypes of thyroid cancer: molecular profiling of FFPE samples using the GC/MS approach. *Mol. Cell Endocrinol.* **417**, 149–157 (2015).
44. Yuan, M., Breitkopf, S. B., Yang, X. & Asara, J. M. A positive/negative ion-switching, targeted mass spectrometry-based metabolomics platform for bodily fluids, cells, and fresh and fixed tissue. *Nat. Protoc.* **7**, 872–881 (2012).
45. Neef, S. K. et al. Optimized protocol for metabolomic and lipidomic profiling in formalin-fixed paraffin-embedded kidney tissue by LC-MS. *Anal. Chim. Acta* **1134**, 125–135 (2020).
46. Kunzke, T. et al. Patterns of carbon-bound exogenous compounds in patients with lung cancer and association with disease pathophysiology. *Cancer Res.* **81**, (2021).
47. WHO Classification of Tumours Editorial Board. Thoracic Tumours. *International Agency for Research on Cancer* (2021).
48. Neppl, C. et al. Comparison of the 7th and 8th edition of the UICC/AJCC TNM staging system in primary resected squamous cell carcinomas of the lung—a single center analysis of 354 cases. *Front. Med.* **6**, 196 (2019).
49. Keller, M. D. et al. Adverse prognostic value of PD-L1 expression in primary resected pulmonary squamous cell carcinomas and paired mediastinal lymph node metastases. *Mod. Pathol.* **31**, 101–110 (2018).
50. Feuchtinger, A. et al. Image analysis of immunohistochemistry is superior to visual scoring as shown for patient outcome of esophageal adenocarcinoma. *Histochem Cell Biol.* **143**, 1–9 (2015).

ACKNOWLEDGEMENTS

The authors thank Ulrike Buchholz, Claudia-Mareike Pflüger, Cristina Hübner Freitas, and Andreas Voss for excellent technical assistance. The study was supported by the Ministry of Education and Research of the Federal Republic of Germany [BMBF; 01ZX1610B and 01KT1615] to A.W.; the Deutsche Forschungsgmeinschaft [SFB 824 C4, CRC/Transregio 205/1] to A.W.; and the China Scholarship Council (No. 201906210076) to J.W.

AUTHOR CONTRIBUTIONS

A.W., S.B., J.W. and N.S. conceived the study design. J.W. wrote the original manuscript. N.S., J.S., T.K. and P.Z. performed sample preparation and measurements. J.W. performed bioinformatics analysis and statistical analysis. N.S., T.K., J.S., V.M.P. and A.F. contributed to bioinformatics assistance. S.B. performed histological review for lung LUSC. A.W. and S.B. acquired ethical permission, collected the samples. A.W., N.S. and S.B. provided overall study oversight. All authors contributed to review and approval of the manuscript.

FUNDING

Open Access funding enabled and organized by Projekt DEAL

COMPETING INTERESTS

The authors declare no competing interests.

ADDITIONAL INFORMATION

Supplementary information The online version contains supplementary material available at https://doi.org/10.1038/s41698-023-00434-4.

Correspondence and requests for materials should be addressed to Sabina Berezowska or Axel Walch.

Reprints and permission information is available at http://www.nature.com/reprints

Publisher's note Springer Nature remains neutral with regard to jurisdictional claims in published maps and institutional affiliations.

Part V

Discussion

7 Cancer Metabolomics and Clinical Therapy

The aim of this thesis was to examine the association between spatial metabolomics and clinically significant factors, including prognosis and therapy prediction, in patients diagnosed with gastric cancer (GC) and lung squamous cell carcinoma (SCC). Using a combination of clustering analysis and MALDI-IMS technology, this study successfully identified metabolic profile-based subtypes in both GC and SCC patients. The primary focus of the first published study was to stratify GC patients based on spatial metabolomics. As a result, the application of spatial metabolomics facilitated the stratification of GC patients, leading to the identification of tumor and stroma-specific metabolic subtypes. Furthermore, an independent validation cohort demonstrated that one specific tumor-specific subtype exhibited a unique benefit from trastuzumab therapy. The second published study aimed to stratify SCC patients based on spatial metabolomics and successfully established tumor and stroma-specific metabolic subtypes. Additionally, the application of an independent cohort revealed that one stroma-specific subtype was uniquely associated with resistance to chemotherapy, while the other two stroma-specific subtypes were associated with a benefit from chemotherapy. Overall, the identification of these metabolic subtypes provides a complementary approach to patient stratification in both GC and SCC.

Our results from the patient stratification of GC and SCC demonstrate that metabolite patterns in tumor-specific and stroma-specific regions within the same patient can convey distinct information. In SCC, notable differences outweigh the similarities between tumor-specific and stroma-specific subtypes, exhibiting substantial variation in patient distribution, except for a large overlap between the T1 subtype and the S2 subtype. Conversely, unique SCC subtypes specific to tumors and the stroma exhibit equivalent significance regarding their clinical prognosis value. In contrast, for GC, there are noteworthy similarities in patient distribution

and their association with clinical molecular features between tumor-specific and stroma-specific subtypes. In this context, the tumor-specific metabolic signature holds greater importance than the stroma-specific metabolic signature in relation to their association with clinical relevance in GC.

7.1 Metabolic subtypes for personalized therapy

This thesis showed that metabolic subtypes with distinct tissue metabolite patterns can be identified in both the first GC study and the second SCC study. In the first GC study, three distinct tumor-specific subtypes, which includes T1(HER2$^+$MIB$^+$CD3$^+$), T2(HER2$^-$MIB$^-$CD3$^-$) and T3(pEGFR$^+$), and three stroma-specific subtypes, which includes S1(FOXP3$^-$), S2(HER2$^-$MIB$^-$CD3$^-$) and S3(HER2$^+$MIB$^+$CD3$^+$FOXP3$^+$) were defined. T1(HER2$^+$MIB$^+$CD3$^+$) was characterized by high immune cell infiltration, presence of Epstein–Barr virus (EBV), high microsatellite instability (MSI), earlier UICC stage, nucleotide metabolism, and favorable prognosis. In contrast, T2(HER2$^-$MIB$^-$CD3$^-$) was characterized by low immune cell infiltration, absence of EBV, low MSI, later UICC stage and poor prognosis; T3(pEGFR$^+$) was characterized by high pEGFR. In the second SCC study, we defined four distinct tumor-specific subtypes, which includes T1(PD-L1$^-$CD3$^-$CD8$^-$), T2(PD-L1$^+$CD3$^+$CD8$^+$), T3, and T4(PD-L1$^+$), and four stroma-specific subtypes, which includes S1, S2(PD-L1$^-$CD3$^-$CD8$^-$), S3 and S4(PD-L1$^+$CD3$^+$CD8$^+$). T1(PD-L1$^-$CD3$^-$CD8$^-$) was characterized by low immune cell infiltration, low PD-L1 expression and poor prognosis. In contrast, T2(PD-L1$^+$CD3$^+$CD8$^+$) was characterized by high immune cell infiltration, high PD-L1 expression and good prognosis; T4(PD-L1$^+$), was characterized by high PD-L1 expression.

This thesis showed that the metabolic differences between established subtypes and their associations with molecular features could offer a tool to aid in selecting specific treatment approaches. In the GC study, the application of the independent trastuzumab-treated cohort revealed that the T1(HER2$^+$MIB$^+$CD3$^+$) subtype benefited from trastuzumab therapy. The expression of PD-1 is found on both CD8-positive infiltrated cells and FOXP3$^+$ Treg cells [49]. Tumors with high immune infiltration respond more actively to immunotherapy [91]. Patients with

these characteristics had improved clinical outcomes in the response to immune checkpoint therapy. Some previous studies have demonstrated that PD-1 blockade could be effective in patients with elevated CD8-positive TILs, even with low PD-L1 expression [92, 93, 94]. Thus, this study also indicates other potential treatment benefit in clinical settings, such as PD-L1 blockade, when we look at the strong correlation of clinical biomarker PD-L1 and tumor-infiltrating lymphocyte features with the metabolic subtypes. Additionally, several recent studies found a close relationship of immune checkpoints with EBV^{+} and MSI-H GC [20, 23]. Thus, we expect T1($HER2^{+}MIB^{+}CD3^{+}$) to be predisposed with immune checkpoint inhibitors, such as PD-1 blockade, because of its higher frequency of EBV positivity, microsatellite instability and positive correlation with $CD8^{+}$ T cell infiltration and $FOXP3^{+}$ Treg cells.

In addition, immunotherapy has been successfully added to HER2-directed therapy [24]. A phase 2 trial demonstrated that pembrolizumab could be safely combined with chemotherapy plus trastuzumab in HER2-positive, metastatic gastroesophageal adenocarcinoma. Notably, there was an impressive 91% response rate and a median overall survival of 27.3 months, which were much higher than what was seen with chemotherapy plus trastuzumab with a response rate of 47%, suggesting that there may be a synergistic benefit of combining checkpoint blockade with standard trastuzumab plus chemotherapy. Efficacy is currently being evaluated in the phase 3 KEYNOTE-811 clinical trial [24]. Recently, it showed that adding pembrolizumab to trastuzumab and chemotherapy subtantially reduced tumor size, induced complete responses in some participants, and significantly improved objective response rate chemotherapy in HER2-positive, metastatic gastroesophageal adenocarcinoma. Notably, there was an surprising 74.4% response rate, which was significantly higher than the 47% response rate achieved with chemotherapy plus trastuzumab. These clinical trials demostrated that T1($HER2^{+}MIB^{+}CD3^{+}$) treatment responsiveness may be improved by combining checkpoint blockade with standard chemotherapy plus trastuzumab .

In the SCC study, the application of the independent chemotherapy-treated SCC cohort reveals that our stroma-specific subtypes can further stratify patient responses to chemotherapy, with SCC patients possessing S1 and S3 experiencing better clinical outcomes to chemotherapy than S2(PD-L1^{-}CD3^{-}CD8^{-}) patients. This evidence suggests that the S1 and S3 subtype assignments are associated with a benefit when initiating chemotherapy. To date only immunotherapy has evolved into a successful therapeutic strategy for patients with SCC [95, 96]. Nevertheless, patients' low response rate to PD-1/PD-L1 inhibitors hinders the clinical application [97]. Effective prediction of treatment response to immunotherapy could dramatically enhance this benefit ratio while preventing overtreatment. T2(PD-L1^{+}CD3^{+}CD8^{+}) captures several immunological features that are predictive of immunotherapy response. The predictive biomarker for this immunotherapeutic class is PD-L1 overexpression [29, 59]. Apart from this, TILs is considered a candidate of predictive marker in a wide tumor types [98, 99, 100]. Moreover, previous studies in the related field confirmed a tight correlation between TILs and PD-1 overexpression in NSCLC [101, 102, 103, 104]. Consequently, we expect T2(PD-L1^{+}CD3^{+}CD8^{+}) to be beneficial from immune checkpoint inhibitors, such as PD-1/PD-L1 blockade, because of its positive correlation with PD-L1 expression, CD3^{+} and CD8^{+} TILs. Regarding the T2(PD-L1^{+}CD3^{+}CD8^{+}) subtype, which includes low expression of CD3 and CD8 molecular features, are known to have a favorable prognosis and PD-L1-negative tumors that resist to PD-L1 blockade. If confirmed in future studies, the molecular classification might be used to identify T2(PD-L1^{+}CD3^{+}CD8^{+}) subtype tumors for directing optimal treatment, such as immune checkpoint inhibitors.

7.2 Potential application of metabolic-based therapies in metabolic subtypes

In general, although determining the responders of metabolic targeted therapies has proven to be challenging, metabolic targeted therapies targeting certain metabolism processes provide alternatives for chemoresistant patients [105, 106]. For instance, glucose metabolism has the potential to guide decisions about neoadjuvant treatment strategies for GC patients [106], in which the changes in glucose metabolism could be determined using fluorodeoxyglucose (FDG)-positron emission tomography (PET) and positron emission tomography-computed tomography (PET-CT) imaging [107]. In the first study of this thesis, compared with T3(pEGFR$^+$) subtype, T1(HER2$^+$MIB$^+$CD3$^+$) and T2(HER2$^-$MIB$^-$CD3$^-$) subtypes were more active in metabolism. Some key metabolites participated in glucose, fatty acid and glutamine metabolic process were enriched in these two metabolic subtypes. For example, T1(HER2$^+$MIB$^+$CD3$^+$) exhibited upregulation of nucleotide associated metabolites such as guanosine and nucleotide phosphates AMP and GMP. It has been pointed out that these nucleotides are associated with TCA energy metabolism, mainly in the form of ATP and GTP which are an alternative energy source of cancer cell proliferation [108]. Additionally, TCA metabolism are closely linked with amino acids metabolism [109]. It is rather remarkable that T1(HER2$^+$MIB$^+$CD3$^+$) also represents with a specific enrichment of glutamine class metabolites involved in D-glutamine and D-glutamate metabolism. Glutamine was one of the most greatly upregulated tissue metabolites in the non-metastasis group stressed by many researches [110, 111]. Furthermore, a previous study identified the anabolic metabolism of DNA as an essential downstream effect of the HER2 oncogene in breast cancer [112]. DNA metabolism in GC tumor cells was identified as a factor influencing response to HER2-targeted trastuzumab therapy in a previous study. The changes in DNA metabolism found in patient tissues were validated in a corresponding

HER2$^+$/sensitive and HER2$^+$/resistant GC cell model [6]. In the first study of this thesis, our established tumor-specific subtypes can further stratify HER2$^+$ patient into trastuzumab sensitive and trastuzumab resistant patients. This study showed that DNA metabolism was potentially important in response to trastuzumab therapy in HER2$^+$ GC.

As for SCC, the metabolites that are correlated within each subtype comprise different classes of biomolecules, such as nucleotides and amino acids. In addition, amino acids play a role in energy generation, maintaining cellular redox homeostasis and driving the synthesis of nucleic acids. Typically, alongside its association with the DNA damage-related protein, T1(PD-L1$^-$CD3$^-$CD8$^-$) also demonstrates a dense cluster which strongly involves deoxycytidine diphosphate, cytidine diphosphate, uridine diphosphate, 2'-Deoxyinosine 5'-phosphate and cytidine, and cytidine in the metabolite network, which can be interpreted as an involvement in nucleotide metabolism occurring in response to DNA damage. Thus, the metabolic subtypes might potentially serve as a metabolic therapeutic target in GC and SCC treatment. Thus, utilizing metabolomics could be also considered to be a promising tool to assess the sensitivity of chemotherapy in virtual conditions and discovering therapeutic targets regarding specific tumor metabolism.

In conclusion, both two studies successfully identified tumor- and stroma-specific metabolic subtypes, and the identification of these metabolic subtypes may serve as a valuable adjunct to current metabolic subtyping approach and help to increase understanding on advancing the patient stratification approach in GC and SCC. Independent cohorts further confirmed that those established metabolic subtypes were associated with clinical therapy response. We hope these results will potentially facilitate the development of clinical trials to explore therapies in defined sets of patients, ultimately improving survival from this deadly disease. Importantly, the scope of a landscape study such as this necessitates that it be understood as hypothesis-generating, and a wider community effort will be required to validate biological

observations and suggested therapeutic alternatives. With the development of molecular detection biotechnology and our understanding of metabolic perturbation in cancer grows, the molecular classification of GC and SCC for associating therapy response will undoubtedly be more precise. Thus, if confirmed and extended in future studies, the classification of GC and SCC reported here may benefit development of therapies tailored to the molecular subtypes. Ultimately, the future cancer treatment would be a clinical-pathological-molecular combined classification and guided individualized approach.

8 Advantages of studies

This study demonstrates for the first time that specific tumor- and stroma-specific classification models could be developed in patients diagnosed with GC and SCC based on tissue metabolomics. The studies of GC and SCC included a total of 362 and 330 patients respectively. The inclusion of a large number of patient samples enhances the reliability and statistical robustness of the results. Additionally, the classification models employed in both studies effectively separate between tumor epithelial cells and stromal cells in patients diagnosed with GC and SCC. This distinction is crucial as many well-established large-scale classification researches did not take into account the exact influence of active, nonmalignant stromal cells [40, 45]. Actually, not only molecular expression profiles deriving from mixed regions of tumor tissues may influence assignment to a specific molecular category, thus creating interpretative troubles, but also novel stroma-based distinctive signatures have been proposed and related to the predominant cancer phenotype [113]. As we found in this project, both tumor and stroma regions play important roles in the GC and SCC stratification, which could be confirmed by the tumor-specific subtype associations for several immune-related markers, including PD-L1, CD3, and CD8, being retained in the stroma-specific subtypes. However, it can be concluded that the tumor and stromal metabolite subtypes exhibit notable differences in patients with GC and SCC in terms of their clinical relevance and impact on survival outcomes. For example, in the first GC study, T1($HER2^+MIB^+CD3^+$) and S3($HER2^+MIB^+CD3^+FOXP3^+$) share a large proportion of common patients with a similar metabolite signature, but result in a difference correlated with histological parameter and clinical parameter. In the second SCC study, stroma-specific subtypes were confirmed to be associated with chemotherapy response, while tumor metabolite signatures were not. This represents that tumor and stroma-specific metabolite pattern would convey different information even if in the same patient individual. So identification of features should be more precise to tumor or stroma

area rather than based on mixed tumor and stroma tissues. From our results we conclude that patterns of moleculars and clinical features in metabolites classification constitute robust surrogate signals for different biochemical processes, which enable a separation of phenotypic metabolic subtypes together with histology. Region-based subtype from the same patient cohort also reveals different prognosis value. Tumor dataset generates a new prognosis-related subtype called T2(HER2^{-}MIB^{-}CD3^{-}) which consists of a larger proportion GC patients in the late stage along with more metastasis status and as a consequence result in short survival, but none significance was found in its related stroma subtype S2(HER2^{-}MIB^{-}CD3^{-}).

9 Limitations of studies

Using FFPE TMAs in this thesis offers a significant advantage as it allows for the direct detection and visualization of metabolites, enabling their assignment to specific tumor or stroma types within their native histological context. Compared to fresh frozen samples, FFPE TMAs exhibit superior preservation of tissue morphology and cellular structures, facilitating more accurate classification of metabolite content in tumors and stroma [81]. This is essential for histopathological examination, where pathologists need to visually inspect tissue samples to make diagnostic assessments. In many clinical settings, FFPE samples are readily available as they are routinely collected during diagnostic procedures such as biopsies and surgeries. Fresh frozen tissue samples require immediate processing and are not as easily accessible. However, it should be noted that a drawback of using FFPE TMAs is the reduced or eliminated intensity of hydrophobic molecules. Previous research has indicated a decline in peak intensities for metabolites in the higher mass range (m/z 600 and above), although metabolite peaks in the low mass range (m/z 50-400) remain comparable to those in fresh frozen tissue [76]. The loss of hydrophobic molecules, such as lipids, can be attributed to the tissue embedding process and the removal of paraffin wax using solvents, but there are certain classes of metabolites preserved both chemically and spatially in FFPE tissue specimens [81]. Additionally, numerous mass spectrometry studies, including those utilizing liquid- and gas-chromatography MS, have demonstrated reliable retention of metabolites in FFPE tissue samples [114, 115]. A recently published protocol for metabolomic and lipidomic profiling in FFPE kidney tissue using LC-MS, followed by the detection of selected lipid species through an independent in situ MS imaging approach, highlights the complementary use of both techniques [116].

Regarding the challenges of MALDI–IMS as a tool in basic research, several issues can not be ignored. Metabolite annotation is the process of finding molecules represented in MS dataset and it is a key challenge

in untargeted metabolomics, including IMS–based spatial metabolomics [117]. In MALDI–IMS, this gap exists due to our limited understanding of ionization pathways or principles of how an analyte forms a signal. MALDI–IMS cannot resolve isomeric molecules as well, but this limitation could be improved by using tandem MS to some degree [117]. Although MS/MS cannot reconstruct the molecular structure completely, it reduces potential ambiguity, as an MS/MS spectrum encodes additional structural information that is missed in MALDI–IMS [118]. In addition, the spatial resolution of MALDI–IMS is often in the range of tens to hundreds of micrometers. Although the spatial resolution is higher than other IMS technologies, such as desorption electrospray ionization mass spectrometry imaging, this is still limited and may not be sufficient to resolve cellular or subcellular structures in highly heterogeneous samples [119].

Opening questions 10

Opening questions should also be acknowledged. Firstly, these classifications are based on a highly complex methodology. The accurate translation of these intricate classifications in the clinical setting requires further validation through larger-scale studies. Such rigorous validation efforts are essential for achieving a universally accepted and standardized classification system in the clinical field. Secondly, different subgroups identified across various molecular level studies need to be aggregated. Cancer is a complex and multifaceted condition with diverse molecular and cellular alterations. Different -omics methods capture distinct aspects of cancer biology. Genomics provides information about the genetic mutations underlying cancer, transcriptomics reveals gene expression patterns, proteomics identifies the proteins level. Metabolomics is located downstream of genomics, transcriptomics, and proteomics. It maps the complete metabolic changes under specific conditions associated with pathogenic factors, host factors, or environmental co-effectors. Integrating these data sources allows researchers to fill gaps in their understanding by combining complementary information. In addition, metabolites often serve as early indicators of disease or therapeutic effects, and integrating metabolomics data with genomic or proteomic data can enhance the precision of biomarker discovery. By the above interpretation, it is evident that while significant progress has been made in defining various genomic and transcriptomic subtypes, it is essential to integrate metabolomics with other -omics methods. It allows for a systems biology perspective, which views cancer as a dynamic, interconnected system rather than isolated genetic or metabolic events and provides a more comprehensive and holistic understanding of the disease. Thus, a collaborative international effort should be undertaken to aggregate a consensus classification by integrated multiomic approaches, enabling more precise prognosis prediction of targeted inhibitors, and a more integrated understanding of underlying cancer development and progression.

Part VI

Conclusion

In summary, this dissertation indicates that metabolically distinct subtypes can be identified based on tissue metabolomics and are associated with prognosis and therapy response in GC and SCC. Patient subtypes derived by tissue-based spatial metabolomics are a valuable addition to existing molecular classification systems in GC and SCC. The deep-information of metabolomics will not only benefit the therapy response at the molecular level but also improve our understanding of the initiation and development of GC and SCC. Overall, these classifications may provide molecular subtyping framework for preclinical, clinical and translational studies of GC and SCC to find effectively targeted agents and explore therapies in defined sets of patients, ultimately improving survival from these deadly diseases in the future.

Part VII

Appendix

List of Publications

A

List of peer-reviewed first-author publications included in this thesis:

Jun Wang, Thomas Kunzke, Verena M. Prade, Jian Shen, Achim Buck, Annette Feuchtinger, Ivonne Haffner, Birgit Luber, Drolaiz HW Liu, Rupert Langer, Florian Lordick, Na Sun, and Axel Walch. Spatial metabolomics identifies distinct tumor-specific subtypes in gastric cancer patients. *Clinical Cancer Research*, 2022; 28(13):2865-2877.
IF: 13.801 (2022)

Jun Wang*, Na Sun*, Thomas Kunzke, Jian Shen, Achim Buck, Annette Feuchtinger, Ivonne Haffner, Birgit Luber, Drolaiz HW Liu, Rupert Langer, Florian Lordick, and Axel Walch. Spatial metabolomics identifies distinct tumor-specific and stroma-specific subtypes in patients with lung squamous cell carcinoma. *npj precision oncology*, 2023; 7(114).
IF: 10.092 (2022)

List of first-author publications not included in this thesis:

Jian Shen*, Na Sun*, **Jun Wang***, Philipp Zens, Thomas Kunzke, Achim Buck, Verena M Prade, Qian Wang, Annette Feuchtinger, Sabina Berezowska, Axel Walch. Patterns of carbon-bound exogenous compounds impact disease pathophysiology in lung cancer subtypes in different ways. *ACS nano*, 2023; 17(17): 16396-16411.
IF: 18.027 (2022)

Jun Wang*, Na Sun*, Thomas Kunzke, et al. Metabolic heterogeneity affects trastuzumab response and survival in HER2-positive advanced gastric cancer. *British Journal of Cancer*, 2024: 1-10.
IF: 9.075 (2022)
* represents authors contributed equally to this work.

List of co-author publications not included in this thesis:

Jian Shen*, Na Sun*, **Jun Wang**, Philipp Zens, Chaoyang Zhang,Thomas Kunzke, Achim Buck, Verena M. Prade, Qian Wang, Annette Feuchtinger, Sabina Berezowska, Axel Walch. Identification of metabolic subtypes of lung adenocarcinoma brain metastases for the development of personalized targeted treatment strategies. (Submitted)

Jian Shen*, Na Sun*, Philipp Zens,Thomas Kunzke, Achim Buck, Verena M. Prade, **Jun Wang**, et al. Metabolic constitution is superior to pathological assessment for evaluating response to neoadjuvant chemotherapy of non-small cell lung cancer patients. *Cancer Communications*, 2022; 42(6): 517–535.
IF: 15.283 (2022)

Twinkle Vohra, Elisabeth Kemter, Na Sun, Britta Dobenecker, Arne Hinrichs, Jacopo Burrello, Elise P. Gomez-Sanchez, Celso EGomez-Sanchez, **Jun Wang**, et al. Effect of Dietary Sodium Modulation on Pig Adrenal Steroidogenesis and Transcriptome Profiles. *Hypertension*, 2020; 76(6):1769-1777.
IF: 10.190 (2022)

Qian Wang*, Na Sun*, Thomas Kunzke, Achim Buck, Jian Shen, Verena M. Prade, Barbara Stöckl, **Jun Wang**, Annette Feuchtinger, and Axel Walch. A simple preparation step to remove excess liquid lipids in white adipose tissue enabling an improved detection of metabolites via MALDI-FTICR imaging MS. *Histochemistry and Cell Biology*, 2022; 157(5):595-605.
IF: 2.531 (2022)

Qian Wang, Na Sun, Raphael Meixner, Ronan Le Gleut, Thomas Kunzke, Annette Feuchtinger, **Jun Wang**, et al. Metabolic heterogeneity in adrenocortical carcinoma impacts patient outcomes. *JCI insight*, 2023; 8(16):e167007.
IF: 8.0 (2022)

Approval letters from publishers

B

1. the first publication published in the Clinical Cancer Research journal

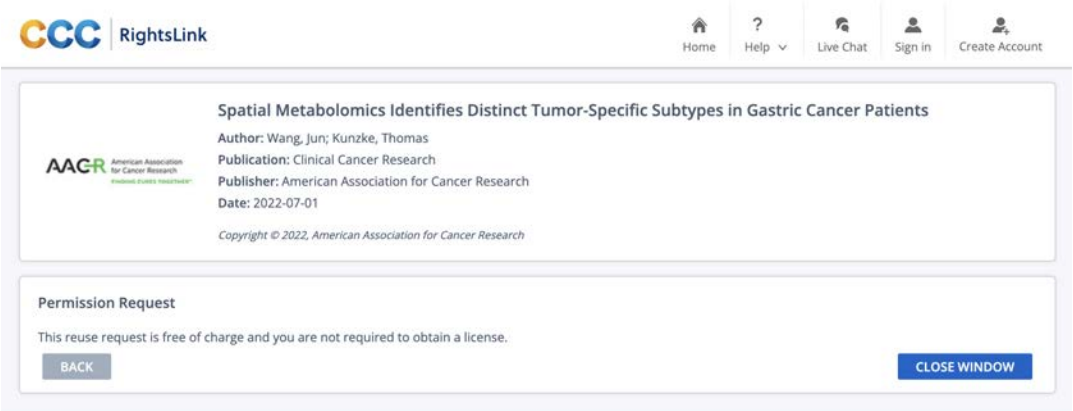

Fig. B.1. Approval letter for the publication in the Clinical Cancer Research [1]. Copyright 2022, American Association for Cancer Research.

2. the second publication published in the npj Precision Oncology journal

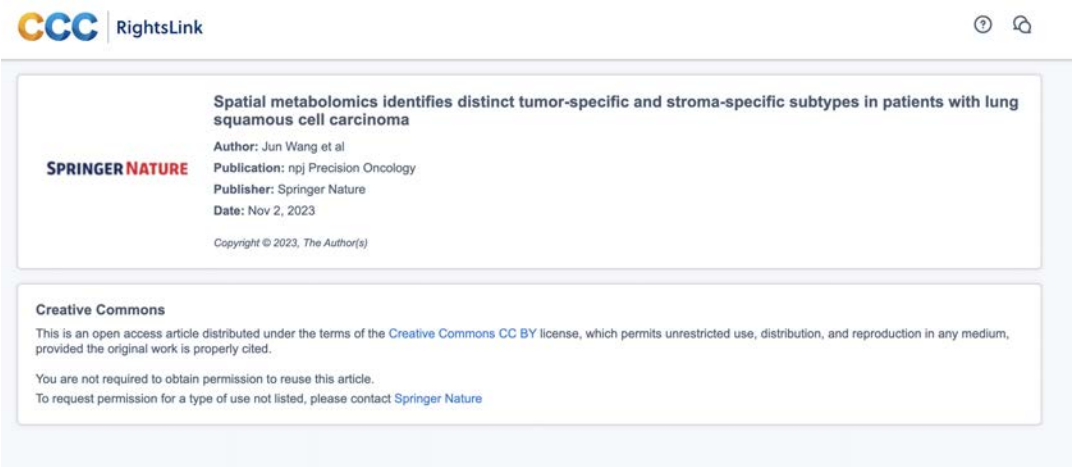

Fig. B.2. Approval letter for the publication in the npj Precision Oncology.

Bibliography

[1] J. Wang, T. Kunzke, V. M. Prade, J. Shen, A. Buck, A. Feuchtinger, I. Haffner, B. Luber, D. H. Liu, R. Langer, et al. “Spatial metabolomics identifies distinct tumor-specific subtypes in gastric cancer patients”. In: *Clinical Cancer Research* 28.13 (2022), pp. 2865–2877 (cit. on pp. 2, 37, 89).

[2] J. Wang, N. Sun, T. Kunzke, J. Shen, P. Zens, V. M. Prade, A. Feuchtinger, S. Berezowska, and A. Walch. “Spatial metabolomics identifies distinct tumor-specific and stroma-specific subtypes in patients with lung squamous cell carcinoma”. In: *npj Precision Oncology* 7.1 (2023), p. 114 (cit. on pp. 2, 51).

[3] H. Sung, J. Ferlay, R. L. Siegel, M. Laversanne, I. Soerjomataram, A. Jemal, and F. Bray. “Global cancer statistics 2020: GLOBOCAN estimates of incidence and mortality worldwide for 36 cancers in 185 countries”. In: *CA: a cancer journal for clinicians* 71.3 (2021), pp. 209–249 (cit. on pp. 9–11).

[4] S. Xiao and L. Zhou. “Gastric cancer: metabolic and metabolomics perspectives”. In: *International Journal of Oncology* 51.1 (2017), pp. 5–17 (cit. on p. 9).

[5] J. Shen, N. Sun, J. Wang, P. Zens, T. Kunzke, A. Buck, V. M. Prade, Q. Wang, A. Feuchtinger, R. Hu, et al. “Patterns of Carbon-Bound Exogenous Compounds Impact Disease Pathophysiology in Lung Cancer Subtypes in Different Ways”. In: *ACS nano* (2023) (cit. on p. 9).

[6] T. Kunzke, F. T. Hölzl, V. M. Prade, A. Buck, K. Huber, A. Feuchtinger, K. Ebert, G. Zwingenberger, R. Geffers, S. M. Hauck, et al. “Metabolomic therapy response prediction in pretherapeutic tissue biopsies for trastuzumab in patients with HER2-positive advanced gastric cancer”. In: *Clinical and Translational Medicine* 11.9 (2021) (cit. on pp. 9, 73).

[7] Z.-F. Lim and P. C. Ma. “Emerging insights of tumor heterogeneity and drug resistance mechanisms in lung cancer targeted therapy”. In: *Journal of hematology & oncology* 12.1 (2019), pp. 1–18 (cit. on p. 9).

[8] N Howlader, A Noone, M Krapcho, J Garshell, N Neyman, S Altekruse, C Kosary, M Yu, J Ruhl, Z Tatalovich, et al. “SEER Cancer Statistics Review, 1975-2010.[Based on the November 2012 SEER data submission, posted to the SEER web site, April 2013.]” In: *Bethesda, MD: National Cancer Institute* 9 (2013) (cit. on p. 10).

[9] M. Alsina, V. Arrazubi, M. Diez, and J. Tabernero. “Current developments in gastric cancer: from molecular profiling to treatment strategy”. In: *Nature Reviews Gastroenterology & Hepatology* 20.3 (2023), pp. 155–170 (cit. on pp. 12, 13).

[10] F. Islami, C. E. Guerra, A. Minihan, K. R. Yabroff, S. A. Fedewa, K. Sloan, T. L. Wiedt, B. Thomson, R. L. Siegel, N. Nargis, et al. “American Cancer Society’s report on the status of cancer disparities in the United States, 2021”. In: *CA: a cancer journal for clinicians* 72.2 (2022), pp. 112–143 (cit. on p. 12).

[11] L. Albarello, L. Pecciarini, and C. Doglioni. “HER2 testing in gastric cancer”. In: *Advances in anatomic pathology* 18.1 (2011), pp. 53–59 (cit. on p. 12).

[12] E. C. Smyth, M. Nilsson, H. I. Grabsch, N. C. van Grieken, and F. Lordick. “Gastric cancer”. In: *The Lancet* 396.10251 (2020), pp. 635–648 (cit. on p. 12).

[13] A. F. Okines and D. Cunningham. “Trastuzumab in gastric cancer”. In: *European Journal of Cancer* 46.11 (2010), pp. 1949–1959 (cit. on p. 12).

[14] Y.-J. Bang, E. Van Cutsem, A. Feyereislova, H. C. Chung, L. Shen, A. Sawaki, F. Lordick, A. Ohtsu, Y. Omuro, T. Satoh, et al. “Trastuzumab in combination with chemotherapy versus chemotherapy alone for treatment of HER2-positive advanced gastric or gastro-oesophageal junction cancer (ToGA): a phase 3, open-label, randomised controlled trial”. In: *The Lancet* 376.9742 (2010), pp. 687–697 (cit. on p. 12).

[15] T. Gutting, N. Schulte, S. Belle, J. Betge, N. Härtel, J. Wilke, J. Weers, M. P. Ebert, and T. Zhan. “Complete remission of metastatic HER2+ oesophagogastric junctional adenocarcinoma under long-term trastuzumab treatment”. In: *J Gastrointest Liver Dis* 28 (2019), pp. 503–517 (cit. on p. 13).

[16] J. H. Yi, J. H. Kang, I. G. Hwang, H. K. Ahn, H. J. Baek, S. I. Lee, D. H. Lim, Y.-W. Won, J. H. Ji, H. S. Kim, et al. “A retrospective analysis for patients with HER2-positive gastric cancer who were treated with trastuzumab-based chemotherapy: in the perspectives of ethnicity and histology”. In: *Cancer Research and Treatment: Official Journal of Korean Cancer Association* 48.2 (2016), p. 553 (cit. on p. 13).

[17] C. Gomez-Martin, J. C. Plaza, R. Pazo-Cid, A. Salud, F. Pons, P. Fonseca, A. Leon, M. Alsina, L. Visa, F. Rivera, et al. “Level of HER2 gene amplification predicts response and overall survival in HER2-positive advanced gastric cancer treated with trastuzumab”. In: *Journal of Clinical Oncology* 31.35 (2013), pp. 4445–4452 (cit. on p. 13).

[18] Y Kurokawa, N Sugimoto, H Miwa, M Tsuda, S Nishina, H Okuda, H Imamura, M Gamoh, D Sakai, T Shimokawa, et al. “Phase II study of trastuzumab in combination with S-1 plus cisplatin in HER2-positive gastric cancer (HERBIS-1)”. In: *British journal of cancer* 110.5 (2014), pp. 1163–1168 (cit. on p. 13).

[19] Y. Miura, T. Takano, Y. Sukawa, K. Nosho, S. Hironaka, M. Mori, K. Nishikawa, S. Tokunaga, H. Okuda, M. Tsuda, et al. *A phase II trial of 5-weekly S-1 plus cisplatin (CDDP) combination with trastuzumab (Tmab) for HER2-positive advanced gastric or esophagogastric junction (EGJ) cancer: WJOG7212G (T-SPACE) study.* 2015 (cit. on p. 13).

[20] J. Chao, C. S. Fuchs, K. Shitara, J. Tabernero, K. Muro, E. Van Cutsem, Y.-J. Bang, F. De Vita, G. Landers, C.-J. Yen, et al. “Assessment of pembrolizumab therapy for the treatment of microsatellite instability–high gastric or gastroesophageal junction cancer among patients in the KEYNOTE-059, KEYNOTE-061, and KEYNOTE-062 clinical trials”. In: *JAMA oncology* 7.6 (2021), pp. 895–902 (cit. on pp. 14, 22, 70).

[21] K. Muro, H. C. Chung, V. Shankaran, R. Geva, D. Catenacci, S. Gupta, J. P. Eder, T. Golan, D. T. Le, B. Burtness, et al. “Pembrolizumab for patients with PD-L1-positive advanced gastric cancer (KEYNOTE-012): a multicentre, open-label, phase 1b trial”. In: *The lancet oncology* 17.6 (2016), pp. 717–726 (cit. on p. 14).

[22] C. S. Fuchs, T. Doi, R. W. Jang, K. Muro, T. Satoh, M. Machado, W. Sun, S. I. Jalal, M. A. Shah, J.-P. Metges, et al. “Safety and efficacy of pembrolizumab monotherapy in patients with previously treated advanced gastric and gastroesophageal junction cancer: phase 2 clinical KEYNOTE-059 trial”. In: *JAMA oncology* 4.5 (2018), e180013–e180013 (cit. on pp. 14, 21).

[23] C. Dai, R. Geng, C. Wang, A. Wong, M. Qing, J. Hu, Y. Sun, A. Lo, and J. Li. “Concordance of immune checkpoints within tumor immune contexture and their prognostic significance in gastric cancer”. In: *Molecular oncology* 10.10 (2016), pp. 1551–1558 (cit. on pp. 14, 22, 70).

[24] Y. Y. Janjigian, A. Kawazoe, P. Yañez, N. Li, S. Lonardi, O. Kolesnik, O. Barajas, Y. Bai, L. Shen, Y. Tang, et al. “The KEYNOTE-811 trial of dual PD-1 and HER2 blockade in HER2-positive gastric cancer”. In: *Nature* 600.7890 (2021), pp. 727–730 (cit. on pp. 14, 70).

[25] W. S. El-Deiry, R. M. Goldberg, H.-J. Lenz, A. F. Shields, G. T. Gibney, A. R. Tan, J. Brown, B. Eisenberg, E. I. Heath, S. Phuphanich, et al. “The current state of molecular testing in the treatment of patients with solid tumors, 2019”. In: *CA: a cancer journal for clinicians* 69.4 (2019), pp. 305–343 (cit. on p. 14).

[26] Z. Niu, R. Jin, Y. Zhang, and H. Li. “Signaling pathways and targeted therapies in lung squamous cell carcinoma: mechanisms and clinical trials”. In: *Signal Transduction and Targeted Therapy* 7.1 (2022), p. 353 (cit. on p. 14).

[27] M. A. Socinski, C. Obasaju, D. Gandara, F. R. Hirsch, P. Bonomi, P. A. Bunn Jr, E. S. Kim, C. J. Langer, R. B. Natale, S. Novello, et al. “Current and emergent therapy options for advanced squamous cell lung cancer”. In: *Journal of Thoracic Oncology* 13.2 (2018), pp. 165–183 (cit. on p. 15).

[28] Food, D. Administration, et al. “Highlights of prescribing information: KEYTRUDA”. In: *Medication Guide, Reference ID* 4449844 (2019) (cit. on p. 15).

[29] K. Shien, V. A. Papadimitrakopoulou, and I. I. Wistuba. “Predictive biomarkers of response to PD-1/PD-L1 immune checkpoint inhibitors in non–small cell lung cancer”. In: *Lung Cancer* 99 (2016), pp. 79–87 (cit. on pp. 15, 23, 71).

[30] M. Reck, D. Rodríguez-Abreu, A. G. Robinson, R. Hui, T. Csőszi, A. Fülöp, M. Gottfried, N. Peled, A. Tafreshi, S. Cuffe, et al. “Pembrolizumab versus chemotherapy for PD-L1–positive non–small-cell lung cancer”. In: *N engl J med* 375 (2016), pp. 1823–1833 (cit. on p. 15).

[31] E. B. Garon, N. A. Rizvi, R. Hui, N. Leighl, A. S. Balmanoukian, J. P. Eder, A. Patnaik, C. Aggarwal, M. Gubens, L. Horn, et al. “Pembrolizumab for the treatment of non–small-cell lung cancer”. In: *New England Journal of Medicine* 372.21 (2015), pp. 2018–2028 (cit. on pp. 15, 23).

[32] R. S. Herbst, P. Baas, D.-W. Kim, E. Felip, J. L. Pérez-Gracia, J.-Y. Han, J. Molina, J.-H. Kim, C. D. Arvis, M.-J. Ahn, et al. “Pembrolizumab versus docetaxel for previously treated, PD-L1-positive, advanced non-small-cell lung cancer (KEYNOTE-010): a randomised controlled trial”. In: *The Lancet* 387.10027 (2016), pp. 1540–1550 (cit. on p. 15).

[33] Z. Lei, I. B. Tan, K. Das, N. Deng, H. Zouridis, S. Pattison, C. Chua, Z. Feng, Y. K. Guan, C. H. Ooi, et al. “Identification of molecular subtypes of gastric cancer with different responses to PI3-kinase inhibitors and 5-fluorouracil”. In: *Gastroenterology* 145.3 (2013), pp. 554–565 (cit. on pp. 17, 18).

[34] Z. Liu, J. Zhang, Y. Gao, L. Pei, J. Zhou, L. Gu, L. Zhang, B. Zhu, N. Hattori, J. Ji, et al. “Large-scale characterization of DNA methylation changes in human gastric carcinomas with and without metastasis”. In: *Clinical cancer research* 20.17 (2014), pp. 4598–4612 (cit. on pp. 17, 18).

[35] M. A. Shah, R. Khanin, L. Tang, Y. Y. Janjigian, D. S. Klimstra, H. Gerdes, and D. P. Kelsen. “Molecular classification of gastric cancer: a new paradigm”. In: *Clinical cancer research* 17.9 (2011), pp. 2693–2701 (cit. on pp. 17, 18).

[36] X. Lin, Y. Zhao, W.-m. Song, and B. Zhang. “Molecular classification and prediction in gastric cancer”. In: *Computational and structural biotechnology journal* 13 (2015), pp. 448–458 (cit. on pp. 17, 18).

[37] S. Satpathy, K. Krug, P. M. J. Beltran, S. R. Savage, F. Petralia, C. Kumar-Sinha, Y. Dou, B. Reva, M. H. Kane, S. C. Avanessian, et al. “A proteogenomic portrait of lung squamous cell carcinoma”. In: *Cell* 184.16 (2021), pp. 4348–4371 (cit. on pp. 17, 20).

[38] Y. Nakamura, A. Kawazoe, F. Lordick, Y. Y. Janjigian, and K. Shitara. “Biomarker-targeted therapies for advanced-stage gastric and gastro-oesophageal junction cancers: an emerging paradigm”. In: *Nature Reviews Clinical Oncology* 18.8 (2021), pp. 473–487 (cit. on p. 17).

[39] M. S.-K. C. C. T. pilot phase only) Socci Nicholas D. 17 Liang Yupu 17 Schultz Nikolaus 17 Borsu Laetitia 17 Lash Alex E. 17 Viale Agnes 17 Sander Chris 17 Ladanyi Marc 18 19, U. of Southern California/Johns Hopkins Cope Leslie 30 Danilova Ludmila 30 Weisenberger Daniel J. 31 Maglinte Dennis T. 31 Pan Fei 31 Van Den Berg David J. 31 Triche Jr Timothy 31 Herman James G. 30 Baylin Stephen B. 30 Laird Peter W. 31, U. of Texas MD Anderson Cancer Center Akbani Rehan 34 Zhang Nianxiang 34 Broom Bradley M. 34 Casasent Tod 34 Unruh Anna 34 Wakefield Chris 34 Craig Cason R. 35 Baggerly Keith A. 34 Weinstein John N. 34 36, et al. "Comprehensive genomic characterization of squamous cell lung cancers". In: *Nature* 489.7417 (2012), pp. 519–525 (cit. on pp. 17, 20, 23).

[40] A. J. Bass, V. Thorsson, I. Shmulevich, S. M. Reynolds, M. Miller, B. Bernard, T. Hinoue, P. W. Laird, C. Curtis, H. Shen, et al. "Comprehensive molecular characterization of gastric adenocarcinoma". In: *Nature* 513.7517 (2014), p. 202 (cit. on pp. 17, 19, 75).

[41] T. Chen, X.-Y. Xu, and P.-H. Zhou. "Emerging molecular classifications and therapeutic implications for gastric cancer". In: *Chinese journal of cancer* 35.1 (2016), pp. 1–10 (cit. on pp. 18, 19).

[42] M. Chénard-Poirier and E. C. Smyth. "Immune checkpoint inhibitors in the treatment of gastroesophageal cancer". In: *Drugs* 79.1 (2019), pp. 1–10 (cit. on p. 19).

[43] H. S. Kim, S.-J. Shin, S.-H. Beom, M. Jung, Y. Y. Choi, T. Son, H.-I. Kim, J.-H. Cheong, W. J. Hyung, S. H. Noh, et al. "Comprehensive expression profiles of gastric cancer molecular subtypes by immunohistochemistry: implications for individualized therapy". In: *Oncotarget* 7.28 (2016), p. 44608 (cit. on pp. 19, 22).

[44] R. Cristescu, J. Lee, M. Nebozhyn, K.-M. Kim, J. C. Ting, S. S. Wong, J. Liu, Y. G. Yue, J. Wang, K. Yu, et al. "Molecular analysis of gastric cancer identifies subtypes associated with distinct clinical outcomes". In: *Nature medicine* 21.5 (2015), pp. 449–456 (cit. on pp. 19, 21).

[45] F. Chen, Y. Zhang, E. Parra, J. Rodriguez, C. Behrens, R. Akbani, Y. Lu, J. Kurie, D. L. Gibbons, G. B. Mills, et al. "Multiplatform-based molecular subtypes of non-small-cell lung cancer". In: *Oncogene* 36.10 (2017), pp. 1384–1393 (cit. on pp. 20, 23, 75).

[46] M. D. Wilkerson, X. Yin, K. A. Hoadley, Y. Liu, M. C. Hayward, C. R. Cabanski, K. Muldrew, C. R. Miller, S. H. Randell, M. A. Socinski, et al. “Lung Squamous Cell Carcinoma mRNA Expression Subtypes Are Reproducible, Clinically Important, and Correspond to Normal Cell TypesLung Squamous Cell Carcinoma mRNA Expression Subtypes”. In: *Clinical cancer research* 16.19 (2010), pp. 4864–4875 (cit. on p. 20).

[47] P. A. Stewart, E. A. Welsh, R. J. Slebos, B. Fang, V. Izumi, M. Chambers, G. Zhang, L. Cen, F. Pettersson, Y. Zhang, et al. “Proteogenomic landscape of squamous cell lung cancer”. In: *Nature communications* 10.1 (2019), p. 3578 (cit. on p. 20).

[48] V. Genitsch, A. Novotny, C. A. Seiler, D. Kröll, A. Walch, and R. Langer. “Epstein–Barr virus in gastro-esophageal adenocarcinomas–single center experiences in the context of current literature”. In: *Frontiers in oncology* 5 (2015), p. 73 (cit. on p. 21).

[49] T. Morihiro, S. Kuroda, N. Kanaya, Y. Kakiuchi, T. Kubota, K. Aoyama, T. Tanaka, S. Kikuchi, T. Nagasaka, M. Nishizaki, et al. “PD-L1 expression combined with microsatellite instability/CD8+ tumor infiltrating lymphocytes as a useful prognostic biomarker in gastric cancer”. In: *Scientific reports* 9.1 (2019), pp. 1–9 (cit. on pp. 21, 22, 69).

[50] M. Fukayama and T. Ushiku. “Epstein-Barr virus-associated gastric carcinoma”. In: *Pathology-Research and Practice* 207.9 (2011), pp. 529–537 (cit. on p. 21).

[51] Y. Y. Janjigian, F. Sanchez-Vega, P. Jonsson, W. K. Chatila, J. F. Hechtman, G. Y. Ku, J. C. Riches, Y. Tuvy, R. Kundra, N. Bouvier, et al. “Genetic predictors of response to systemic therapy in esophagogastric cancer”. In: *Cancer discovery* 8.1 (2018), pp. 49–58 (cit. on p. 21).

[52] S. T. Kim, R. Cristescu, A. J. Bass, K.-M. Kim, J. I. Odegaard, K. Kim, X. Q. Liu, X. Sher, H. Jung, M. Lee, et al. “Comprehensive molecular characterization of clinical responses to PD-1 inhibition in metastatic gastric cancer”. In: *Nature medicine* 24.9 (2018), pp. 1449–1458 (cit. on p. 21).

[53] A. Panda, J. M. Mehnert, K. M. Hirshfield, G. Riedlinger, S. Damare, T. Saunders, M. Kane, L. Sokol, M. N. Stein, E. Poplin, et al. “Immune activation and benefit from avelumab in EBV-positive gastric cancer”. In: *JNCI: Journal of the National Cancer Institute* 110.3 (2018), pp. 316–320 (cit. on p. 21).

[54] A. A. d. A. Jácome, E. M. d. Lima, A. I. Kazzi, G. F. Chaves, D. C. d. Mendonça, M. M. Maciel, and J. S. d. Santos. "Epstein-Barr virus-positive gastric cancer: a distinct molecular subtype of the disease?" In: *Revista da Sociedade Brasileira de Medicina Tropical* 49 (2016), pp. 150–157 (cit. on p. 21).

[55] C. Díaz del Arco, L. Estrada Muñoz, E. Molina Roldán, M. Cerón Nieto, L. Ortega Medina, S. García Gómez de las Heras, and M. Fernández Aceñero. "Immunohistochemical classification of gastric cancer based on new molecular biomarkers: a potential predictor of survival". In: *Virchows Archiv* 473.6 (2018), pp. 687–695 (cit. on p. 22).

[56] E.-M. Birkman, N. Mansuri, S. Kurki, A. Ålgars, M. Lintunen, R. Ristamäki, J. Sundström, and O. Carpén. "Gastric cancer: immunohistochemical classification of molecular subtypes and their association with clinicopathological characteristics". In: *Virchows Archiv* 472.3 (2018), pp. 369–382 (cit. on p. 22).

[57] M. Yi, D. Jiao, H. Xu, Q. Liu, W. Zhao, X. Han, and K. Wu. "Biomarkers for predicting efficacy of PD-1/PD-L1 inhibitors". In: *Molecular cancer* 17.1 (2018), pp. 1–14 (cit. on p. 22).

[58] M. Kwon, M. An, S. J. Klempner, H. Lee, K.-M. Kim, J. K. Sa, H. J. Cho, J. Y. Hong, T. Lee, Y. W. Min, et al. "Determinants of response and intrinsic resistance to PD-1 blockade in microsatellite instability–high gastric cancer". In: *Cancer Discovery* 11.9 (2021), pp. 2168–2185 (cit. on p. 22).

[59] P. K. Paik, R. N. Pillai, C. S. Lathan, S. A. Velasco, and V. Papadimitrakopoulou. "New treatment options in advanced squamous cell lung cancer". In: *American Society of Clinical Oncology Educational Book* 39 (2019), e198–e206 (cit. on pp. 23, 71).

[60] Y. K. Chae, A. Pan, A. A. Davis, K. Raparia, N. A. Mohindra, M. Matsangou, and F. J. Giles. "Biomarkers for PD-1/PD-L1 blockade therapy in non–small-cell lung cancer: Is PD-L1 expression a good marker for patient selection?" In: *Clinical lung cancer* 17.5 (2016), pp. 350–361 (cit. on p. 23).

[61] A. M. Newman, C. L. Liu, M. R. Green, A. J. Gentles, W. Feng, Y. Xu, C. D. Hoang, M. Diehn, and A. A. Alizadeh. "Robust enumeration of cell subsets from tissue expression profiles". In: *Nature methods* 12.5 (2015), pp. 453–457 (cit. on p. 23).

[62] A. O. Kamphorst, R. N. Pillai, S. Yang, T. H. Nasti, R. S. Akondy, A. Wieland, G. L. Sica, K. Yu, L. Koenig, N. T. Patel, et al. “Proliferation of PD-1+ CD8 T cells in peripheral blood after PD-1–targeted therapy in lung cancer patients”. In: *Proceedings of the National Academy of Sciences* 114.19 (2017), pp. 4993–4998 (cit. on p. 23).

[63] M. E. Ardini-Poleske, R. F. Clark, C. Ansong, J. P. Carson, R. A. Corley, G. H. Deutsch, J. S. Hagood, N. Kaminski, T. J. Mariani, S. S. Potter, et al. “LungMAP: the molecular atlas of lung development program”. In: *American Journal of Physiology-Lung Cellular and Molecular Physiology* 313.5 (2017), pp. L733–L740 (cit. on pp. 23, 24).

[64] S. O. Group et al. “Lung-MAP: Biomarker-Targeted Second-Line Therapy in Treating Patients With Recurrent Stage IV Squamous Cell Lung Cancer”. In: *ClinicalTrials. gov [Internet]. Bethesda (MD): National Library of Medicine (US). Available from: URL: https://clinicaltrials. gov/ct2/show/NCT02154490* () (cit. on pp. 23, 24).

[65] C. M. Gay, C. A. Stewart, E. M. Park, L. Diao, S. M. Groves, S. Heeke, B. Y. Nabet, J. Fujimoto, L. M. Solis, W. Lu, et al. “Patterns of transcription factor programs and immune pathway activation define four major subtypes of SCLC with distinct therapeutic vulnerabilities”. In: *Cancer cell* 39.3 (2021), pp. 346–360 (cit. on p. 24).

[66] Y. Xiao, T.-J. Yu, Y. Xu, R. Ding, Y.-P. Wang, Y.-Z. Jiang, and Z.-M. Shao. “Emerging therapies in cancer metabolism”. In: *Cell Metabolism* 35.8 (2023), pp. 1283–1303 (cit. on p. 24).

[67] S. Qiu, Y. Cai, H. Yao, C. Lin, Y. Xie, S. Tang, and A. Zhang. “Small molecule metabolites: discovery of biomarkers and therapeutic targets”. In: *Signal Transduction and Targeted Therapy* 8.1 (2023), p. 132 (cit. on p. 24).

[68] J. Shen, N. Sun, P. Zens, T. Kunzke, A. Buck, V. M. Prade, J. Wang, Q. Wang, R. Hu, A. Feuchtinger, et al. “Spatial metabolomics for evaluating response to neoadjuvant therapy in non-small cell lung cancer patients”. In: *Cancer communications* 42.6 (2022), pp. 517–535 (cit. on pp. 24, 28).

[69] D. R. Schmidt, R. Patel, D. G. Kirsch, C. A. Lewis, M. G. Vander Heiden, and J. W. Locasale. “Metabolomics in cancer research and emerging applications in clinical oncology”. In: *CA: a cancer journal for clinicians* 71.4 (2021), pp. 333–358 (cit. on p. 24).

[70] L.-W. Yuan, H. Yamashita, and Y. Seto. “Glucose metabolism in gastric cancer: The cutting-edge”. In: *World Journal of Gastroenterology* 22.6 (2016), p. 2046 (cit. on p. 24).

[71] A. A. Cluntun, M. J. Lukey, R. A. Cerione, and J. W. Locasale. “Glutamine metabolism in cancer: understanding the heterogeneity”. In: *Trends in cancer* 3.3 (2017), pp. 169–180 (cit. on p. 24).

[72] S. Huang, Y. Guo, Z. Li, Y. Zhang, T. Zhou, W. You, K. Pan, and W. Li. “A systematic review of metabolomic profiling of gastric cancer and esophageal cancer”. In: *Cancer biology & medicine* 17.1 (2020), p. 181 (cit. on p. 24).

[73] Q. Wei, Y. Qian, J. Yu, and C. C. Wong. “Metabolic rewiring in the promotion of cancer metastasis: mechanisms and therapeutic implications”. In: *Oncogene* 39.39 (2020), pp. 6139–6156 (cit. on p. 25).

[74] F. André, A. Trinh, S. Balayssac, P. Maboudou, S. Dekiouk, M. Malet-Martino, B. Quesnel, T. Idziorek, J. Kluza, and P. Marchetti. “Metabolic rewiring in cancer cells overexpressing the glucocorticoid-induced leucine zipper protein (GILZ): Activation of mitochondrial oxidative phosphorylation and sensitization to oxidative cell death induced by mitochondrial targeted drugs”. In: *The International Journal of Biochemistry & Cell Biology* 85 (2017), pp. 166–174 (cit. on p. 25).

[75] X. Peng, Z. Chen, F. Farshidfar, X. Xu, P. L. Lorenzi, Y. Wang, F. Cheng, L. Tan, K. Mojumdar, D. Du, et al. “Molecular characterization and clinical relevance of metabolic expression subtypes in human cancers”. In: *Cell reports* 23.1 (2018), pp. 255–269 (cit. on p. 25).

[76] A. Buck, A. Ly, B. Balluff, N. Sun, K. Gorzolka, A. Feuchtinger, K.-P. Janssen, P. J. Kuppen, C. J. van de Velde, G. Weirich, et al. “High-resolution MALDI-FT-ICR MS imaging for the analysis of metabolites from formalin-fixed, paraffin-embedded clinical tissue samples”. In: *The Journal of pathology* 237.1 (2015), pp. 123–132 (cit. on pp. 27, 77).

[77] B. Balluff, C. K. Frese, S. K. Maier, C. Schöne, B. Kuster, M. Schmitt, M. Aubele, H. Höfler, A. M. Deelder, A. J. Heck, et al. “De novo discovery of phenotypic intratumour heterogeneity using imaging mass spectrometry”. In: *The Journal of pathology* 235.1 (2015), pp. 3–13 (cit. on p. 27).

[78] J. Kriegsmann, M. Kriegsmann, and R. Casadonte. “MALDI TOF imaging mass spectrometry in clinical pathology: a valuable tool for cancer diagnostics”. In: *International journal of oncology* 46.3 (2015), pp. 893–906 (cit. on p. 27).

[79] J. Yao, M. Yang, and Y. Duan. “Chemistry, biology, and medicine of fluorescent nanomaterials and related systems: new insights into biosensing, bioimaging, genomics, diagnostics, and therapy”. In: *Chemical reviews* 114.12 (2014), pp. 6130–6178 (cit. on p. 27).

[80] B. Balluff, S. Rauser, M. P. Ebert, J. T. Siveke, H. Höfler, and A. Walch. “Direct molecular tissue analysis by MALDI imaging mass spectrometry in the field of gastrointestinal disease”. In: *Gastroenterology* 143.3 (2012), pp. 544–549 (cit. on pp. 27–29).

[81] A. Ly, A. Buck, B. Balluff, N. Sun, K. Gorzolka, A. Feuchtinger, K.-P. Janssen, P. J. Kuppen, C. J. van de Velde, G. Weirich, et al. “High-mass-resolution MALDI mass spectrometry imaging of metabolites from formalin-fixed paraffin-embedded tissue”. In: *Nature protocols* 11.8 (2016), pp. 1428–1443 (cit. on pp. 28, 77).

[82] D. Lambrechts, E. Wauters, B. Boeckx, S. Aibar, D. Nittner, O. Burton, A. Bassez, H. Decaluwé, A. Pircher, K. Van den Eynde, et al. “Phenotype molding of stromal cells in the lung tumor microenvironment”. In: *Nature medicine* 24.8 (2018), pp. 1277–1289 (cit. on p. 28).

[83] J. L. Norris and R. M. Caprioli. “Analysis of tissue specimens by matrix-assisted laser desorption/ionization imaging mass spectrometry in biological and clinical research”. In: *Chemical reviews* 113.4 (2013), pp. 2309–2342 (cit. on p. 28).

[84] J. M. Neumann, H. Freitag, J. S. Hartmann, K. Niehaus, M. Galanis, M. Griesshammer, U. Kellner, and H. Bednarz. “Subtyping non-small cell lung cancer by histology-guided spatial metabolomics”. In: *Journal of cancer research and clinical oncology* (2022), pp. 1–10 (cit. on p. 28).

[85] V. M. Prade, T. Kunzke, A. Feuchtinger, M. Rohm, B. Luber, F. Lordick, A. Buck, and A. Walch. “De novo discovery of metabolic heterogeneity with immunophenotype-guided imaging mass spectrometry”. In: *Molecular metabolism* 36 (2020), p. 100953 (cit. on pp. 29, 30).

[86] T. Alexandrov, I. Chernyavsky, M. Becker, F. von Eggeling, and S. Nikolenko. “Analysis and interpretation of imaging mass spectrometry data by clustering mass-to-charge images according to their spatial similarity”. In: *Analytical chemistry* 85.23 (2013), pp. 11189–11195 (cit. on p. 31).

[87] P. Inglese, G. Correia, P. Pruski, R. C. Glen, and Z. Takats. “Colocalization features for classification of tumors using desorption electrospray ionization mass spectrometry imaging”. In: *Analytical chemistry* 91.10 (2019), pp. 6530–6540 (cit. on p. 31).

[88] X. Song, J. He, X. Pang, J. Zhang, C. Sun, L. Huang, C. Li, Q. Zang, X. Li, Z. Luo, et al. “Virtual calibration quantitative mass spectrometry imaging for accurately mapping analytes across heterogenous biotissue”. In: *Analytical chemistry* 91.4 (2019), pp. 2838–2846 (cit. on p. 31).

[89] A. R. Konicek, J. Lefman, and C. Szakal. “Automated correlation and classification of secondary ion mass spectrometry images using ak-means cluster method”. In: *Analyst* 137.15 (2012), pp. 3479–3487 (cit. on p. 31).

[90] S.-O. Deininger, M. P. Ebert, A. Futterer, M. Gerhard, and C. Rocken. “MALDI imaging combined with hierarchical clustering as a new tool for the interpretation of complex human cancers”. In: *Journal of proteome research* 7.12 (2008), pp. 5230–5236 (cit. on p. 31).

[91] J. B. Haanen. “Converting cold into hot tumors by combining immunotherapies”. In: *Cell* 170.6 (2017), pp. 1055–1056 (cit. on p. 69).

[92] P. C. Tumeh, C. L. Harview, J. H. Yearley, I. P. Shintaku, E. J. Taylor, L. Robert, B. Chmielowski, M. Spasic, G. Henry, V. Ciobanu, et al. “PD-1 blockade induces responses by inhibiting adaptive immune resistance”. In: *Nature* 515.7528 (2014), pp. 568–571 (cit. on p. 70).

[93] J.-Y. Sun, D. Zhang, S. Wu, M. Xu, X. Zhou, X.-J. Lu, and J. Ji. “Resistance to PD-1/PD-L1 blockade cancer immunotherapy: mechanisms, predictive factors, and future perspectives”. In: *Biomarker Research* 8.1 (2020), pp. 1–10 (cit. on p. 70).

[94] T. S. Nowicki, S. Hu-Lieskovan, and A. Ribas. “Mechanisms of resistance to PD-1 and PD-L1 blockade”. In: *Cancer journal (Sudbury, Mass.)* 24.1 (2018), p. 47 (cit. on p. 70).

[95] R. Kelly, A Thomas, A Rajan, G Chun, A Lopez-Chavez, E Szabo, S Spencer, C. Carter, U Guha, S Khozin, et al. “A phase I/II study of sepantronium bromide (YM155, survivin suppressor) with paclitaxel and carboplatin in patients with advanced non-small-cell lung cancer”. In: *Annals of oncology* 24.10 (2013), pp. 2601–2606 (cit. on p. 71).

[96] N. Karachaliou, M. Fernandez-Bruno, and R. Rosell. “Strategies for first-line immunotherapy in squamous cell lung cancer: are combinations a game changer?” In: *Translational Lung Cancer Research* 7.Suppl 3 (2018), S198 (cit. on p. 71).

[97] Z. Y. Xu-Monette, M. Zhang, J. Li, and K. H. Young. “PD-1/PD-L1 blockade: have we found the key to unleash the antitumor immune response?” In: *Frontiers in immunology* 8 (2017), p. 1597 (cit. on p. 71).

[98] G. T. Motz and G. Coukos. “Deciphering and reversing tumor immune suppression”. In: *Immunity* 39.1 (2013), pp. 61–73 (cit. on p. 71).

[99] M. W. Teng, S. F. Ngiow, A. Ribas, and M. J. Smyth. “Classifying cancers based on T-cell infiltration and PD-L1”. In: *Cancer research* 75.11 (2015), pp. 2139–2145 (cit. on p. 71).

[100] G. Mazzaschi, D. Madeddu, A. Falco, G. Bocchialini, M. Goldoni, F. Sogni, G. Armani, C. A. Lagrasta, B. Lorusso, C. Mangiaracina, et al. “Low PD-1 Expression in Cytotoxic CD8+ Tumor-Infiltrating Lymphocytes Confers an Immune-Privileged Tissue Microenvironment in NSCLC with a Prognostic and Predictive ValuePrognostic and Predictive Role of NSCLC Immune Context”. In: *Clinical cancer research* 24.2 (2018), pp. 407–419 (cit. on p. 71).

[101] V. Velcheti, K. A. Schalper, D. E. Carvajal, V. K. Anagnostou, K. N. Syrigos, M. Sznol, R. S. Herbst, S. N. Gettinger, L. Chen, and D. L. Rimm. “Programmed death ligand-1 expression in non-small cell lung cancer”. In: *Laboratory investigation* 94.1 (2014), pp. 107–116 (cit. on p. 71).

[102] Y. Zhang, S. Huang, D. Gong, Y. Qin, and Q. Shen. “Programmed death-1 upregulation is correlated with dysfunction of tumor-infiltrating CD8+ T lymphocytes in human non-small cell lung cancer”. In: *Cellular & molecular immunology* 7.5 (2010), pp. 389–395 (cit. on p. 71).

[103] J. Konishi, K. Yamazaki, M. Azuma, I. Kinoshita, H. Dosaka-Akita, and M. Nishimura. “B7-H1 expression on non-small cell lung cancer cells and its relationship with tumor-infiltrating lymphocytes and their PD-1 expression”. In: *Clinical cancer research* 10.15 (2004), pp. 5094–5100 (cit. on p. 71).

[104] S. Cui, L. Dong, J. Qian, L. Ye, and L. Jiang. “Classifying non-small cell lung cancer by status of programmed cell death ligand 1 and tumor-infiltrating lymphocytes on tumor cells”. In: *Journal of Cancer* 9.1 (2018), p. 129 (cit. on p. 71).

[105] L. G. Boros. “Metabolic targeted therapy of cancer: current tracer technologies and future drug design strategies in the old metabolic network”. In: *Metabolomics* 1 (2005), pp. 11–15 (cit. on p. 72).

[106] S. R. Rosario, M. D. Long, H. C. Affronti, A. M. Rowsam, K. H. Eng, and D. J. Smiraglia. “Pan-cancer analysis of transcriptional metabolic dysregulation using The Cancer Genome Atlas”. In: *Nature communications* 9.1 (2018), pp. 1–17 (cit. on p. 72).

[107] M. Aichler, B. Luber, F. Lordick, and A. Walch. “Proteomic and metabolic prediction of response to therapy in gastric cancer”. In: *World journal of gastroenterology: WJG* 20.38 (2014), p. 13648 (cit. on p. 72).

[108] S. Nie, Y. Zhao, X. Qiu, W. Wang, Y. Yao, M. Yi, and D. Wang. “Metabolomic study on nude mice models of gastric cancer treated with modified Si Jun Zi Tang via HILIC UHPLC-Q-TOF/MS analysis”. In: *Evidence-Based Complementary and Alternative Medicine* 2019 (2019) (cit. on p. 72).

[109] A. M. Weljie and F. R. Jirik. “Hypoxia-induced metabolic shifts in cancer cells: moving beyond the Warburg effect”. In: *The international journal of biochemistry & cell biology* 43.7 (2011), pp. 981–989 (cit. on p. 72).

[110] J.-L. Chen, H.-Q. Tang, J.-D. Hu, J. Fan, J. Hong, and J.-Z. Gu. “Metabolomics of gastric cancer metastasis detected by gas chromatography and mass spectrometry”. In: *World journal of gastroenterology: WJG* 16.46 (2010), p. 5874 (cit. on p. 72).

[111] J. Ye, Q. Huang, J. Xu, J. Huang, J. Wang, W. Zhong, W. Chen, X. Lin, and X. Lin. “Targeting of glutamine transporter ASCT2 and glutamine synthetase suppresses gastric cancer cell growth”. In: *Journal of Cancer Research and Clinical Oncology* 144.5 (2018), pp. 821–833 (cit. on p. 72).

[112] B. C. Nikolai, R. B. Lanz, B. York, S. Dasgupta, N. Mitsiades, C. J. Creighton, A. Tsimelzon, S. G. Hilsenbeck, D. M. Lonard, C. L. Smith, et al. “HER2 signaling drives DNA anabolism and proliferation through SRC-3 phosphorylation and E2F1-regulated genes”. In: *Cancer research* 76.6 (2016), pp. 1463–1475 (cit. on p. 72).

[113] Q. Ren, P. Zhu, H. Zhang, T. Ye, D. Liu, Z. Gong, and X. Xia. “Identification and validation of stromal-tumor microenvironment-based subtypes tightly associated with PD-1/PD-L1 immunotherapy and outcomes in patients with gastric cancer”. In: *Cancer cell international* 20.1 (2020), pp. 1–13 (cit. on p. 75).

[114] A. Wojakowska, M. Chekan, Ł. Marczak, K. Polanski, D. Lange, M. Pietrowska, and P. Widlak. “Detection of metabolites discriminating subtypes of thyroid cancer: Molecular profiling of FFPE samples using the GC/MS approach”. In: *Molecular and Cellular Endocrinology* 417 (2015), pp. 149–157 (cit. on p. 77).

[115] M. Yuan, S. B. Breitkopf, X. Yang, and J. M. Asara. “A positive/negative ion–switching, targeted mass spectrometry–based metabolomics platform for bodily fluids, cells, and fresh and fixed tissue”. In: *Nature protocols* 7.5 (2012), pp. 872–881 (cit. on p. 77).

[116] S. K. Neef, S. Winter, U. Hofmann, T. E. Muerdter, E. Schaeffeler, H. Horn, A. Buck, A. Walch, J. Hennenlotter, G. Ott, et al. “Optimized protocol for metabolomic and lipidomic profiling in formalin-fixed paraffin-embedded kidney tissue by LC-MS”. In: *Analytica Chimica Acta* 1134 (2020), pp. 125–135 (cit. on p. 77).

[117] T. Alexandrov. “Spatial metabolomics and imaging mass spectrometry in the age of artificial intelligence”. In: *Annual review of biomedical data science* 3 (2020), p. 61 (cit. on p. 78).

[118] A. Rajkomar, J. Dean, and I. Kohane. “Machine learning in medicine”. In: *New England Journal of Medicine* 380.14 (2019), pp. 1347–1358 (cit. on p. 78).

[119] M. J. He, W. Pu, X. Wang, W. Zhang, D. Tang, and Y. Dai. “Comparing DESI-MSI and MALDI-MSI mediated spatial metabolomics and their applications in cancer studies”. In: *Frontiers in Oncology* 12 (2022), p. 891018 (cit. on p. 78).

List of Figures